12-16-2020

Development of Point-of-Care Assays for Different Biologically Relevant Analytes

Dandan Liu

DEVELOPMENT OF POINT-OF-CARE ASSAYS FOR DIFFERENT BIOLOGICALLY RELEVANT ANALYTES

by

DANDAN LIU

Under the Direction of Suri S. Iyer, PhD

ABSTRACT

This thesis focuses on the development of assays that could potentially be used in Point-Of-Care (POC) diagnostics. We present our discovery and development efforts for three targets, influenza, norovirus and inflammatory bowel disease.

Influenza is a respiratory infection caused by influenza viruses, a highly contagious pathogen that primarily spreads through respiratory droplets. Influenza pandemics has led to millions of deaths. A significant number of patients have complications because of secondary infections caused by *S. pneumoniae*, after the initial infection caused by influenza. Thus, differentiation of influenza and *S. pneumoniae* is very important for appropriate treatment options. Here, we have synthesized fluorescent sialic acid derivatives that are cleaved by influenza neuraminidases (NAs) and not by *S. pneumoniae*. We have also developed assays that could

differentiate between influenza viruses and *S. pneumoniae* by taking advantage of the structural differences between NAs from these pathogens and assay conditions.

In the second project, we present our efforts to identify and develop biomarkers for inflammatory bowel disease (IBD), which is characterized by chronic inflammation in gastrointestinal tract. People diagnosed with IBD are required to monitor their status of inflammation routinely. The gold standard to monitor IBD is to perform endoscopic evaluation with biopsies. However, this method is invasive, and patients often experience pain and discomfort during these procedures, highlighting the need for a non-invasive and cost-effective technique to monitor inflammation. Here, we explore the use of alternate biomarkers, matrix metallopeptidase 9 (MMP-9) and tumor necrosis factor alpha (TNF-α) in stool and sera, respectively, that can increase in inflammatory conditions. We explored the correlation between MMP-9, TNF-α levels and severity of colitis in IL10-/- mouse model, with a view to designing an effective tool for POC diagnostics for human IBD, since IL10-/- mouse model reflects inflammation in human IBD patients. We also present our initial studies to detect and monitor these biomarkers using a novel mesoporous silica bead-based method.

In the third project, we targeted human noroviruses in an effort to develop assays that could detect noroviruses at POC. Human noroviruses are the major cause of epidemic outbreaks of gastroenteritis. At the present time, there are no antivirals or vaccine for norovirus infection; the treatment options are primarily supportive care, and reverse dehydration and electrolyte abnormality. Therefore, prevention and early diagnostics of norovirus is important. When noroviruses infect humans, it binds to human histo-blood group antigens (HBGAs). However, the interactions between norovirus and HBGAs are poorly understood. Here, we have studied the interactions between norovirus virus like particles (VLPs) and chemically synthesized HBGAs by

surface plasmon resonance (SPR) with the ultimate goal being able to use some of these carbohydrates as recognition molecules in diagnostics to capture norovirus. We found that the interactions between HBGA and VLPs are complex and highly dependent on the structure of the VLP and the carbohydrate.

INDEX WORDS: Point-of-care, Diagnostics, Influenza, IBD, Norovirus.

DEVELOPMENT OF POINT-OF-CARE ASSAYS FOR DIFFERENT BIOLOGICALLY RELEVANT ANALYTES

by

DANDAN LIU

A Dissertation Submitted in Partial Fulfillment of the Requirements for the Degree of

Doctor of Philosophy

in the College of Arts and Sciences

Georgia State University

2020

DEVELOPMENT OF POINT-OF-CARE ASSAYS FOR DIFFERENT BIOLOGICALLY RELEVANT ANALYTES

by

DANDAN LIU

Committee Chair: Suri Iyer

Committee: Donald Hamelberg

Jenny Yang

Electronic Version Approved:

Office of Graduate Studies

College of Arts and Sciences

Georgia State University

December 2020

DEDICATION

I would like to dedicate my family for their supporting me to pursue my PhD career. I want to thank my friend Shanshan Li, without her help I would not be able to make the decision to study aboard.

ACKNOWLEDGEMENTS

First and foremost, I want to thank my advisor, Dr. Suri Iyer, for giving me the opportunity to join his research group. He was kind and patient in guiding my research in Georgia State University. He taught me knowledge, skills and improve my critical analysis skills. Without his help, I would not be able to finish my work in the dissertation.

I also want to thank my committee members, Dr. Jenny Yang and Dr. Donald Hamelberg, for giving me suggestions during my research and my dissertation. I would like to thank Dr. Mingzhen Zhang for cooperation, with his help, I published my first scientific paper.

I also want to thank my group members, Dr. Abasaheb N. Dhawane, Dr. Xiaohu Zhang, Dr. Xikai Cui, Dr. Hieu Dinh, Dr. Amrita Das, Dr. Varma Saikam, Ying Luo, Tianwei Jia, Xiaolin Sheng, Jieqiong Fang and Ethan, for their support, collegiality and guidance.

Finally, I want to thank the Centers for Diagnostics and Therapeutics (CDT) followship and for NIH to support my research.

TABLE OF CONTENTS

LIST OF TABLES

LIST OF FIGURES

LIST OF ABBREVIATIONS

Ethyl acetate, EtOAc;

Tetrabutylammonium hydrogen sulfate, TBAHS;

Sodium carbonate, Na_2CO_3;

Sodium methoxide, NaOMe;

Methanol, MeOH;

Sodium hydroxide, NaOH;

4-Methlumbelliferone, 4-MU;

Dichloromethane, DCM;

2′-(4-Methylumbelliferyl)-α-D-N-acetylneuraminic acid sodium salt hydrate, MUNANA;

Sodium azide, NaN_3;

Dimethylformamide, DMF;

(3-Aminopropyl) triethoxysilane, APTES;

2-(1H-benzotriazol-1-yl)-1,1,3,3-tetramethyluronium hexafluorophosphate, HBTU;

N, N-Diisopropylethylamine, DIPEA;

Sodium sulfate, Na_2SO_4;

Sodium metabisulfite, $Na_2S_2O_5$.

1 CHAPTER 1 POINT-OF-CARE TESTING

1.1 Introduction

This thesis focuses on the development of assays that could potentially be used in Point-Of-Care tests (POCTs). Therefore, in this chapter, we discuss some of the requirements of POCTs. As defined by the National Academy of Clinical Biochemistry (NACB), POCT refers to any testing performed outside of the traditional, core and central laboratory. It is an excellent method to provide laboratory testing or near the site of patient care so that medical treatment does not have to be delayed. POCT can be undertaken in many places, for example, home use, pharmacy, ambulance, nursing home, primary care, health clinic, major hospital and workplace drug screening, **Table 1.1** showed the application of POCT. The analytical process of POCT in healthcare is innovative and it can offer other options for disease prevention, diagnosis and patients monitoring.[1] POCT systems make up an important part of the in-vitro diagnostics market and the global market is estimated to reach $ 38 billion by 2022 from $ 23 billion in 2017.[2] A major segment of the POCT market comes from the blood glucose strips and test meter for diabetes, which utilizes the electrochemical biosensor for detection.[3]

Table 1.1 *The application of POCT in different places. Table is taken from publisher with permission.*[4]

ICU/operating room	Critical care testing: Blood gases, electrolytes, lactate
Emergency department	Emergency parameters: Blood gases, electrolytes, lactate
Outpatient department	Monitoring parameters: Glucose, HbA_{1c}
Ambulance	Critical care testing:

	Glucose, cardiac markers
Physician's practice	Monitoring parameters: Glucose, HbA_{1c}, global coagulation tests
Patient at home	Self-monitoring: Glucose, global coagulation tests

Several reasons could be contributed to the fast growth of POCT systems market. Improvement in analytical methods; increasing demand for continuous measurement; increasing patients and consumer interest; a rapidly increasing demand in the outpatient setting. There are numerous POCT devices developed and different biosensor techniques have been applied in the test, such as, electrochemical biosensor, optical biosensor and microgravimetry biosensor.[5, 6] The POCT devices can be classified as: qualitative device (such as lateral flow assays), benchtop instrument (such as spectrophotometric devices, chemistry test strips), viscoelastic coagulation analyzers[7] (such as bleeding time testing) and continuous testing device[8] (such as Free Style Libre from Abbott Diabetes Care).

An important factor to be considered for widespread use of POCT devices was developed by the WHO. This ASSURED (Affordable, Sensitive, Specific, User-friendly, Rapid and robust, Equipment-free and Deliverable to end-users) criteria provided by World Health Organization (WHO) can be used to identify the most appropriate POCT for the resource-limited areas .[9] In addition, WHO also provided six steps for selecting an appropriate in vitro diagnostic test[10], which is shown in **Table 1.2**.

Table 1.2 *Six steps in selecting an appropriate diagnostic test. Table is taken from publisher with permission.*[11]

Step 1	Define the purpose of the test
Step 2	Review the market and check each product's specification

Step 3	Review the test's regulatory approval
Step 4	Obtain data on the diagnostic accuracy of the test under ideal conditions
Step 5	Obtain data on the diagnostic accuracy of the test in clinical practice
Step 6	Monitor the test's performance in routine use

1.2 Biosensor Technology

There are several techniques used to develop POC diagnostics. Given below are some of the techniques used for analyte sensing. These examples are not meant to be a comprehensive review but are chosen to give the reader a broad view of the technologies could be used to develop POCTs.

1.2.1 Electrochemical sensor

Electrochemical sensor is based on transducing biochemical reactions to electrical signals.[11] Normally, the sensor consists three electrodes: reference electrode, working electrode and counter electrode. A reference electrode commonly made from silver metal coated with silver chloride (Ag/AgCl) or saturated calomel electrode (SCE); a working electrode consists conductive materials, such as gold, carbon and platinum; a counter electrode connects the electrolytic solution to apply the current to the working electrode.[5] While a two electrode system only need working electrode and reference electrode. The signal comes from the electron exchange between chemical component and the electrode. There are mainly three types of electrochemical sensors: amperometric sensor, potentiometric sensor and conductometric sensor.

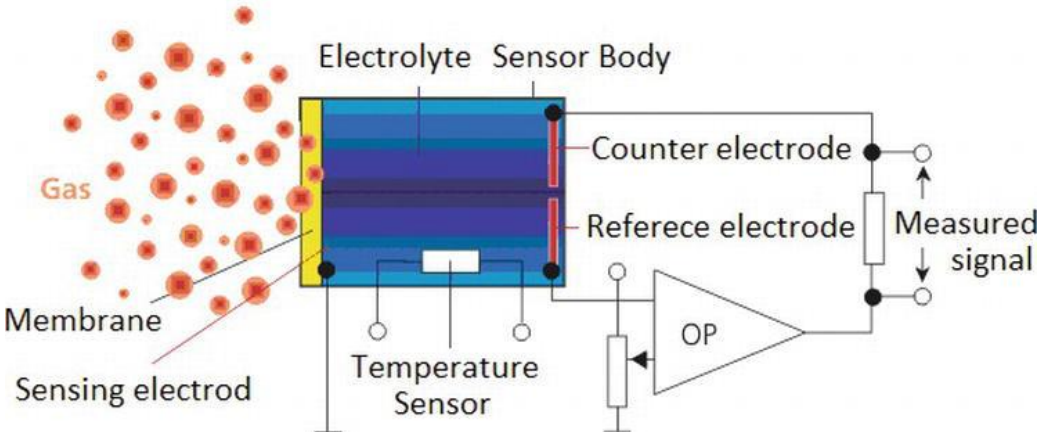

Figure 1.1 *The principle of electrochemical sensor. Figure is taken from publisher with permission.*[12]

Amperometric sensor continuously measures the current generated by the electrochemical oxidation or reduction at a given potential which is maintained at the working electrode as regards a reference electrode.[13] The measured current is proportional to the analyte concentration. The fixed potential in the detection leading to a negligible current needed to apply the potential to the system, minimizing the background signal, which makes it excellent sensitivity. This technique is applied in glucose meter to measure blood glucose and oxygen electrode is applied. Potentiometric sensor measures the potential change at the working electrode in respect with the reference electrode when no significant current between them.[14] The main types of potentiometric transducer electrodes are: transmembrane potential (Based on the accumulation of a potential from a sensor membrane), electrode potential (Based on a potential from the electrode, similar to transmembrane potential) and field effect transistor (FET). Conductometric sensor measures the change of electric conductivity from chemical reaction at stable voltage.[15]

Table 1.3 *Different types of electrochemical sensor.*

Electrochemical sensor type	**Principle**
Amperometric sensor	Oxidation / reduction

Potentiometric sensor	Electric potential
Conductometric sensor	Electric conductivity

1.2.2 Optical Sensor

Optical biosensor measures the interactions of analytes based on the measurement of photons in the process. The detection involving the measurement of fluorescence, reflection, absorbance, Förster Resonant Energy Transfer (FRET) and refractive index. Most commonly used optical techniques including fluorescence, absorbance, luminescence. They are widely used in the immunoassay, whereas they require the use of appropriately labeled substances. The label-free optical surface techniques are barely used in POC, although they have excellent analytical sensitivity. For example, surface plasmon resonance (SPR) is a label-free, quantum-physical phenomenon-based sensor.[16] It takes advantage of total reflection between two mediums, causing the formation of evanescent waves, which results in the excitation of electron on the gold and form plasmon resonance. When the analytes binding with the immobilized ligand, the refractive index changes leading to the change of signal.

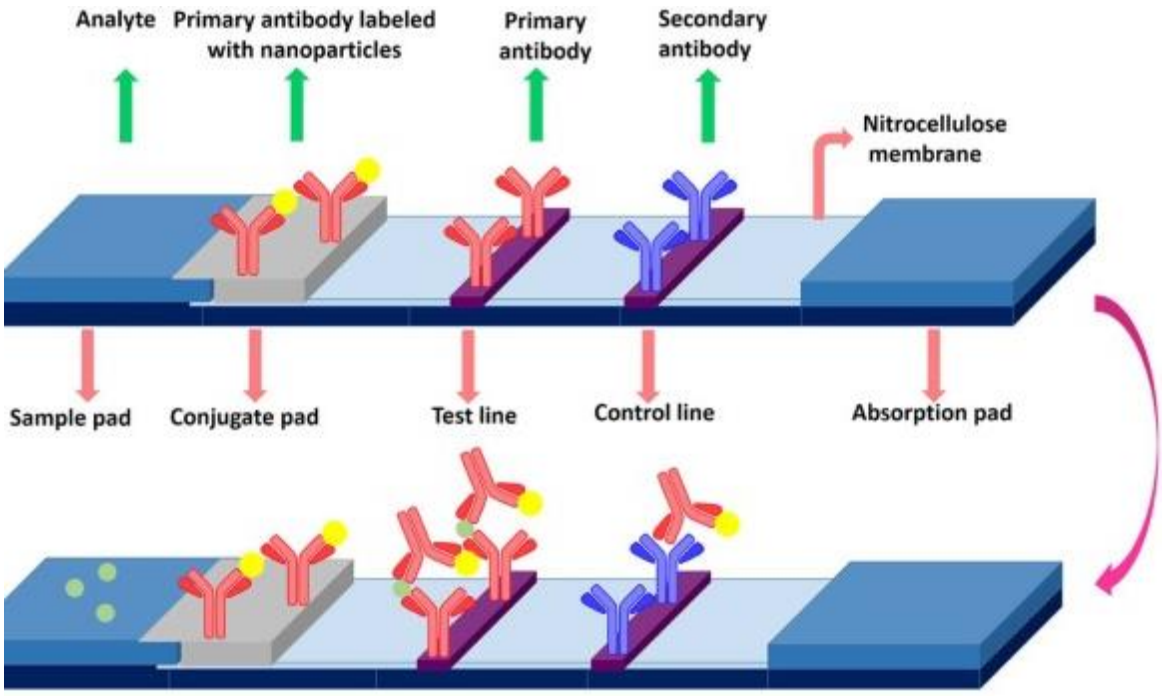

Figure 1.2 *The principle of lateral flow assay. Figure is taken from publisher with permission.*[17]

1.2.3 Microgravimetry sensor

Microgravimetry biosensor is mass sensitive sensor, which can be classified into three types according to the signal transduction methods: Quartz crystal microbalance, surface acoustic wave-based systems and microcantilevers.[18] In the quartz crystal microbalance method, the surface of crystal is covered with a thin gold in its resonant frequency by changing voltage. The signal resonant frequency is proportional to the mass of chemicals on the surface. In the surface acoustic wave system, the surface wave is excited electrically by interdigital transducers. The acoustic waves are restricted on the surface and decay as far away from the surface. Microcantilever measures the changes of cantilever bending or vibrational frequency. When a specific mass of material is absorbed on the surface, the bending will change.[19]

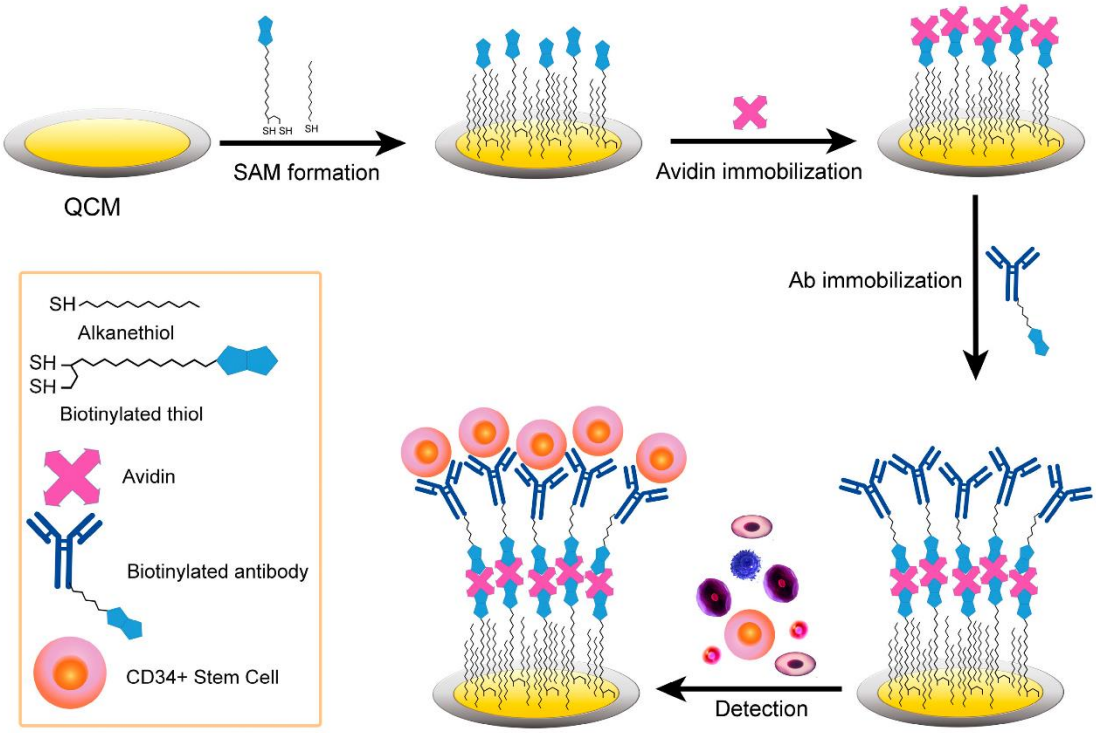

Figure 1.3 *The principle of Quartz crystal microbalance immunosensor. Figure is taken from publisher with permission.*[20]

1.3 POCT Application

1.3.1 Patient self-monitoring

Blood glucose meter is one of the most commonly used self-monitoring device. About 90% of blood glucose test is to monitor the glucose level of diabetes and modify the medication for the patients. The first blood glucose meter and glucose self-monitoring system were developed by Anton H. Chemens. Now glucose meter has been widely used in identifying hypoglycemia and hyperglycemia. The measurement of glucose is based enzymatic assay reaction.[3] On the glucose meter strips, glucose is oxidized to gluconic acid by glucose oxidase in the presence of water and oxygen. The enzyme cofactor flavin adenine dinucleotide (FAD) receives the first electron and is reduced to FADH. Followed by FADH is oxidized by oxygen and form H_2O_2, the electron transfer can be measured by electrochemical methods. The mechanism was shown in **Figure 1.4**.

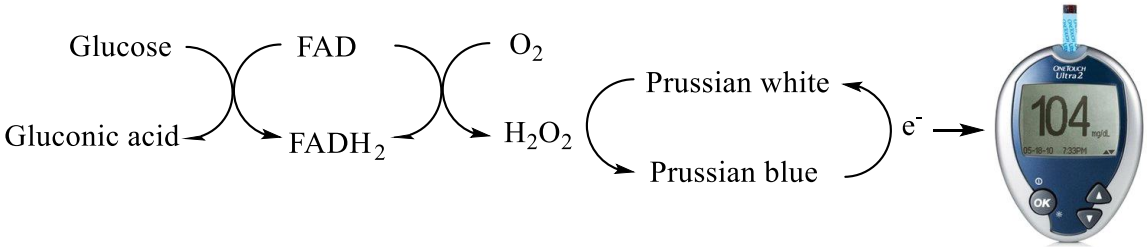

Figure 1.4 *The mechanism of glucose meter. Figure is taken from publisher with permission.*[21]

International Normalized Ratio (INR) was introduced by WHO in 1983 to measure the anticoagulation treatment with vitamin K antagonist. The prothrombin time was measured and converted to INR based on the thromboplastin in the test. The value of 1.0 in INR is for normal coagulation individuals not on medication. When patients are treated with vitamin K antagonists, the value increases, which ranges from 2 to 3.

1.3.2 Emergency care

Preclinical rescue systems include emergency ambulances and vehicles staffed by clinicians. The responsibility of emergency clinician is to restore and stabilize the vital functions of the patient. POCT can do initial diagnosis and is helpful for quick and efficient treatment decision. The applications of POCT in emergency department include measure acid-base status, blood gases, CO oximetry, electrolytes, metabolites, cardiac markers.

Table 1.4 *Mean analytical performance of common methods for POCT. Table is taken from publisher with permission.*[22]

Analytes	**Analytical performance**
Blood gas and electrolytes	Optimal
Cardiac markers	Variable
Basic biochemistry	Acceptable
Inflammation markers	Acceptable

Complete blood count	Acceptable
Coagulation	Acceptable
Pregnancy test	Acceptable
Urinalysis	Acceptable
Infection, molecular	Acceptable
Serology	Acceptable
Drugs of abuse	Limited
Toxicology	Limited

1.3.3 Physician's practice

POCT is mainly used in smaller hospital, where a 24-hour laboratory service is not available. The reasons to apply POCT in hospital are the waiting time from the central laboratory is normally too long; in the hospital without central laboratory, the detection can be carried out with POCT. Some examples of POCT in the physician practice was listed in **Table 1.4**.

Table 1.5 *Examples of POCT in the physician practice setting. Table is taken from publisher with premission.*[4]

Urologist	Prostate-specific antigen for cancer screening
Gynecologist	Human chorionic gonadotropin for pregnancy testing
Cardiologist	Brain natriuretic peptide for monitoring the clinical course in patients with heart failure
Oncologist	Blood count prior to chemotherapy
Sports physician	Lactate as performance check
General practitioner	INR for monitoring anticoagulation
Diabetologist	Blood sugar and HbA_{1c} for monitoring the clinical course of blood glucose control
Pediatrician	Rapid streptococcal detection test prior to antibiotic therapy
Nephrologist	Albumin as microalbuminuria screening in diabetic nephropathy
Psychiatrist	Drug screening during therapy for withdrawal

1.4 Summary

Described in the previous section is a snapshot of some of the techniques used in POCTs. The goal in our research group is to develop POC assay to detect biological relevant analytes. I was involved in three of those projects: development of POC assay to detect influenza, norovirus and inflammatory bowel disease.

To detect influenza, we have synthesized fluorescent sialic acid derivatives that are cleaved by influenza neuraminidases (NAs) and not by *S. pneumoniae*. We have also attempted to develop assays that could differentiate between influenza viruses and *S. pneumoniae* by taking advantage of the structural differences between NAs from these pathogens. we can perform this assay with handheld fluorometer. Handheld fluorometer is a small, lightweight and highly durable equipment, which is ideal for POC measurement. Upon cleaving of the substrate by influenza, the fluorophore can be released and detected by handheld fluorometer in seconds. This allows patients self-test at home or in low resource settings.

In the second project, we present our efforts to identify and develop biomarkers for Inflammatory bowel disease (IBD). Here, we explore the use of alternate biomarkers, MMP-9 and TNF-α, that can increase in inflammatory conditions. We explored the correlation between MMP-9, TNF-α levels and severity of colitis in IL10-/- mouse model, with a view to design an effective POCT for human IBD, since IL10-/- mouse model has similar condition with human IBD. We also present our initial studies to detect and monitor these biomarkers using a novel mesoporous silica bead-based method, which can be used for POCT.

In the third project, we targeted human noroviruses in an effort to develop assays that could detect noroviruses at POC. We studied the interactions between norovirus virus like particles

(VLPs) and chemically synthesized HBGAs by surface plasmon resonance (SPR) with the goal being able to use some of these carbohydrates as recognition molecules in diagnostics to capture norovirus. We found that the interactions between HBGA and VLPs are complex and highly dependent on the structure of the VLP and the carbohydrate. It can be applied to FilmArray™ Gastrointestinal (GI) Panel quick test. Different types of HBGAs can be attached on the bottom of array, when the norovirus flow through the array, it can be captured by HBGAs. According to the binding pattern results, different genotypes of norovirus can be identified.

2 CHAPTER 2 FLUORESCENT SIALIC DERIVATIVES FOR THE SPECIFIC DETECTION OF INFLUENZA VIRUSES

* Most of the work described in this chapter has been published in the publication:

Dandan Liu, Xikai Cui, Abasaheb N. Dhawane, Vasanta Chivukula, Suri S. Iyer*. Fluorescent Sialic Derivatives for the Specific Detection of Influenza Viruses. *Bioorganic & Medicinal Chemistry Letters*, **2019,** 29 (24), 126773.

2.1 Influenza Introduction

2.1.1 Influenza epidemiology

Influenza is a respiratory infection caused by influenza virus, which is highly contagious and spread through respiratory droplets. Influenza outbreaks lead to millions of deaths and hospitalizations. The first pandemic influenza was reported from Russian in May 1889.[23] At first it spreads slowly, then it began to spread in lighting speed in October 1889. Till spring 1890, it spread through the whole world. It killed 1 million of people worldwide.[23] Around 30 years later, another pandemic influenza appeared in 1918 (Spanish flu) which was caused by influenza H1N1. It spread very fast, leading to estimated 50-100 million deaths.[24] Most deaths in this pandemic were caused by secondary bacterial pneumonias, which lagged by approximately 7-10 days after influenza.[25] After around another 30 years, a new pandemic H2N2 influenza outbreak in Guizhou, China, leading to estimated 1.1 million deaths worldwide, which is known as Asian flu.[26] Most of the deaths are influenza and pneumonia related. In a decade, pandemic influenza happened again in Hongkong in 1968.[27] This pandemic was caused by H3N2 influenza, which is believed to rise from H2N2 through a process antigenic shift, in which hemagglutinin antigen on the influenza

went through a genic mutation to H3 antigen. Although fewer deaths in this Hongkong flu, H3N2 is very contagious and still considered as seasonal flu.[28] There's no pandemic influenza after a long time until 2009, which was caused by swine-origin H1N1 flu, very different from HIN1 from 1918. Less people (estimated 18,500 – 150,000) were killed by swine flu due to the flu vaccine.[29] Although pandemic influenza doesn't occur every year, seasonal flu typically peaks between December and February each year and kills around 291,000-646,000 people worldwide.[29]

2.1.2 Influenza life cycle

There are three transmembrane proteins on the surface of influenza virus: haemagglutinin (HA), neuraminidase (NA) and matrix 2 (M2).[30] When influenza virus infects host cell, the HA on the surface will recognize the terminal sialic acid of glycoconjugates on the surface of host cell and enter the cell by endocytosis. It has low pH around 5 to 6 in the endosome, which triggers the fusion of virus.[31] The acidic environment also opens M2 ion channel to acidify the viral core to release viral ribonucleoprotein (vRNP), hence the vRNP can be free to enter the cytoplasm of the host cell.[32]

The influenza virus contains negative sense viral RNA.[33] After the vRNP enters the nucleus, it can transcribe into mRNA and translate to make viral proteins, also it can be replicated to make more vRNP. Then the viral proteins and vRNP assembly to make viral progeny.[32] The progeny will be budding to exit to the cell and the NA will cleave the sialic acid residues to release the newly formed viral particles. These particles will continue to infect the other cells. (**Figure 2.1**)

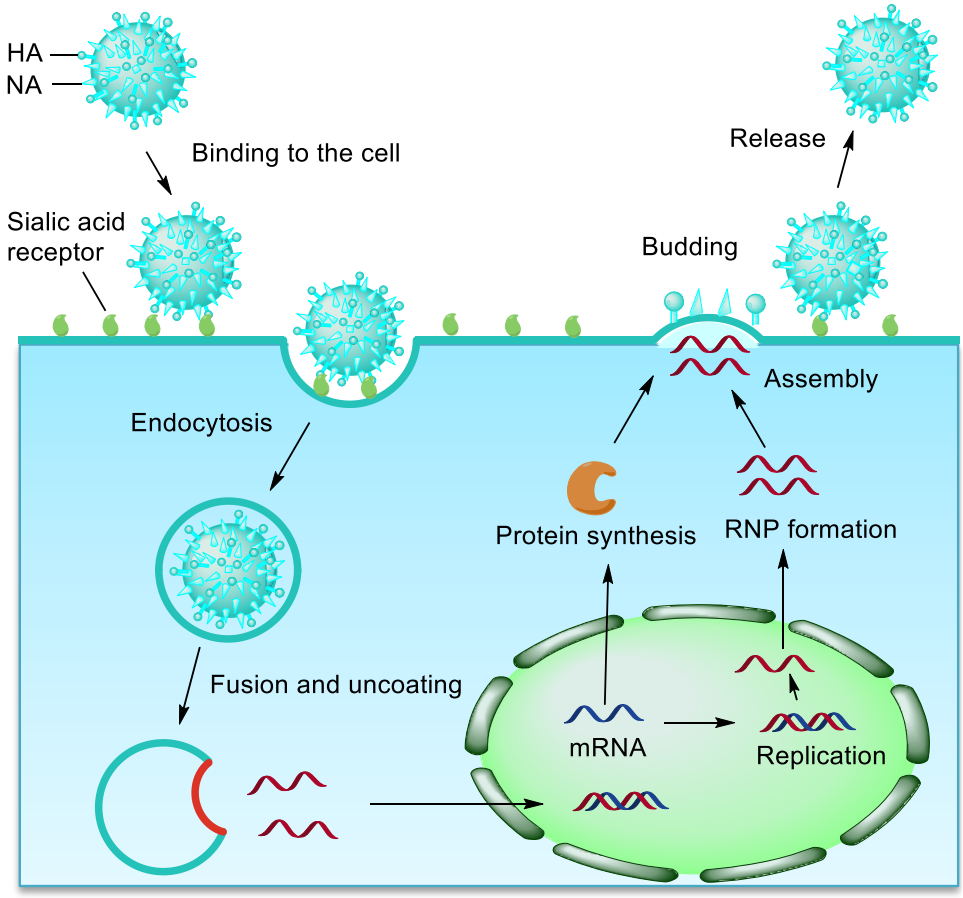

Figure 2.1 *Life cycle of influenza virus. Figure is modified from journal with permission.*[34]

2.1.3 Influenza proteins

In the process of influenza infection, there are two proteins, haemagglutinin (HA) and neuraminidase (NA), play important roles and they are also important biomarkers to detect and treat influenza infection.

HA

HA is a homotrimer that can bind to sialic acid receptor on the surface of host cell and mediates the release of influenza vRNP to cytoplasm.[33] HA processor is made of two subunits: HA1 and HA2, they are connected by disulfide bond.[35] HA1 contains sialic acid receptor domain, which allows the virus to enter the host cells by endocytosis. HA2 contains fusion peptide which

can attach to the endosomal membrane to promote the releasing of vRNP to cell cytoplasm.[36] There are two major binding between sialic acid and glycoproteins: α (2,3) linkage and α (2,6) linkage.[37] They are very important for the specificity of HA binding to sialic acid receptor. Influenza virus from human only recognizes α (2,6) linkage, influenza from avian only recognizes α (2,3) linkage, influenza from swine recognizes both.[37] That explains why swine influenza is more contagious and harmful.

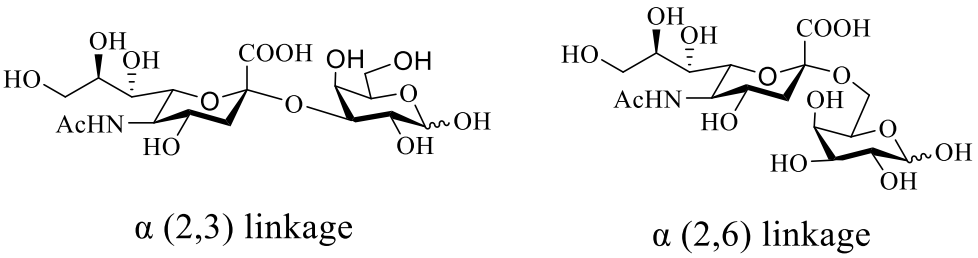

Figure 2.2 *α (2,3) linkage and α (2,6) linkage of sialic acid.*

When HA binding to the sialic acid unit on the host cell, a receptor-mediated endocytosis process helps the virus get into the host cell. The pH (5~6) of the endosome will trigger the fusion process and induce the conformational changes in HA0 to expose the HA2 fusion domain. The HA2 is released to the endosomal membrane and helps the endosomal membrane contact with the viral.[38] The low pH environment of the endosome is important to induce the HA0 conformation changing to expose the HA2 fusion peptide. Another biological process is also triggered by the low pH environment of the endosome, the M2 ion channel on the surface of the virus opens up in low pH environment. This process will acidify the virus core and help the release of the vRNP from M1, which is the M1 part of the ion channel. Consequently, the vRNP is free to enter to the cytoplasm of the host cell.[39]

NA

Influenza NA is a homo tetramer, which consists four identical subunits (**Figure 2.3**).[40] There are usually 50~100 copies of NA on virus surface. NA is essential for the influenza virus leaving the host cell by catalyzing hydrolysis of both α (2,3) and α (2,6) linkages of glycosidic bonds.[40] NA is an exoglycohydrolase which hydrolyzes terminal sialic acid residues from glycoproteins and glycoconjugates.[41] Cleavage of terminal sialo side initiate with the binding to the active sites of NA. After binding, the stable chair conformation is forced into a less stable boat conformation due to the highly conserved triarginyl cluster (Arg-118, Arg-292, and Arg-371). Conformational changes facilitate the leaving group falling down and form an oxocarbocation ion intermediate, a sialosyl cation. The sialosyl cation undergoes a nucleophilic attack to form a glycosyl-enzyme intermediate. The glycosyl-enzyme intermediate breaks to generate a sialosyl cation again, where it undergoes nucleophilic attack by a water molecule to form an α-Neu5aAc as the initial product. The α-Neu5Ac product is further isomerize into β-Neu5Ac, the more thermodynamically favored product.[41]

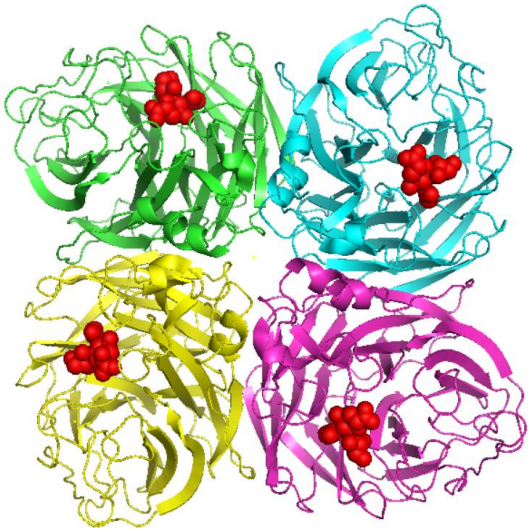

Figure 2.3 *3D dimension of influenza NA binding with sialic acid. The structure was downloaded from NIH PDB database (PDB: 1NNA).[40] Different monomers were shown in green, cyan, purple and yellow colors, sialic acid molecule was shown in red sphere.*

2.1.4 Influenza therapeutics

Several FDA-approved anti-influenza antivirals have been used for influenza treatment. These drugs can be divided into three groups: the M2 ion channel blockers, the neuraminidase inhibitors (NAIs) and the virus polymerase inhibitors.[34, 42] In recent years, influenza virus has developed high assistance to some of the drugs, hence some of them are no longer used.

M2 ion channel blockers

M2 ion channel is a single-pass membrane protein, which is important in the process of unpacking viral genome into cell.[43] The adamantane-based anti-influenza drugs amantadine and rimantadine (**Figure 2.4**) target the M2 ion channel to block it, that have been used as first choice antiviral drugs for influenza A virus.[44] However, influenza A H3N2 and H1N1 are highly resistant to these drugs.[45] The center for disease control and prevention (CDC) does not recommend these antiviral drugs to treat influenza anymore.

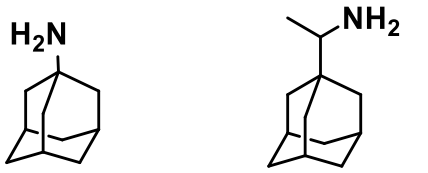

Amantadine Rimantadine

Figure 2.4 *The structure of amantadine and rimantadine.*

NAIs

NAIs target neuraminidase and prevent its cleavage, therefore inhibiting the release of viral progeny.[46] FDA approved NAIs include oseltamivir, zanamivir, peramivir and laninamivir, they are sialic acid analogues, that can specifically bind to neuraminidase enzyme active site.[42, 47]

Oseltamivir (**Figure 2.5A**) and zanamivir (**Figure 2.5B**) are globally available. Oseltamivir is a prodrug of oseltamivir carboxylate, a potent inhibitor for neuraminidase of influenza A and B. Oseltamivir is the first approved NAI drug, the bioavailability of its active

metabolite is around 80%.[48] Zanamivir is approved for inhalation delivery with intravenous administration due to its low oral bioavailability. Intravenous zanamivir can be used for seriously ill patients with influenza, especially those patients resist to oseltamivir.[49] Peramivir (**Figure 2.5C**) is approved in China, Japan, South Korea, and the United States. It also has low bioavailability and is therefore delivered intravenously. Peramivir-treated patients have rapid and greater reduction of influenza A and B viral titers than oseltamivir in the first 48 hours.[50] Antiviral resistance to zanamivir, oseltamivir and peramivir is very low for current influenza strains.[42]

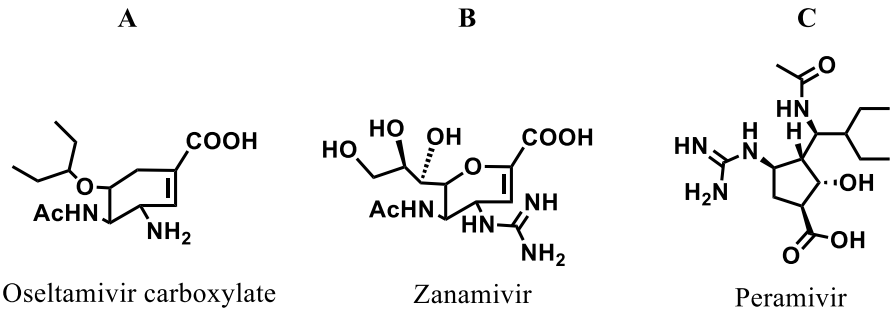

Figure 2.5 *The structure of oseltamivir carboxylate, zanamivir and peramivir.*

Laninamivir octanoate (**Figure 2.6**) was approved in Japan in 2010 to treat influenza A and B. It is prodrug, which converts to its active form laninamivir in lung. Laninamivir octanoate performs as inhalation delivery, with long-lasting action (Half-life of as long as 41.4 hours), displays antiviral effect for treatment of oseltamivir-resistant H275Y-mutated virus.[47]

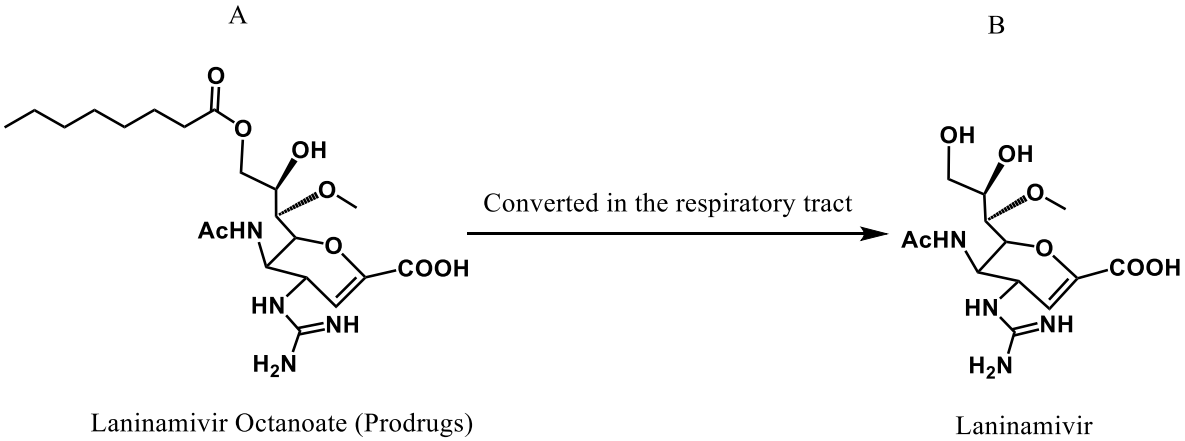

Figure 2.6 *Prodrug laninamivir octanoate (A) and its active form laninamivir (B).*

2.1.5 Influenza diagnostics

Diagnostic tests for influenza basically include viral culture, molecular assays and antigen detection assays.[51, 52] Molecular assays include rapid molecular assays, reverse transcription polymerase chain reaction (RT-PCR and other nucleic acid amplification assays). Antigen detection assays include rapid influenza test and immunofluorescence assays.

Viral culture

Viral culture test, original from 1940s, is highly sensitive and selective, and it is one of the gold standard method to detect influenza.[53] This method uses infectious samples to inoculate with permissive cell lines or embryonated eggs, propagation for 7 - 10 days to monitor development of cytopathic effect, then confirm influenza infection with staining, immunofluorescence microscopy or erythrocytes hemadsorption.[54] Influenza virus isolation using this approach is usually performed on two types of cell lines: first, established cell lines, such as Madin Darby canine kidney (MDCK), A549, mink lung epithelial cell line (Mv1Lu), rhesus monkey kidney (LLC MK2), and buffalo green monkey kidney (BGMK); second, primary cell lines, such as rhesus monkey kidney (RhMK) or African green monkey kidney (AGMK).[55] This assay has high specificity and requires well-trained personnel and takes long time to perform.[56]

Molecular assays

Molecular assays include RT-PCR and other nucleic acid amplification assays. RT-PCR can identify influenza viral RNA in respiratory specimens. It is believed to be most powerful nucleic acid-based test (NAT) approach to detect influenza.[55] Other nucleic acid amplification assays include ligase chain reaction, sequencing-based tests and loop-mediated isothermal amplification-based assay (LAMP), *etc*.[57-59] The basic procedure for RT-PCR includes extraction

of RNA from specimens and reverse transcript viral RNA to single-stranded complementary DNA (cDNA) using enzyme reverse transcriptase, and product amplification with fluorescent detection.[60] This method is highly sensitive and selective, while it takes few hours and it is the most expensive test, also it requires well-trained personnel.[60]

Antigen detection assays

Antigen detection assays include rapid influenza tests (RIDTs) and immunofluorescent assays. RIDTs are antigen-based tests developed to rapid diagnose influenza in around 15 min.[52] Several FDA-approved RIDTs are available, such as: BD Directigen EZ Flu A+B test (Becton Dickinson), BinaxNOW Influenza A&B (Inverness Medical), and QuickVue Influenza A+B Test (Quidel), but none of these can differentiate different A subtypes.[52, 61] Immunofluorescent assays detect antigen with fluorescence, which takes around 1 hour.[51] And it cannot distinguish different A subtype either. These assays have high selectivity and medium sensitivity.[62]

Summary

All these tests above are expensive and none of them can measure drug susceptibility rapidly in a POC setting. The lack of good rapid diagnostic tests leads to asymptomatic treatment and overuse of drugs, which increases drug resistance.[63] Additionally, the initial infection caused by the virus often leads to secondary infection caused by bacterial pathogens.[64] It is very important for a physician to ascertain if the infection is viral or bacterial, because the treatment is different. For influenza infections, antiviral drugs like Tamiflu or Relenza are prescribed;[65] in contrast, for bacteria, antibiotics such as Azithromycin Zpak, is prescribed.[66] Secondary infections can increase burden, for example, infections caused by Streptococcus pneumoniae, can lead to otitis media, especially in immunocompromised people and children five years old or younger.[67] It takes 1–4 days for symptoms of influenza related sickness to appear after exposure to the virus. The time

when secondary infection due to S. pneumoniae or other bacteria occurs is not very clear, as the interplay between viral, bacterial and the host immune system is complex[68] and to compound the issue further, overall morphological symptoms due to viral/bacteria are quite similar. Thus, by the time the patient enters the clinic, it is unclear if the patient is suffering from viral, bacterial or coinfections. Therefore, differentiate between influenza and secondary bacterial infection is important.

We recently developed an electrochemical assay to detect enzymes using a repurposed glucose meter. Briefly, we developed substrates bearing a glucose molecule and expose it to samples containing the enzyme.[69] If enzyme is present and is active, glucose is released, which can be quantified using a glucose meter and correlated to the activity of the enzyme. Our first target was influenza virus; we synthesized sialic acid bearing molecules that release glucose.[69] These molecules, when exposed to NA (or sialidase) from any source resulted in release of glucose, which was detected using a glucose meter. In further iterations, we demonstrated that molecules like galactose[70] and paracetamol[71] can also be detected using glucose meters; and we synthesized sialic acid derivatives that were highly specific for influenza viruses. Similar biochemiluminescent molecules, when exposed to influenza or *S. pneumoniae*, were cleaved only by influenza viral strains with high specificity.[72] By using a combination of natural and modified sialic acid derivatives, we could differentiate between influenza and *S. pneumoniae*.[70] While electrochemical detection using repurposed glucometers are very valuable in diagnostics, fluorescence based detection of pathogens cannot be understated, especially when it is integrated with smartphones.[73] Here, we report a fluorescence based assay that could lead to the accurate detection of influenza virus by exploiting structural differences between NAs from influenza and *S. pneumoniae*.

2.2 Experiment Design

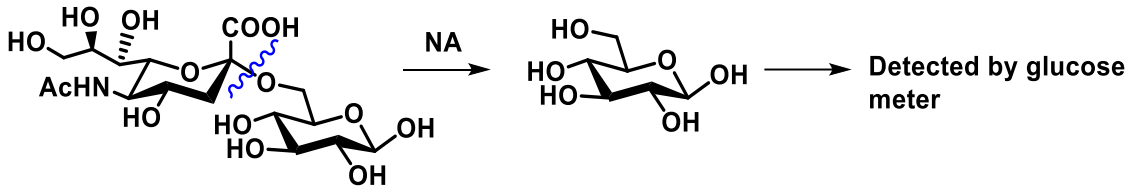

Figure 2.7 *Electrochemical assay to detect enzymes using glucose meter. Figure is taken from publisher with permission.*[74]

Previously, we have developed electrochemical assay to detect NA using a repurposed glucose meter (**Figure 2.7**). Briefly, we developed a substrate bearing a glucose molecule, which can be cleaved by NA and release glucose that can be detected by glucose meter.[69] By using a combination of natural and modified sialic acid derivatives, we could differentiate between influenza and *S. pneumoniae*.[70] Electrochemical assay plays an important role in POC diagnostics, while the fluorescent assay can't be understated. Here we report a fluorescent assay to detect influenza accurately by exploiting the structure difference between influenza NA and *S. pneumoniae* NA.[74]

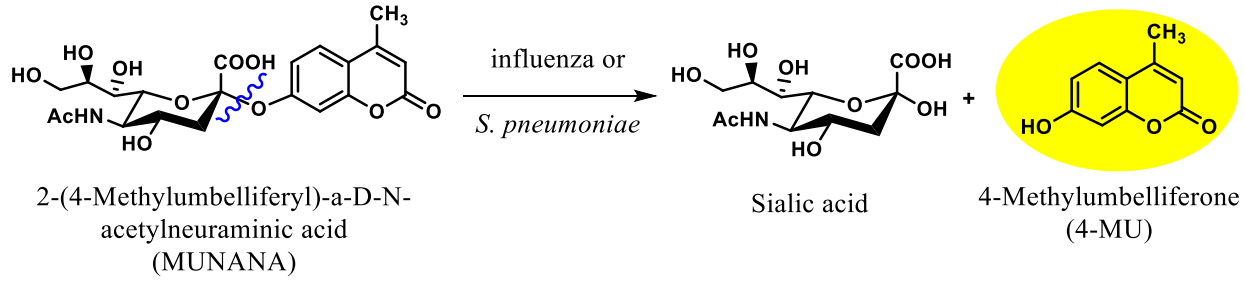

Figure 2.8 *Sialic acid derivatives for influenza and S. pneumoniae. When the substrate MUNANA is cleaved by influenza or S. pneumoniae, 4-MU is released and detected at 360/460 nm. The substrate MUNANA (4,7 OMe) only can be cleaved by influenza and release 4-MU. Figure is taken from publisher with permission.*[74]

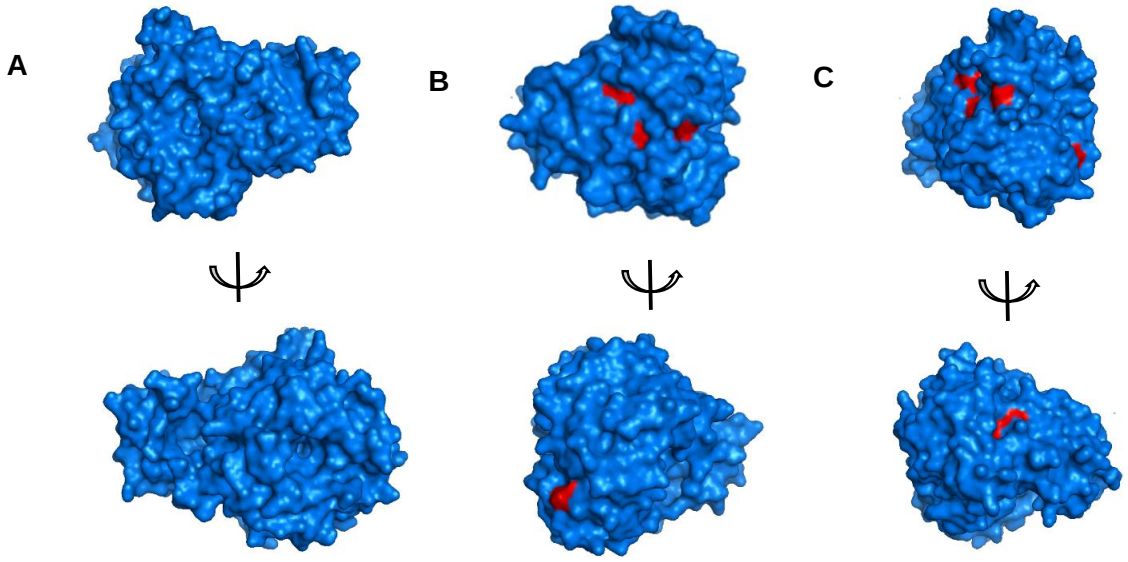

Figure 2.9 *The disulfide bonds in NA monomer from S. pneumoniae and influenza virus. The disulfide bonds in NA monomer from S. pneumoniae and influenza virus. The structures are downloaded from NIH PDB database. The surface is showed in blue color, the disulfide bond is showed in red color. A. The structure of S. pneumoniae Nan A monomer (PDB: 2ya5) which shows no disulfide bond. B. The structure of H1N1 NA monomer (PDB: 3ti6) which shows eight disulfide bonds, four of them are buried inside, the other four are exposed on the surface. C. The structure of H3N2 NA monomer (PDB: 4gzp) which shows nine disulfide bonds, four of them are buried inside, the other five are exposed on the surface. Figure is taken from publisher with permission.*[74]

2′-(4-methylumbelliferyl)-α-D-N-acetylneuraminic acid (MUNANA) and synthetic sialic acid derivative substrate, MUNANA (4,7 OMe), were used to detect influenza and *S. pneumoniae*.

Because the binding pocket of influenza NA is considerably larger than *S. pneumoniae* NA, especially in 4 and 7 positions. Therefore, we synthesized a fluorescent sialic acid derivative bearing OMe groups at the 4 and 7 positions. The natural substrate MUNANA (**Figure 2.8**) and sialic acid derivative, MUNANA (4,7 OMe) (**Figure 2.8**) were exposed to different influenza virus strains and *S. pneumoniae* and the fluorescence was recorded for 2 hours. Next, we attempted to destroy the activity of influenza with high pH since it's reported high pH can reduce the activity of influenza. Also, we used dithiothreitol (DTT) to break the disulfide bonds in influenza NA. Because there are several disulfide bonds in influenza NA, four of them are exposed on the surface (**Figure 2.9 B and C**). When the bond was broken, the structure of influenza NA can be destroyed, results in the minimal or no activity of influenza NA. While *S. pneumoniae* NA doesn't contain any disulfide bond (**Figure 2.9 A**), whose activity will have negligible change.

2.3 Results and Discussions

The X-ray crystal structure shows that influenza NA has a larger binding pocket than *S. pneumoniae* NA. (**Figure 2.10**) Although both influenza and *S. pneumoniae* NA can cleave natural substrate MUNANA, the MUNANA (4,7 OMe) bearing OMe group at 4 and 7 positions can only cleaved by influenza NA. To his end, MUNANA (4,7 OMe) was synthesized as **Scheme 2.1**.

A

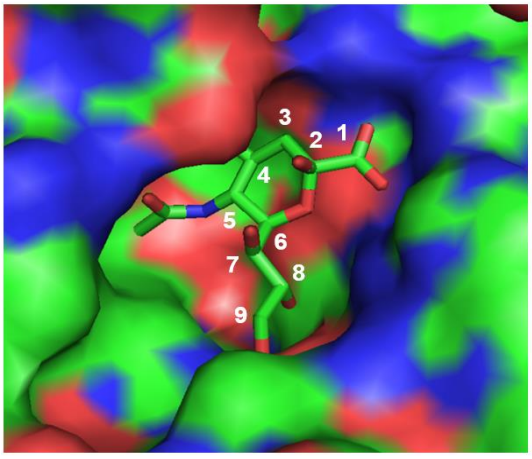

B

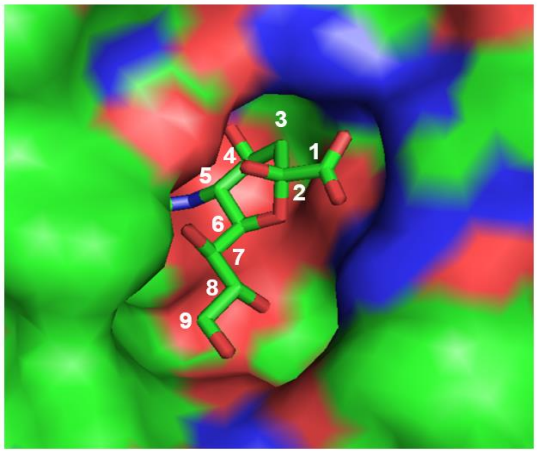

Figure 2.10 *The binding pocket of NA complexed with sialic acid downloaded from NIH PDB database and PyMOL was used to show the surface and binding pocket. The binding pocket of NA complexed with sialic acid downloaded from NIH PDB database and PyMOL was used to show the surface and binding pocket. The carbon atom was showed in green color, the oxygen atom element was showed in red color, the nitrogen atom was showed in blue color. A. The binding pocket of influenza NA (PDB: 4gzq). B. The binding pocket of S. pneumoniae NA (PDB: 3h72). Which shows the binding pocket of influenza NA is larger than S. pneumoniae NA. Figure is taken from publisher with permission.*[74]

Briefly, we introduced the methoxy groups to the 4 and 7 positions of protected sialic acid before coupling to 4-Methylumbelliferone sodium salt acceptor. The known compound, **2-1**, is reacted with 4-methylumbelliferone sodium salt to yield compound **2-3** in high yield. The α linkage was confirmed by the H_{3eq} peak at 2.8 ppm in the 1H NMR spectroscopy. Deprotection of the acetate and ester groups resulted in the desired compound MUNANA (4,7 OMe), which was characterized extensively by NMR and mass spectroscopies.

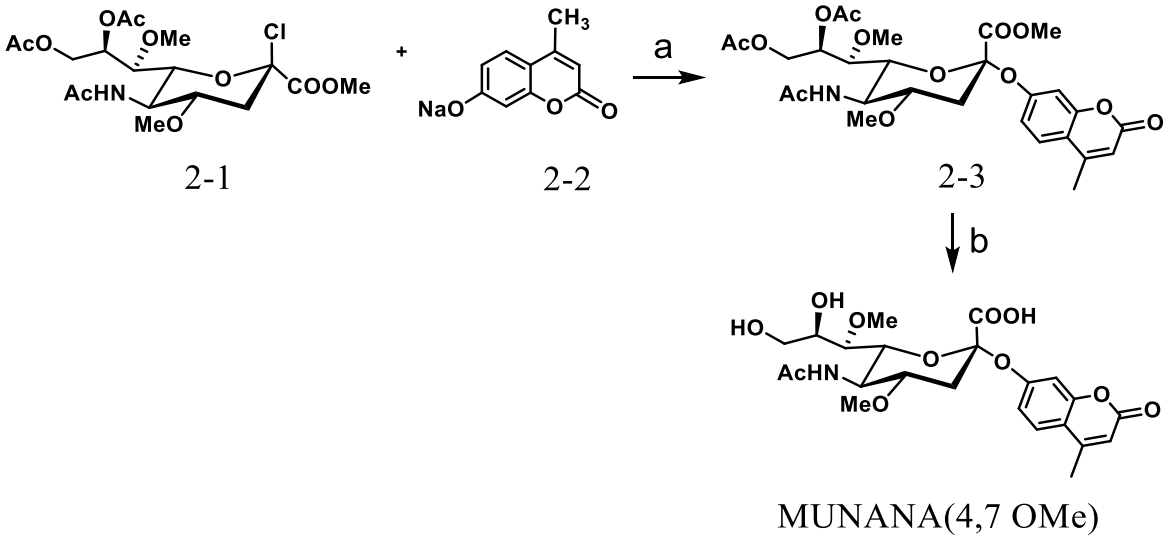

Scheme 2.1 *Reagents and conditions:* a) EtOAc, TBAHS, Na_2CO_3, RT, 16 h, 60%; b) i) NaOMe, MeOH, RT, 30 min; ii) 0.05 M NaOH in H_2O, RT, 2 h, 84% yield after two steps. *Scheme is taken from publisher with permission.*[74]

Next, we tested the enzyme activities of influenza NA and *S. pneumoniae* NA cleaving natural substrate MUNANA in different pH. Inactivated A/Aichi/2/1968 H3N2 (sample AC), A/Winsconsin/15/2009 H3N2 (sample WS), A/Netherlands/2629/2009 H1N1 (sample NL), *S. pneumoniae* B (sample SB) were used for the experiment. The result was shown in **Figure 2.11**. Both influenza and *S. pneumoniae* can cleave MUNANA in different pH. Although higher pH can decrease the activity of influenza, it can't destroy its activity. However, when modified sialic acid derivative MUNANA (4,7 OMe) was used, only influenza can cleave it (**Figure 2.12**), which demonstrates the high specificity of MUNANA (4,7 OMe) to influenza. Our results are similar to previous reports that introduction of larger groups at the 4 and 7 positions of sialic acid make the compounds highly specific towards influenza virus. Next, we attempted to identify conditions where fluorescence would be realized upon exposure to *S. pneumoniae* and not influenza. Because activity of all NAs decreased at higher pH, NAs from these influenza viral strains still retain their activity. Therefore, we can't use this condition to differentiate influenza and *S. pneumoniae*.

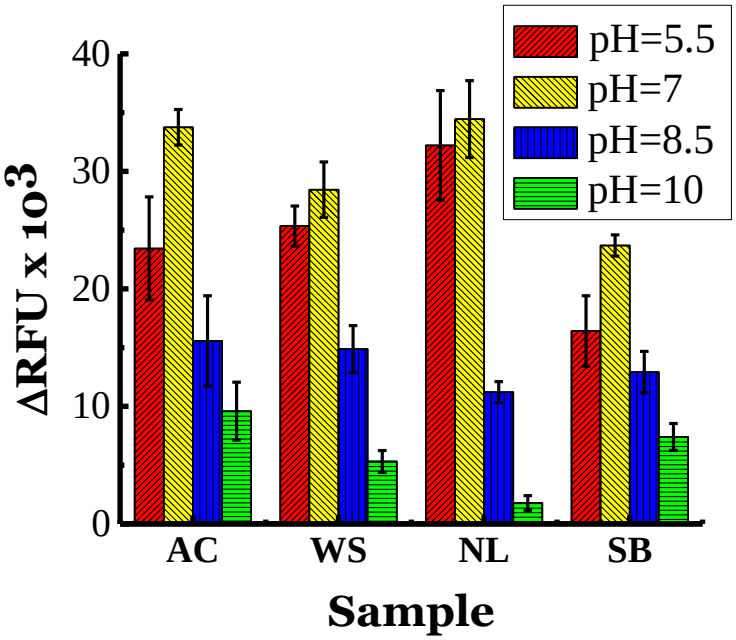

Figure 2.11 *Detection of influenza and S. pneumoniae with natural substrate MUNANA. Sample AC, WS, NL and SB were incubated with different buffers (pH = 5.5, pH =7, pH = 8.5, pH = 10) for 30 min. Then MUNANA was added, the fluorescence intensity was detected at 37℃, 360 nm/460 nm for 2 h. Then 1 M, 100 µL tris solution was added, fluorescence intensity was detected*

at 37ºC, 360 nm/460 nm for 10 min. All experiments were performed in triplicate. Figure is taken from publisher with permission.[74]

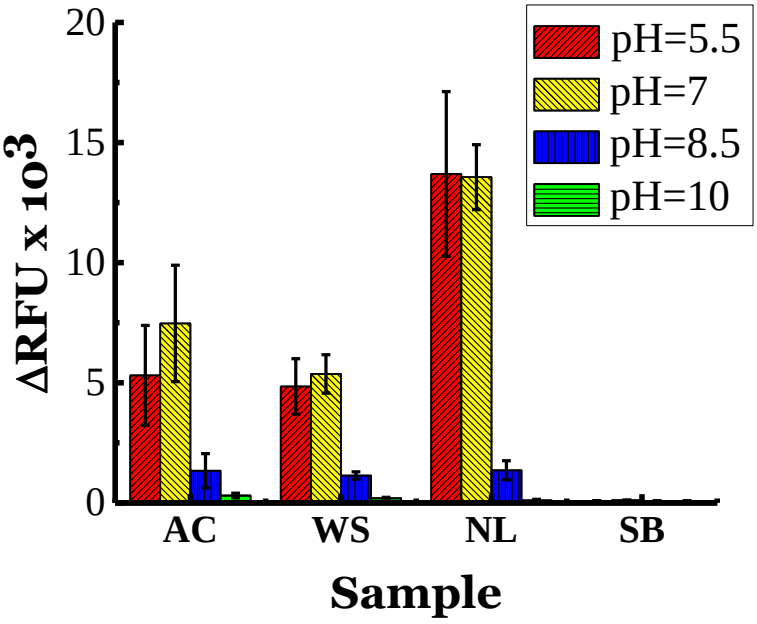

Figure 2.12 *Detection of influenza or S. pneumoniae by MUNANA (4,7 OMe) in different pH. The influenza or S. pneumoniae samples were incubated in MUNANA (4, 7 OMe) solution with different buffers (pH = 5.5, pH =7, pH = 8.5, pH = 10), the fluorescence intensity was detected at 37°C, 360 nm/460 nm for 2 h. Then 1 M, 100 µL tris solution was added, fluorescence intensity was detected at 37ºC, 360 nm/460 nm for 10 min. All experiments were performed in triplicate. Figure is taken from publisher with permission.*[74]

Next, we used DTT, a reducing agent can reduce disulfide bond, to cleave the disulfide bonds present in influenza NA not *S. pneumoniae* NA. (**Figure 2.9**) From the X-ray structure of influenza H1N1 NA and H3N2 NA, there are eight disulfide bonds in one monomer of H1N1 influenza NA, nine disulfide bonds in one monomer of H3N2 NA.[75-77] Four of them are buried inside the enzyme, whereas the others are exposed on the surface, which can be reduced by DTT,

resulting in the deactivation of NA. Upon this fact, we introduced DTT to tris buffer (pH=10), used influenza and *S. pneumoniae* to cleave the natural substrate MUNANA, resulting in minimal or no activity in influenza. In the contrast, *S. pneumoniae* still can cleave the substrate. (**Figure 2.13**)

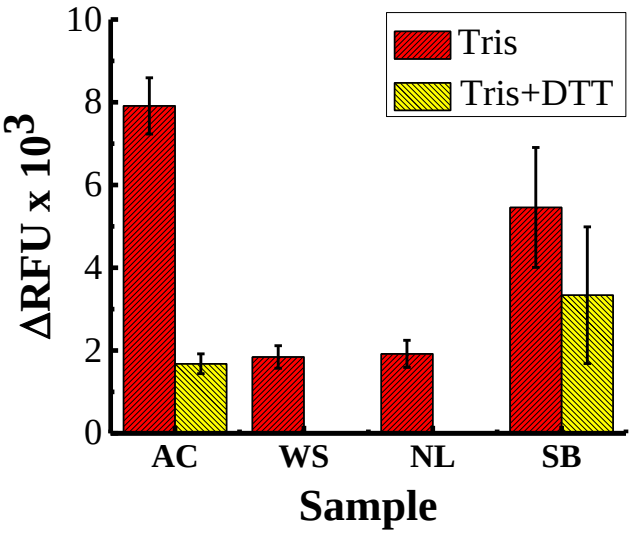

Figure 2.13 *The results for the influence of DTT. The influenza or S. pneumoniae samples were incubated in MUNANA solution with or without DTT. After 2 h, 1 M, 100 µL tris solution was added, fluorescence intensity was detected at 37ºC, 360 nm/460 nm for 10 min. All experiments were performed in triplicate. Figure is taken from publisher with permission.*[74]

2.4 Conclusion

We have designed fluorescent molecules specific for influenza virus. Influenza is very contagious infection, which leads to death for patients of weak (Children and senior citizens) or compromised immune systems (Patients with human immune deficiency virus, tuberculosis or organ transplants). Influenza infection is always companied with *S. pneumoniae* infection, which results in a secondary infection. Hence early detection and differentiation of influenza and *S. pneumoniae* is important for treatment. We have attempted to exploit structural differences

between *S. pneumoniae* and influenza neuraminidases to develop assay conditions to specifically detect *S. pneumoniae* with limited success.

We have been developing POC diagnostics using glucose meters for the past several years. Our previous detection strategy involved the development of glucose or galactose-based substrates. The exposure of these substrates to enzymes or pathogens released glucose or galactose, which was readily detected using a personal glucose meter.[69] Afterwards, we have developed paracetamol-based substrate. Which can remove the background of glucose in human blood and lead to a higher sensitivity. However, none of those can detect *S. pneumoniae* specifically when there are influenza resistant strains exist. Here we took advantage of the structure differences between influenza and *S. pneumoniae* NA, use DTT to break the disulfide bonds in influenza NA, leading to the minimum the activity of influenza. Hence, we can detect *S. pneumoniae* specifically with limited success.

In the future, we will optimize the DTT condition to minimize the activity of influenza NA, make the activity destroyed completely. Afterwards, we can perform this assay with handheld fluorometer. Handheld fluorometer is a small, lightweight and highly durable equipment, which is ideal for quick in situ measurement. Upon cleaving of the substrate by influenza, the fluorophore can be released and detected by handheld fluorometer in seconds. This allows patients self-test at home.

2.5 Experimental

2.5.1 Synthesis and characterization

General:

Chemical reagents were of analytical grade, used as supplied, without further purification unless indicated. The acidic ion exchange resin used was Amberlite® IR-120 (H+) resin.

Analytical thin layer chromatography (TLC) was performed on silica gel 230-400 mesh (Silicycle, Quebec City, Canada). Plates were visualized under UV light, and/or by staining with acidic $CeH_8Mo_3N_2O_{12}$, followed by heating. 1H and 13C NMR spectra were recorded on Bruker 400 MHz spectrometer. Chemical shifts are reported in δ (ppm) units using 13C and residual 1H signals from deuterated solvents as references. Spectra were analyzed with MNova® (Mestrelab Research, Escondido, CA, USA). Electrospray ionization mass spectra were recorded on a Micromass QT 2 (Waters) and data were analyzed with MassLynx® 4.0 (Waters, Milford, MA, USA) software. Reported yields refer to spectroscopically and chromatographically pure compounds that were dried under high vacuum (10^{-2} mbar) before analytical characterization, unless otherwise specified.

Abbreviations:

Ethyl acetate, EtOAc; Tetrabutylammonium hydrogen sulfate, TBAHS; sodium carbonate, Na_2CO_3; Sodium methoxide, NaOMe; Methanol, MeOH; Sodium hydroxide, NaOH; 4-methlumbelliferone, 4-MU; Dichloromethane, DCM; MUNANA (2′-(4-Methylumbelliferyl)-α-D-N-acetylneuraminic acid sodium salt hydrate).

2-(4-Methylumbelliferyl)-5-acetamido-8,9-di-O-acetyl-4,7-di-O-methyl-D-glycero-α-D-galacto-nonulopyranosidonate (2-3)

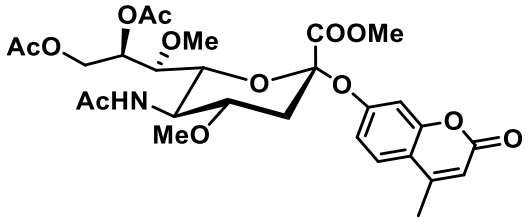

To a solution of **2-2** [72] (60 mg, 0.13 mmol) in ethyl acetate (5mL) was added a solution of **2-1** (56 mg, 0.26 mmol) and TBAHS (53 mg, 0.15 mmol) in 1M solution of Na_2CO_3 (3 mL). The mixture was stirred at rt.[78] After completion of reaction (TLC) then a solution of ethyl acetate :

$NaHCO_3$ (1:1) was added. The organic phase was separated and washed twice with $NaHCO_3$. The organic phase was dried over Na_2SO_4 and concentrate under reduced pressure. The residue was purified by silica gel column chromatography MeOH : DCM = (5 : 95) to afford **2-3** as a solid white material, yield = 46 mg (60%). 1H NMR (400 MHz, $CDCl_3$) δ 7.51 (d, J = 8.7 Hz, 1H), 7.11 (d, J = 8.9 Hz, 1H), 6.99 (s, 1H), 6.19 (s, 1H), 5.35 – 5.28 (m, 2H), 4.60 (d, J = 12.4 Hz, 1H), 4.35 (d, J = 10.5 Hz, 1H), 4.22 (dd, J = 12.5, 5.0 Hz, 1H), 3.69 (s, 3H), 3.59 (d, J = 7.4 Hz, 1H), 3.55 (s, 3H), 3.44 – 3.35 (m, 4H), 2.84 (dd, J = 4.0, 12.0 Hz, 1H), 2.42 (s, 3H), 2.15 (s, 3H), 2.09 (s, 6H), 2.06 – 2.03 (m, 1H). 13C NMR (100 MHz, $CDCl_3$) δ 170.6, 170.4, 170.1, 161.1, 157.0, 154.4, 152.4, 127.1, 115.9, 115.6, 113.3, 107.5, 100.4, 77.2, 76.2, 74.5, 70.6, 62.6, 61.3, 56.2, 53.0, 50.1, 37.2, 23.8, 20.9, 18.7, 14.2.

4,7-dimethoxy-2-(4-methylumbelliferyl)-a-D-N-acetylneuraminic acid. [MUNANA (4,7 OMe)]

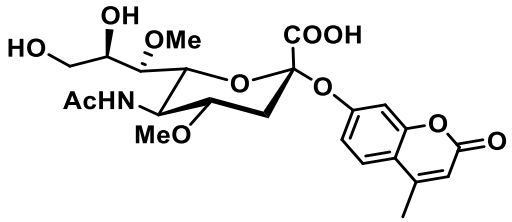

Compound **2-3** (46 mg, 0.08 mmol) was dissolved in MeOH (7mL) and treated with a solution of NaOMe (20 µL) and stirred at rt for 1 h. The solution was neutralized with Amberlite® IR 120 (H^+) resin, filtered and concentrate to dryness. The dried compound was treated with NaOH (0.05 N, 3.0 mL) and reaction was stirred for 4h. After completion of reaction, as monitored by TLC using DCM:MeOH:NH_4OH (8:1.5:0.5), reaction was neutralized with Amberlite® IR 120 (H^+) resin, filter, concentrate, then subjected to P-2 gel column to afford **MUNANA (4,7 OMe)**, yield = 33 mg (84% over two steps). 1H NMR (400 MHz, D_2O) δ 7.57 (d, J = 8.8 Hz, 1H), 7.08 – 7.02 (m, 2H), 6.12 (s, 1H), 4.15 (d, J = 10.3 Hz, 1H), 3.98 (t, J = 9.9 Hz, 1H), 3.88 – 3.83 (m, 1H),

3.80 (d, J = 12.1 Hz, 1H), 3.59 (dd, J = 12.0, 5.8 Hz, 1H), 3.38 – 3.30 (m, 8H), 2.88 (dd, J = 12.7, 3.9 Hz, 1H), 2.31 (s, 3H), 1.98 (s, 3H), 1.84 (t, J = 12.1 Hz, 1H). 13C NMR (100 MHz, D_2O) δ 174.1, 172.7, 164.5, 157.3, 156.2, 153.3, 126.1, 117.3, 116.0, 111.5, 107.6, 102.5, 78.1, 78.0, 73.5, 71.3, 62.3, 60.3, 56.7, 49.8, 37.5, 22.2, 17.9. HRMS (ESI): Calculated for C23H29NO11Na [M+Na] 518.1638; Found 518.1641.

2.5.2 Biological assays

Materials:

Influenza A virus strains: H3N2 (A/Aichi/2/1968), H3N2 (A/Winsconsin/15/2009), H1N1(A/Netherlands/2629/2009) were obtained from Beiresources (NIAID). *S. pneumoniae* (ATCC 6301) were obtained from American Type Culture Collection (ATCC). Enspire plate reader. 400 µL, 96 well black plates were purchased from Thermo Scientific.

***S. pneumoniae* bacterial growth:**

S. pneumoniae (ATCC 6301) was inoculated in brain heart infusion (BHI) broth that was augmented with 0.16 g/L of sialic acid to enhance NA production by the bacteria.[71] The bacterial concentration was determined to be 1.2×10^6 CFU/mL using the colony count method. 100 µL of bacterial solution was lysed using 0.01% SDS, and 20 µL of chloroform was added to it. The sample was then lysed by vertexing for 30 s and incubating at a temperature of 28 °C for 5 min.

Influenza virus growth:

MDCK (Madin-Darby canine kidney) cells were purchased from ATCC® (CCL-34™, Manassas, VA) and maintained in Dulbecco's Modified Eagle Medium (DMEM, Gibco, Grand Island NY) supplemented with 10% Fetal Bovine Serum (FBS Gibco, Grand Island NY). Influenza A virus strains used in this study were obtained from BEI Resources (Manassas, VA).

Virus titers of different influenza strains were determined using standard plaque assays in MDCK cells to quantify the amount of virus.[69, 70] MDCK cells were grown to confluency in 6-well plates. Once confluent, media was removed from the cells and were washed three times with plain DMEM to remove residual FBS. Virus suspension was serially diluted 10-fold and added to duplicate wells at 400 µL/well. Virus was adsorbed for 1 h at 37 °C in a 5.0% CO_2 incubator. One-hour post-adsorption, virus suspension was removed and Avicel (1.2%, 2.0 mL, FMC Biopolymer) supplemented with 2 µg/mL TPCK-trypsin (Sigma-Aldrich, St. Louis, MO) was added to each well. Avicel was prepared as described previously. 77 Plates were incubated for 5 days to allow for plaque formation. On day 5, the Avicel overlay was removed carefully from each well and the wells were washed two times with 1X PBS followed by methanol (100%) fixation. Fixed wells were stained with 0.2% crystal violet and plaques were counted to determine virus titers.

The influence of pH to the activity of virus and *S. pneumoniae*:

Inactivated A/Aichi/2/1968 H3N2 (sample AC), A/Winsconsin/15/2009 H3N2 (sample WS), A/Netherlands/2629/2009 H1N1 (sample NL), *S. pneumoniae* B (sample SB) were incubated with different buffers (pH = 5.5, pH =7, pH = 8.5, pH = 10) for 30 min. Then the substrate was added, the fluorescence intensity was detected at 37ºC, 360 nm/460 nm for 2 h. Then 1 M, 100 µL tris solution was added, fluorescence intensity was detected at 37ºC, 360 nm/460 nm for 10 min.

The influence of DTT to the activity of virus and *S. pneumoniae*:

Inactivated A/Aichi/2/1968 H3N2 (sample AC), A/Winsconsin/15/2009 H3N2 (sample WS), A/Netherlands/2629/2009 H1N1 (sample NL), *S. pneumoniae* B (sample SB) were incubated with tris or tris + DTT buffer for 5 min. Then MUNANA was added, the fluorescence intensity was detected at 37ºC, 360 nm/460 nm for 2 h. Then 1 M, 100 µL tris solution was added, fluorescence intensity was detected at 37ºC, 360 nm/460 nm for 10 min.

3 CHAPTER 3 DEVELOPMENT OF POINT-OF-CARE ASSAYS TO MONITOR MMP-9 AND TNF-α LEVEL IN INFLAMMATORY BOWEL DISEASE

* Most of the work described in this chapter has been submitted in two publications:

1. Dandan Liu, Emilie Viennois, Didier Merlin, and Suri S. Iyer*. Towards Point-of-Care Assays to Monitor MMP9 and TNF-α Levels in Inflammatory Bowel Disease. Submitted to *ACS Omega*. Under review.

2. Dandan Liu, Katie A. Skrada, Didier Merlin, Suri S. Iyer*. Inflammatory Bowel disease biomarkers. Submitted to *Medicinal Research Reviews*. Under review.

3.1 Inflammatory Bowel Disease (IBD) Introduction

3.1.1 Classification of IBD

Inflammatory bowel disease (IBD) is characterized by chronic inflammation in gastrointestinal tract and has no cure.[79] There are estimated 6.8 million U.S. adults have been diagnosed IBD by 2017, which is a large increase since 1999 (2 million)[80]. Ulcerative colitis (UC) and Crohn's disease (CD) are two major subtypes of IBD.

Ulcerative colitis (UC)

UC is a chronic inflammatory disease affects the colon, most commonly afflicting adults aged 30-40 years old and resulting in disability.[81] The factors that lead to UC include: genetic predisposition, epithelial barrier defects, dysregulated immune responses and environmental factors. UC is frequently associated with inflammation starting in the rectum and extending to proximal segments of the colon, mainly the inner side of colon,[82] characterized by bloody diarrhea, tenesmus and abdominal pain.[83] Patients with UC can have the following symptoms: urgency,

incontinence, fatigue, mucus discharge, nocturnal defecations, increased frequency of bowel movement and abdominal discomfort. UC can be classified into 3 types regarding to the extent of colonic involvement: proctitis, left-side colitis and extensive colitis.[82] (**Figure 3.1**) Proctitis involves 30-60% patients, the symptoms could be rectal bleeding, tenesmus and urgency; 16-45% patients were involved in left-side colitis, the symptoms could be proctitis, diarrhea and abdominal cramping; 15-35% patients were involved in extensive colitis, the symptoms could be left-side colitis symptoms plus constitutional symptoms, fatigue and fever. The symptoms can be different depends on different patients.

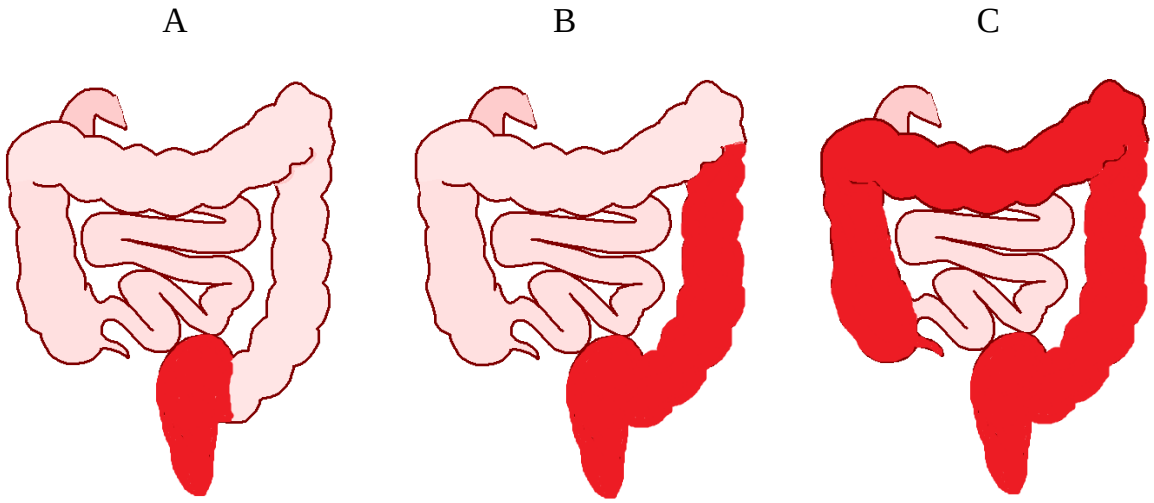

Figure 3.1 *Classification of UC regarding to the extent of colonic involvement. A. Proctitis; B. Left-side colitis; C. Extensive colitis. Figure is modified from publisher with permission.*[82]

Crohn's disease (CD)

CD is a chronic inflammatory bowel disease affecting any portion of the gastrointestinal tract from the mouth to the anus, normally afflicting people between 15 and 30 years old. CD is a relapsing and remitting disease, which only involves a small segment of the gastrointestinal tract, while it has potential to progress extensively. Factors contribute to CD include immunological,

genetic and environmental factors. Recently, 163 of rick loci have been identified to trigger IBD, of which 110 are associated with both CD and UC.[84] Environmental factors such as Western diet are believed contributing to CD. CD is un-continuous disease which can affect all the layers of the bowel wall. Patients get CD could have symptoms: abdominal pain, fever and clinical signs of bowel obstruction or diarrhea with passage of blood or mucus.[85]

3.1.2 Therapeutics of IBD

UC and CD are two main subtypes of IBD, inflammation of UC is limited to the mucosal layer and the inflammation is continuous, while the inflammation of CD is transmural and it's not continuous. Although there are significant differences between UC and CD, most treatment approaches are effective for both diseases.

Anti-inflammatory drugs

Anti-inflammatory drugs are often the first step to treat IBD, including 5-aminosalicylates (5-ASA) and corticosteroids.[86] Sulfasalazine is a prodrug to treat IBD, which will release active form 5-ASA through colonic bacteria (**Figure 3.2**). This drug was developed as a treatment for rheumatoid arthritis, later was found to effective for IBD patients.[87] Due to the poor toleration of sulfasalazine in up to 30% of patients, a variety of mesalamine derivatives have been developed to deliver 5-ASA, including azo-linked two molecules of 5-ASA (Olsalazine, **Figure 3.3A**) and inert carrier linked 5-ASA (Balsalazide, **Figure 3.3B**).[88, 89] There are also other drugs coated with protective materials to control (Pentasa) or delay (Asacol, Apriso and Lialda) the delivery of 5-ASA.[90] 5-ASA is effective for treatment of active CD, but not recommended for the maintenance. For treatment of UC, 5-ASA is effective for the induction and maintenance of remission in mild to moderate active UC.[90]

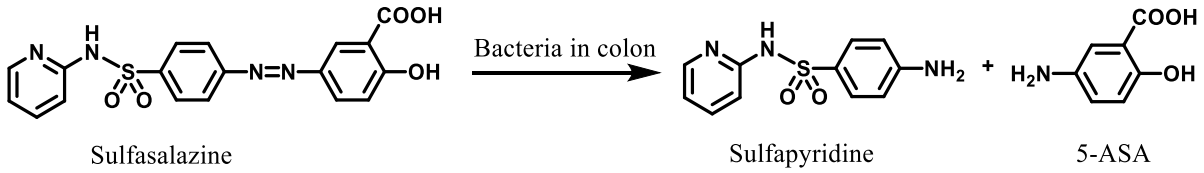

Figure 3.2 *Prodrug sulfasalazine and active form 5-ASA.*

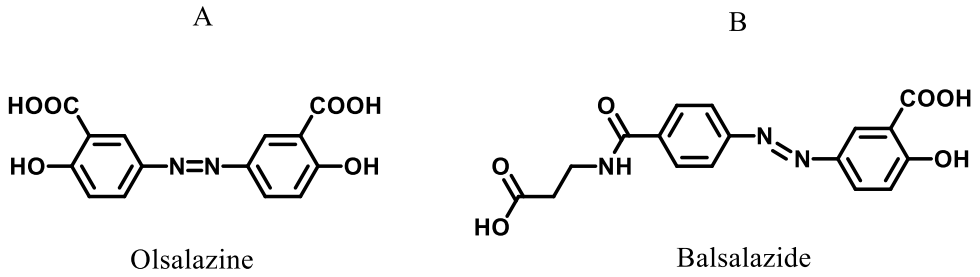

Figure 3.3 *Structure of Olsalazine and Balsalazide. A. Olsalazine; B. Balsalazide.*

Corticosteroids are another kind of anti-inflammation drug, which can bind to a cytoplasmic receptor and enter the nucleus to introduce a variety of anti-inflammatory effects.[91] Common types of corticosteroids used in the treatment of IBD include prednisone, methylprednisolone, hydrocortisone and budesonide (**Figure 3.4**).[92] Prednisone and methylprednisolone are used to treat moderate to severe cases of IBD[93]; hydrocortisone is used for short treatment[94]; budesonide is used to treat moderate cases of CD[95].

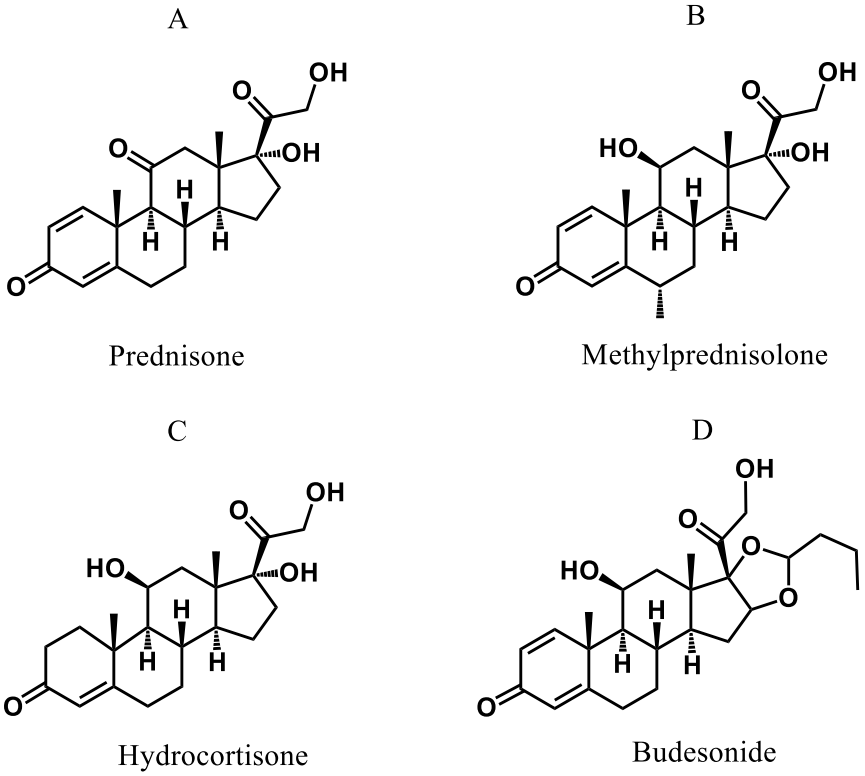

Figure 3.4 *Structure of prednisone, methylprednisolone, hydrocortisone and budesonide. A. Prednisone; B. Methylprednisolone; C. Hydrocortisone; D. Budesonide.*

Immunosuppressive agents

Immunosuppressive agents are mainly used when patients were failed with treatment of 5-ASA and steroids.[96] Immunomodulators include 6-mercaptopurine (6-MP), azathioprine (AZA), methotrexate (MTX) and cyclosporine (CSA). 6-MP is active form of AZA, (**Figure 3.5**) both of them can inhibit lymphocyte proliferation, which might lead to anti-inflammatory effects through suppression of natural kill cell and T cell activity.[97]

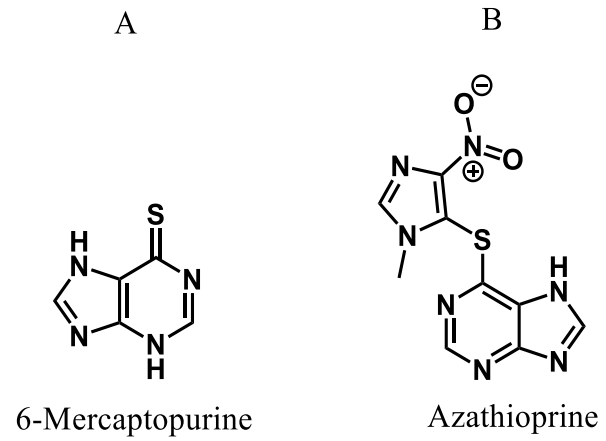

Figure 3.5 *Structure of 6-mercaptopurine and azathioprine. A. 6-Mercaptopurine B. Azathioprine.*

MTX is a folic acid antagonist, which can inhibit interleukin (IL)-1 and suppress T cell function. It has been reported that MTX was used for the induction and maintenance of CD[98], but no convincing data for UC. The structure of MTX was shown in **Figure 3.6**. CSA is a calcineurin inhibitor, which can form a complex with cyclophilin to block the phosphatase activity of calcineurin, resulting in the decrease of inflammatory cytokines produced from T cell.[99] It is effective for the induction and maintenance of UC, while no convincing data for treatment of CD.[100]

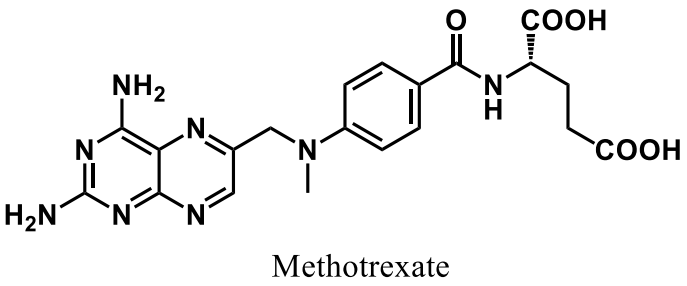

Figure 3.6 *The structure of methotrexate.*

Biological agents

Tumor necrosis factor-alpha (TNF-α) inhibitors, also called biologics, are proved as biological agents to treat IBD. Human TNF is a family of proteins and receptors that involved in immune regulation.[101] TNF-α is trimer, produced by macrophages or monocytes during acute inflammation, high concentration of TNF leads to excess inflammation, which is considered as a proinflammatory cytokine. There are two forms of TNF-α: soluble and transmembrane form, both forms can perform their biological functions by binding to TNF-α receptors.[102] Anti-TNF-α can neutralize TNF-α, blocking the proinflammation signals.

The first biological agent approved is infliximab to treat moderate to severe IBD in the late 1990s. Infliximab is a chimeric monoclonal IgG1 antibody created by combing mouse and human TNF, which has a half-life of approximately 14 days.[103] This can be used for treatment of CD, UC, rheumatoid arthritis, ankylosing spondylitis and plaque psoriasis.[104] Infliximab is administered intravenously by weight-based dosing, normally dosed every 4-8 weeks after an initial treatment of 0-6 weeks. The recommended dose for UC and CD patients is 5 mg/kg at 0, 2, 6 weeks, followed by the maintenance dose of 5 mg/kg every 8 weeks. Data shows infliximab is very effective for treating IBD, while up to 30% patients show no clinical benefit after induction phase and up to 50% of patients have to discontinue the treatment because of the secondary loss of response or serious side effect.[105-107]

Adalimumab is the first fully human monoclonal antibody against TNF-α approved by FDA in 2002 to treat rheumatoid arthritis. It inhibits TNF-α and its interaction with TNF-α receptor on the surface of p55 and p75 cell, which has a half-life approximately 2 weeks.[108] Adalimumab was approved to treat moderately to severely active CD and UC in 2007 and 2012 respectively.[109] It treats patients who have an inadequate response to conventional therapy or immunosuppressant, or who are intolerant to or have medical contraindications for such therapies. The recommended

dose for treating CD and UC is 160 mg on day 1, 80 mg on day 15, followed by a maintenance dose of 40 mg every two weeks starting at day 29 for less than one year.[104]

Certolizumab pegol is a monoclonal antibody against TNF-α approved by FDA in 2008 to treat CD. It is a recombinant antigen-binding fragment (Fab) antibody conjugated to polyethylene, which is the only PEGylated TNF-α inhibitor without crystallizable fragment (Fc). By conjugating to polyethylene, the bioavailability, drug stability and plasma half-life were enhanced.[110] The recommended dose to treat CD is 400 mg initially and week 2 and 4, followed by 400 mg every 4 weeks for maintenance if there is response.[104]

Golimumab is another fully human IgG1 monoclonal antibody against TNF-α, which was approved by FDA to treat rheumatoid arthritis in 2009. Golimumab is administered by subcutaneous injection which allows self-administration.[111] It was approved to treat moderate to severe UC in 2013. The recommended dose to treat UC is 200 mg initially and 100 mg at week 2 followed by maintenance dose of 100 mg every 4 weeks.[104]

Table 3.1 *Anti-TNF-α developed to treat IBD.*

Drug	**Indication**	**Dose**
Infliximab	UC, CD	5 mg/kg at 0, 2, 6 weeks, followed by the maintenance dose of 5 mg/kg every 8 weeks.
Adalimumab	UC, CD	160 mg on day 1, 80 mg on day 15, followed by a maintenance dose of 40 mg every two weeks starting at day 29 for less than one year.
Certolizumab pegol	CD	400 mg initially and week 2 and 4, followed by 400 mg every 4 weeks for maintenance.
Golimumab	UC	200 mg initially and 100 mg at week 2 followed by maintenance dose of 100 mg every 4 weeks.

3.1.3 Current diagnostics for IBD

Endoscopy

The only way to establish a diagnosis for UC and CD is through the combination of endoscopy procedure with biopsy of the targeted area. This can accurately differentiate UC from CD and monitor the disease activity.[112]

CD can affect any part of gastrointestinal tract; with the most commonly affected area being the colon. Ileocolonoscopy with collection of multiple biopsy specimens is a well-established first line diagnostic in CD.[113] The features of endoscopic finding of CD including the discontinuous chronic and patchy distribution of inflammation with skip lesions.[114] During endoscopic procedures in patients with CD, the inflammation can present in different ways: erythema, altered vascular pattern, friability, granularity and small discrete superficial and aphthous ulcers. As the inflammation becomes more severe, deep, serpiginous and linear ulcerations and a "cobblestone" appearance of the inner wall can develop.[115] Anatomical criteria of severe inflammation in CD includes deep ulcerations across the muscle layer, mucosal detachments, or ulceration limited to the submucosa but extending to more than one-third of a defined colonic segment.[116] Endoscopy in a patient suffering from UC will show inflammation that is continuous throughout the colon; while the specific characteristics depend on the severity of UC. Mild inflammation in UC presents as edema, erythema and abnormal vascularity. Moderate inflammation can have a "wet sand-paper" appearance, erosions, superficial ulcers and friability. Severe inflammation in UC appears as confluent ulcerations, worsened friability of epithelium, and has the potential to develop into spontaneous bleeding.[117, 118] The endoscopy might also reveal rectum sparing or patchy rectal inflammation after treatment.

In order to obtain a reliable diagnosis, a minimum of two biopsies from five sites around the colon should be obtained, including rectum and ileum.[119, 120] The microscopic features identified in CD include discontinuous chronic and patchy chronic inflammation, discontinuous crypt and granulomas. The features above combined with irregular villous architecture can be used to identify the biopsy samples taken from the ileum.[114] UC biopsy samples are characterized by diffused mucosal granularity, edema and erythema.[121] Obtaining a full set of biopsy samples from the colon can improve the diagnostic yield for both UC and CD, which also might reveal inflammation not seen in endoscopy alone. Though, this method may be time-consuming and invasive, the use of endoscopy combined with biopsy sampling has the advantage to diagnose IBD at an early stage which proves useful for the patient. The differences between UC and CD from endoscopy are listed in **Table 3.2**.

Table 3.2 *Different endoscopic appearance between UC and CD. Table is taken from publisher with permission.*[122]

Endoscopic appearance	**UC**	**CD**
Distribution	Continuous spread from the rectum	Any segment of the gastrointestinal tract
Small bowel involvement	Rare	Frequent
Rectal involvement	Almost always	30-50%
Uniform, continuous disease	Always	Infrequent
Longitudinal, polycyclic ulcers	No	Frequent
Cobblestone appearance of ileum	No	Frequent
Normal mucosa within inflamed areas strictures	No	Frequent
Mucosal edema	Frequent	Occasional
Ulceration	Often flat and extensive	Deep
Circumferential inflammation	Frequent	Rare

Imaging

Numerous studies have been done to investigate less-invasive imaging methods to potentially diagnose IBD such as magnetic resonance imaging (MRI), computed tomography (CT), ultrasonography (US), scintigraphy and positron emission tomography (PET).[123-125] Imaging plays an important role in early diagnostics for IBD. It can provide evidence of abnormal bowel in patients with suspected IBD, particularly CD, and further see where the abnormalities are distributed in the gastrointestinal tract.[126] A meta-analysis, done by *Horsthuis, K. et al.*, discussed a total of 33 studies to compare the accuracies of US, MRI, CT and scintigraphy imaging to diagnose patients with suspected IBD.[127] The sensitivity and specificity for each method were respectively: 89.7% and 95.6% for US, 93.0% and 92.8% for MRI, 84.3% and 95.1% for CT, 87.8% and 84.5% scintigraphy.[127] CT and MRI are used primarily to view the small intestine. Both of them can establish the locations and activity of IBD through wall thickness and increased intravenous contrast enhancement. Meanwhile, imaging with US and scintigraphy can be used to take images of the colon. MRI and US hold the most accuracy, and furthermore are not involved in the use of ionizing radiation, which can be harmful to patients over time.[128] Considering the relapsing nature of IBD, frequent reevaluation for most patients is necessary. Therefore, MRI and US should be considered as a means for initial diagnosis and follow-up evaluation tools for IBD.

Transabdominal ultrasound

Ultrasound, rapidly improving resolution, has become an important tool for diagnostics of IBD. The diagnosis is based on the assessment of bowel wall diameter and blood flow. The thickness of the bowel wall can differentiate moderate and severe disease.[129] Pathologic findings like enlarged lymph nodes, abscesses, stenoses and fistulae can be detected by ultrasound. This method is also sensitive and specific, but it requires well-trained personnel.

Biomarkers

Since endoscopy and other methods discussed in the previous section require invasive and uncomfortable procedures, efforts to diagnose and monitor inflammation have been proposed. Ideally, non-invasive or minimally invasive self-testing methods are ideal as it would decrease hospital visits and subsequent discomfort to the patient. Towards this end, there has been considerable effort directed towards the development of discovering new biomarkers and assays for diagnosing and monitoring IBD. A biomarker is defined as a substance that can be objectively measured or evaluated from a tissue or biofluid present in the targeted specimens.[130] Several biomarkers have been identified and proposed as IBD specific biomarkers (**Table 3.3**). These biomarkers are discussed in detail in the following sections.

Table 3.3 *Biomarkers used for diagnosis of IBD.*

Biomarker		**Concentration**		
		UC	CD	Healthy or remission disease
Serological biomarker	CRP	20 mg/L	40 mg/L	1 mg/L - 3 mg/L
	ESR*	~30 mm/h		~20 mm/h
	ASCA and p-ANCA			
	NO	15.3 µM	14.5 µM	13.3 µM
	Cytokine (TNF-α, IL-6, 8, 10, 17, 22)	7.6 pg/ml (TNF-α)	12.7 pg/ml (TNF-α)	0.02 pg/ml (TNF-α)
	ST2	56.8 pg/ml		30.7 pg/ml
	TNFAIP6	5.8 ng/ml	5.6 ng/ml	2.4 ng/ml
	NGAL	87 ng/ml	90 ng/ml	60 ng/ml
	Calprotectin	1900 µg/g	3200 µg/g	34 µg/g

Fecal biomarker	S100A12	400 ng/ml	470 ng/ml	70 ng/ml
	Lactoferrin	1100 µg/g	440 µg/g	1 µg/g
	NGAL	6 µg/g	5 µg/g	0.3 µg/g
	MPO	100 µg/g	60 µg/g	4 µg/g
	MMP-9	6 ng/ml	2 ng/ml	0.6 ng/ml
	IAP	20% less	22% less	--
Urine biomarker	MMP-9	95%	91%	20%
	MMP-2	90%	89%	25%
	MMP-9/NGAL	90%	86%	3%

A. Serological biomarkers.

1. C-reactive protein (CRP). CRP is considered one of the most important proteins present in acute inflammation, and was first discovered in 1930 in patients with pneumococcal pneumonia.[131] The production of CRP is amplified in response to most forms of inflammation, infection, and tissue damage in endothermic animals.[132] Human CRP consists of 187 amino acids and is composed of five identical non-glycosylated polypeptide subunits (**Figure 3.7**).[132] The correlation between elevated CRP levels and IBD in patients has been investigated through various studies. Under normal bowel conditions, the concentration of CRP detected in serum is between 1 mg/L – 3 mg/L; while in patients with mild to moderate inflammation, the CRP levels can increase to 50 – 100 mg/L in 4 to 6 hours.[133, 134] A population-based data study showed that at the time of diagnosis, the median CRP concentration for CD patients is 40 mg/L and in UC patients is 20 mg/L.[135] To further examine the correlation of CRP levels to IBD, a study by Solem, C. et al. was performed to examine the clinical, endoscopic, and histologic activity of both CD and UC. The results revealed that patients with CD had elevated levels of CRP. They were most associated with active irritable bowel during colonoscopy (OR, 3; 95% CI, 1-18), as well as histologically severe

forms of the disease (OR, 10; 95% CI; 1-104). In UC patients, CRP levels were only associated with histologically severe forms (P = 0.029).[136] In more recent years, several studies have been conducted to compare the levels of CRP in patients treated with the drug infliximab. Louis, E. et al. compared the CRP levels in CD patients before and after treatment with the drug;[137] while Iwasa, R. et al. compared them in patients with UC, also before and after treatment.[138] The results indicated that the concentration levels of CRP in patients that positively responded to infliximab, had significantly decreased.[137, 138] CRP accurately reflects the decrease in inflammation when patients positively respond to the infliximab treatment. These results, in conjunction with the significant difference between concentration levels in IBD patients and healthy subjects, demonstrate that CRP is an effective tool in monitoring inflammation flareups in IBD.

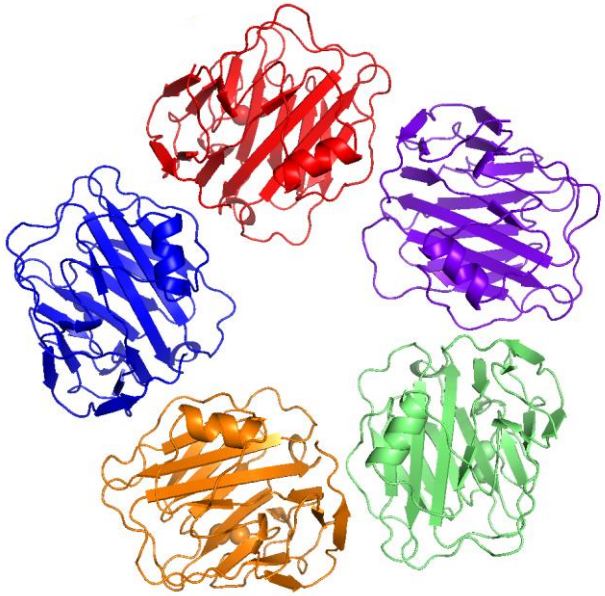

Figure 3.7 *Molecular structure of CRP. The structure was downloaded from the NIH PDB database. Molecular structure for CRP (PDB: 1GNH)[132] consists of five identical polypeptide subunits, each represented by a different color.*

2. Erythrocyte sedimentation rate (ESR). ESR determination is a test that can indicate acute inflammation in patients in a simple and inexpensive way. The test measures the rate of erythrocytes falling through a vertical column of anticoagulated blood under the influence of gravity.[139, 140] The two main factors that determine ESR are the degree of red blood cell aggregation and hematocrit, also known as packed cell-volume. Red blood cell aggregation is affected by the proteins present in blood plasma, which are different based on disease presence.[141] In cases of positive inflammatory response, the erythrocytes will fall at a faster rate and more aggregation will be present. This positive correlation allows this test to be used to measure the inflammatory activity that is caused by IBD.[142] Turner, D. et al. evaluated the use of ESR to monitor UC in patients, and also compared it to use of CRP.[142] They found the median ESR values for different severity levels of UC to be as follows: around 17 mm/h in patients in remission from UC, 26 mm/h in mild UC patients, 37 mm/h in moderate UC patients, and 39 mm/h in severe UC patients (**Figure 3.8**). A meta-analysis performed by Holtman, G. et al. showed that the sensitivity and specificity values for ESR to diagnose IBD were 66% and 84%, respectively.[143] While ESR is less accurate than CRP for the diagnosis of IBD, it still proves to be a useful tool. However, ESR could potentially be used to monitor inflammation flareups.

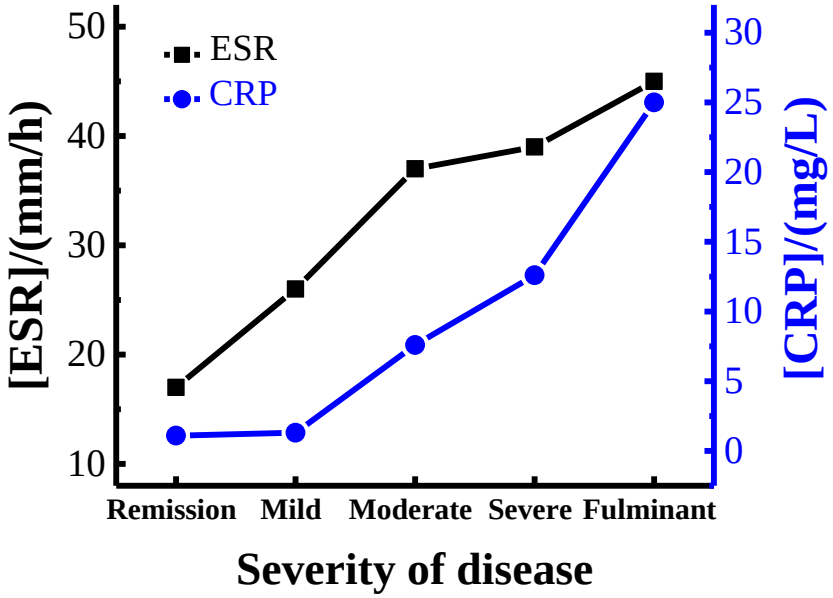

Figure 3.8 *Levels of ESR and CRP measured in patients with UC for comparison of usefulness.*[142] *Samples were taken from UC patients with varying severity of disease. The Kruskal Wallis test was used to compare test results across the levels of disease activity.*

3. ASCA, p-ANCA, and other antibody markers. Anti-Saccharomyces cerevisiae antibodies (ASCA) and perinuclear anti-neutrophil cytoplasmic antibodies (p-ANCA) have been characterized as serological markers for inflammation for many years. They were first discovered in UC patients in 1990.[144] ASCAs were detected in the serum of 50 – 60% of patients with CD; and had diagnostic values for sensitivity and specificity of 67% and 92%, respectively.[145] P-ANCAs were detected in the serum of 60 – 70% of UC patients, with only 15% of CD patients presenting with antibodies.[146] Most studies used enzyme-linked immunosorbent assay (ELISA) to detect ASCA and p-ANCA; a sample was considered positive when a concentration of >15 U/ml was detected. Indirect immunofluorescence assay (IIF) was also used to measure p-ANCA to differentially diagnose patients with CD or UC; a sample was considered positive when >24

U/ml.[147] Mokhtarifar, A. et al. tested patients at a one-year follow up exam, for ASCAs and p-ANCAs to re-examine their diagnoses of UC or CD.[147] The results showed that ASCA+/p-ANCA- can diagnose CD with a sensitivity of 67% and specificity of 78%; while, ASCA-/p-ANCA+ can diagnose UC with a sensitivity of 78% and specificity of 67%, respectively. Other antibody markers have shown positive correlations with IBD patients; these include anti-outer-membrane porin C (OmpC) and anti-Cbir1 antibodies. These have been positively detected in around 50 – 55% of CD patients, 5% - 10% of UC patients, and 5 – 8% of healthy subjects.[148-151] Combining multiple antibodies in a single test is preferred as it decreases false positives and negatives. In one study, a group of four genetic markers (ATG16L1, NKX2-3, ECM1, and STAT3), five inflammatory markers (CRP, SAA, ICAM-1, VCAM-1, and VEGF), and two serological markers (A4-Fla2 and FlaX) were selected for the diagnosis of IBD in combination with a six serological marker panel (ASCA-IgA, ASCA-IgG, ANCA, pANCA, OmpC, CBir1).[152] The results of the combination test were then compared to the results from the six serological marker panel for comparison.[152] The outcome showed that with this extended marker panel, discrimination area under the curve of IBD versus non-IBD increased to 0.87 (95% CI, -0.4 – 0.4) from 0.80 (95% CI, -0.5 – 0.5; $P < 0.001$). In addition, the discrimination area under the curve for differential diagnosis of UC from CD increased to 0.93 (95% CI, -0.4 – 0.4) from 0.78 (95% CI, -0.6 -0.6; $P < 0.001$).

4. Nitric oxide (NO). NO is a stable, yet mildly reactive free radical and gaseous signaling molecule present in mammalian cells, that plays a vital role in the regulation of various physiological and pathophysiological responses.[153] Some of these processes include vascular homeostasis, neurotransmission of the central nervous system and in peripheral nerves, as well as hemostasis and host defense.[153, 154] The possibility of NO working as a mediator in the inflammatory processes of IBD has fuelled many studies over the years.[155] Several manifestations

of IBD have been found to directly or indirectly correspond with NO, such as vasodilation and increased vascular permeability. A study done by Avdagić, N. et al. investigated the potential of serum NO as biomarker to diagnose UC and CD.[156] The result showed the level of serum NO was statistically different between UC patients, CD patients, and healthy controls. The median NO concentrations in UC patients, CD patients, and healthy controls were 15.3 μM, 14.5 μM, and 13.3 μM, respectively. With a cut-off of 17.4 μM, the sensitivity and specificity of NO to differentiate between active and inactive UC patients were both 100%. And with a cut-off of 14 μM, the sensitivity and specificity of NO to differentiate between active and inactive CD patients were 88% and 69%, respectively. These results indicate that serum NO could be a potential biomarker for IBD.

5. Cytokines. Tumor necrosis factor- α (TNF-α) was first identified in the 1970's as a soluble cytokine capable of significant cytotoxic activity against tumor cell lines, and is released upon activation of the immune system.[157] TNF-α is important for pro-inflammatory activity and have vital roles in the pathogenesis of chronic inflammatory diseases. The effects of TNF-α are carried out when this trimer (**Figure 3.9**) protein binds to and forms clusters with high-affinity receptors TNF-R1 and TNF-R2 on cell membranes.[158, 159] Once TNF-α is bound to its receptor, depending on the type of cell membrane, it will play part in numerous physiological and pathological responses.[159] TNF-α can be found in elevated levels in the GI tract of colitis patients, and has a major role in mucosal inflammation.[159, 160] A study conducted by Komatsu, M. et al. tested the concentrations of TNF- α using highly sensitive immuno-PCR, which resulted in concentrations that were significantly different between IBD patients and healthy controls.[161] Results for median TNF-α concentrations are as follows: 7.6 pg/ml in patients with UC, 12.7 pg/ml in patients with CD patients, and 0.02 pg/ml in healthy controls. This study was the first to result

in strikingly higher concentrations of TNF- α in IBD patients than in healthy controls; most likely due to the use of immune-PCR assay in comparison to conventional serum assay methods used in the past. TNF- α in the inflamed mucosa of IBD patients need further exploration but should be considered as a potential biomarker for its strong correlation to inflammation in the body.

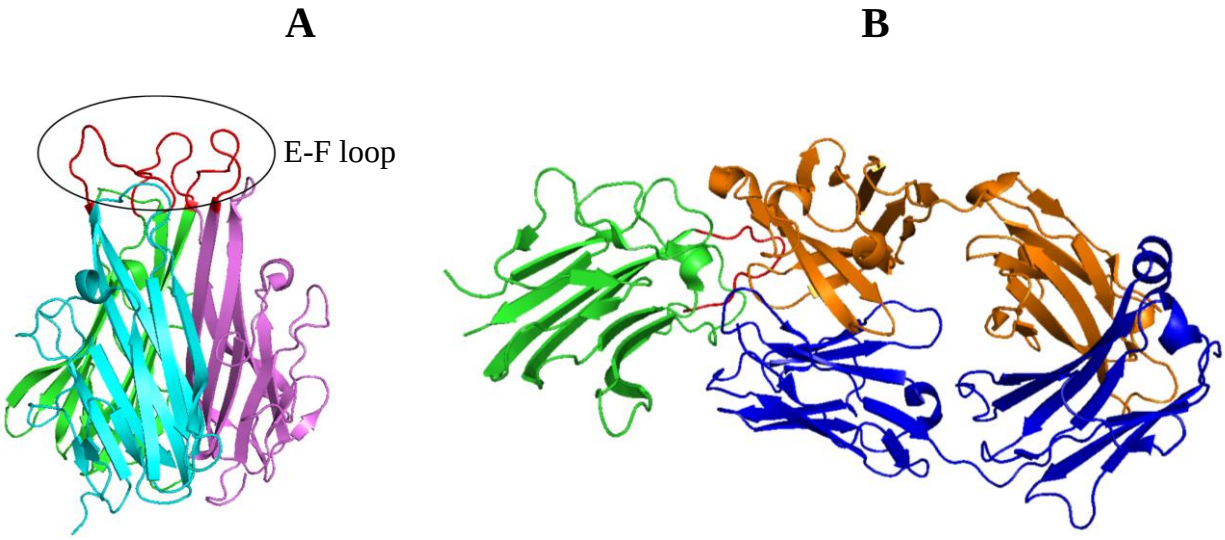

Figure 3.9 *Overall structure of human TNF-α and its monomer binding with infliximab. Structures downloaded from NIH PDB database. A. Overall structure of TNF-α (PDB: 1NTF).*[162] *It is a trimer, each monomer shown in different colors (green, cyan, purple). The E-F loop is shown in red, which plays a central role in antibody-antigen binding. B. TNF-α monomer binding with infliximab Fab (PDB: 4G3Y).*[163] *Infliximab Fab heavy chain is shown in orange, while the light chain is shown in dark blue. The TNF-α monomer is shown in green and the E-F loop is shown in red. One trimer of TNF-α can bind at most three infliximab molecules.*[163]

There are several other cytokines indicate the inflammation in IBD, such as interleukin-6 (IL-6), IL-8, IL-10, IL-17 and IL-22.[164-166] ILs are a group of cytokines first discovered express in leukocytes and there are more than 50 ILs in human.[167] IL-10 is a dimer, each monomer consists of six helices . Each IL-10 molecule can bind with two molecules of IL-10 receptor to induce

cellular responses.[168] IL-10 is an immunoregulatory cytokine inhibiting the production of proinflammatory cytokines, such as TNF-α, IL-1, IL-6 and IL-12.[169-171] It is also a growth and differentiation factor for B cells, thymocytes and mast cells, and it plays an important role in preventing inflammatory and autoimmune pathologies.[172, 173] IL-10 is mainly secreted by monocytes and release to serum and stool.[174] Kühn, R. et al. found that IL-10 deficient mice develop chronic intestinal inflammation.[175] Therefore, IL-10 knocked mice model normally are used for colitis study. Mitsuyama, K. et al. compared the concentration of IL-10 in active UC, CD patients and healthy subjects with ELISA.[164] The result showed the concentration of IL-10 increased in active UC and CD patients, which might be a helpful biomarker for IBD.

6. ST2. Suppression of tumorigenicity 2 (ST2) was first discovered in 1989, and belongs to interleukin 1 receptor family.[176] ST2 is mainly expressed in cardiac fibroblasts and cardiomyocytes in response to injury or stress. However, non-myocardial sources of ST2 are known, and are associated in inflammatory and immune processes.[177] Overexpression of ST2 has been positively identified in correlation with UC, and Boga, S. et al. set out to investigate the endoscopic, clinical, and histopathological assessment for serum ST2 levels in patients with UC and CD, in comparison to healthy controls.[178] A total of 143 IBD patients participated in this study, 83 UC subjects and 60 CD subjects, along with 50 healthy controls. ST2 serum levels were detected using ELISA testing; and endoscopic disease activity was measured by the CD activity index (CDAI) and the clinical colitis activity index (CCAI). The median concentrations of serum ST2 in UC patients, CD patients, and healthy controls were 54 pg/ml, 64 pg/ml, and 31 pg/ml respectively. Which showed a significant increase in IBD patients compared to healthy controls. In addition, this study found that the serum ST2 levels were positively correlated with endoscopic

activity for both UC and CD patients.[178] The results of these studies indicate that ST2 serum is a useful biomarker to measure the clinical course of IBD patients.

7. TNFAIP6. Tumor necrosis factor alpha-induced protein 6 (TNFAIP6), also known as TSG-6, is a protein that is secreted during times of inflammation in various cell types.[179] It has been suggested that TNFAIP6 plays a vital role in extracellular matrix formation or developmental properties.[180] High levels of TNFAIP6 have been detected in mucosal samples taken from patients with IBD; specifically in mucosal smooth muscle cells.[179] However, there has not been much investigation into the link between serum levels of TNFAIP6 and disease activity in patients with IBD. The serum levels for TNFAIP6 and CRP were tested against the disease activity in IBD using the CD Activity Index in CD patients, and Mayo Score in UC patients. Results showed that the correlation coefficients (r) were comparable for the CD activity index with values of 0.378 and 0.39 for TNFAIP6 and CRP, respectively; and for the UC Mayo Score, TNFAIP6 serum had a higher correlation value than that of CRP with values of 0.65 and 0.51, respectively.[181] While CRP shows higher accuracy for measurement, TNFAIP6 still proves useful for the monitoring of IBD disease activity and should be considered in further studies as a potential biomarker for diagnosing IBD.

B. Fecal biomarkers.

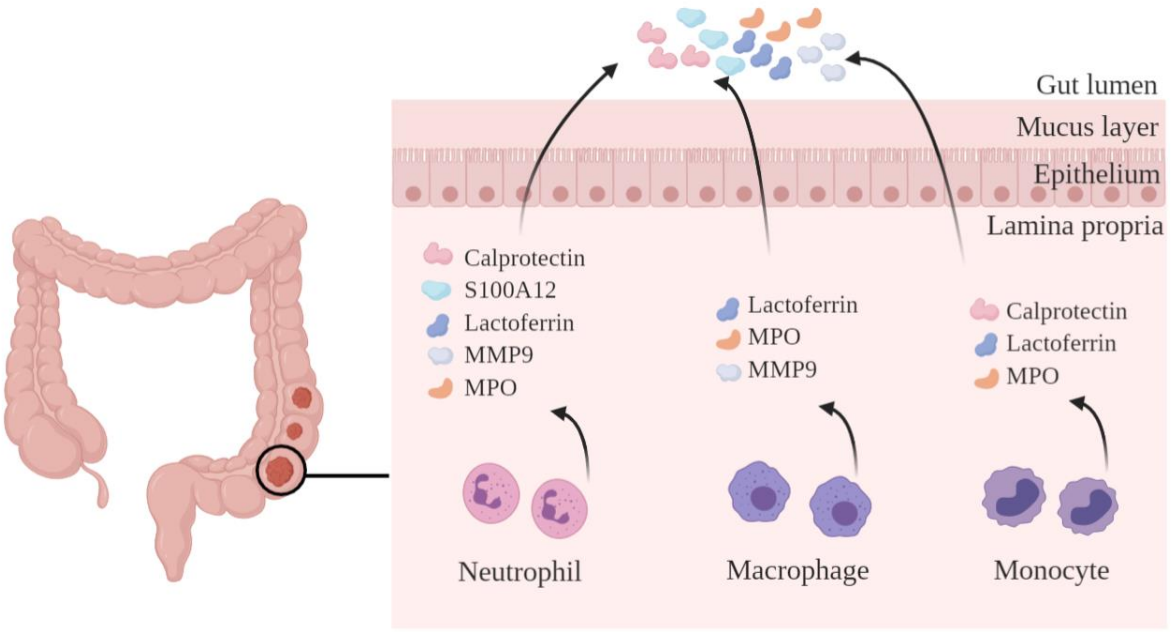

Figure 3.10 *The fecal biomarkers secretion of IBD. The inflammation in the gut mucosa leads to enhanced migration of innate immune cells, such as monocytes, macrophages and neutrophils to the affected mucosa. These cells secrete inflammatory mediators, such as calprotectin, lactoferrin, MMP9 et al. actively and the mediators are released to gut lumen, which can be detected from feces. Figure is modified from publisher with permission.*[182]

1. Calprotectin. Calprotectin is a calcium-binding protein that was first isolated from granulocytes back in 1980. It is mainly found in the cytosol of neutrophils, but can also be detected in monocytes and reactive macrophages in lower quantities.[183] Calprotectin possesses antimicrobial and antiproliferative properties and belongs to the S100 family of proteins, which are responsive to acute and chronic inflammation, as well as various malignancies.[184] Calprotectin is a heterodimeric protein composed of subunits S100A8 and S100A9 (**Figure 3.11**).[185] During inflammation, calprotectin can be detected in elevated levels in blood plasma, cerebrospinal fluid, synovial fluid, urine, and feces.[185] The concentration levels of calprotectin present in the feces of subjects is around six times greater than those found in plasma.[186] The calprotectin concentration

in healthy subjects is found to be around ~ 34 µg/g in feces. For patients with CD, the concentration increases significantly to ~ 3200 µg/g; and for UC patients it is around ~1900 µg/g.[187] Due to the large difference in concentration of calprotectin between healthy patients and those with CD or UC, For these reasons, numerous studies have used fecal calprotectin as an indicator for inflammation in patients.[184, 186, 188, 189] A meta-analysis performed by Freeman, K. et al. examined the use of fecal calprotectin to diagnose IBD, through various methods of measurement: ELISA, fluorescence enzyme immunoassay (FEIA), and Quantum-Blue point-of-care test.[190] It showed that the sensitivity from different assays ranged from 85% to 94%, and the specificity ranged from 67% to 88%. Calprotectin concentration can also be used to measure effect of interventions. Sipponen, T. et al. studied the effect of anti-TNF-α treatment on calprotectin levels, and found that the median fecal concentration in CD patients decreased from 1200 µg/g to 130 µg/g through treatment .[191] To summarize, fecal calprotectin is a very useful biomarker for the diagnosis and monitoring of inflammation in IBD patients.

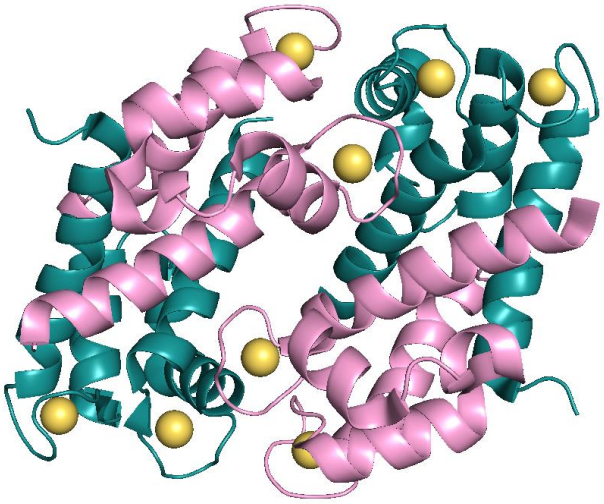

Figure 3.11 *Overall molecular structure of calprotectin heterotetramer. The structure downloaded from the NIH PDB database. The heterotetramer structure of calprotectin (PDB: 1XK4)*[189] *is composed of two heterodimer protein subunits: S100A8 and S100A9, forming the total formation structure (S100A8/S100A9)*$_2$*. S100A8 subunit is shown in pink color, S100A9 is shown in teal color. Calcium ions bound to each EF-hand formation are shown as yellow spheres.*

2. S100A12. S100A12, also known as Calgranulin C, is a calcium-binding pro-inflammatory protein that belongs to the S100 protein family.[192] S100A12 binds to cell surface receptor RAGE on inflammatory cells, which results in the activation of several intracellular signal cascades.[193] This ligation specifically activates nuclear factor (NF)-□B transduction pathway and MAP-kinase pathway—leading to the production of proinflammatory cytokines, such as tumor necrosis factor (TNF)-α and IL-1b.[194, 195] Several reports elaborate S100A12 and its role in various inflammatory diseases, these include rheumatoid and psoriatic arthritis[193], cystic fibrosis[196], various respiratory disorders[197], and IBD.[192] Since S100A12 is secreted by activated human neutrophils, which play a vital role in the inflammatory processes of IBD, the levels of serum S100A12 in IBD patients have been investigated. A study performed by Foell, D. et al. determined the tissue expression of S100A12 in IBD patients.[198] The results of the study show that concentration levels for S100A12 were around 470 ng/ml in patients with active CD, and 400 ng/ml in patients with active UC; compared to 75 ng/ml in healthy controls.[198] Since S100A12 has been positively identified in the feces of IBD patients, this biomarker could potentially be used as an effective non-invasive self-testing method.

3. Lactoferrin. Lactoferrin (LTF) is an iron-binding glycoprotein whose function is to transport iron in blood serum, but also plays an important role in first line immune defense.[199] This protein can be found in most mammalian exocrine secretions, such as tears, saliva, gastrointestinal

fluids, or breastmilk; or in the secondary granules of neutrophils. LTF levels are shown to increase significantly in the biological fluids of patients who suffer from various inflammatory diseases.[200] It has been of interest to measure IBD activity in patients through the use of fecal LTF sampling. Kane, S. V. et al. compared the concentration levels of fecal lactoferrin in patients with IBD to healthy controls using ELISA.[201] In healthy subjects, the concentration was found to be around ~1 µg/g, in CD patients it increases to ~440 µg/g, and in UC patients it is ~1100 µg/g.[201] The sensitivity and specificity of fecal LTF to diagnose UC in patients were 81% and 82%, respectively; while the sensitivity and specificity to diagnose CD were 82% and 0.71%, respectively.[141]

4. Lipocalin-2/NGAL. Neutrophil gelatinase-associated lipocalin (NGAL), also known as lipocalin-2, is a glycoprotein originally isolated from neutrophils that can be found in monomeric and homodimeric forms, as well as in a NGAL-gelatinase complex.[202] The presence of NGAL is expressed in elevated levels in chronic and acute inflammation and a wide array of benign and malignant diseases effecting various organ including digestive, respiratory, endocrine, and reproductive organs.[203, 204] High NGAL expression has been positively identified in IBD patients with inflamed colonic epithelium.[203] In one study with a limited number of patients, i.e. 21 patients with IBD and 23 healthy patients, the median concentration of NGAL present in UC patients was 6 (4 – 15) µg/g, and in CD patients at 5 (2 – 8) µg/g in contrast to healthy subjects expressed lower concentrations at around 0.3 (0.1 – 0.4) µg/g.[205] The sensitivity and specificity to diagnose active IBD from the subjects were 94.7% and 95.7%, respectively. Based on these studies, NGAL is also considered as a potential biomarker for IBD.

5. Myeloperoxidase (MPO). MPO is an enzyme found in the azurophil granules of neutrophils, and is used as a microbicidal agent that can attack foreign materials.[206] The MPO

concentration is directly proportional to the number of neutrophils.[207] Since neutrophils play a vital role in the inflammatory processes of IBD and are directly correlated to MPO, studies to correlate inflammation to MPO levels were undertaken.[208] It was demonstrated that median concentration of MPO was < 4, 100 and 60 µg/g in healthy, UC and CD patients, respectively. These results show a significant difference in the MPO levels of IBD patients compared to healthy subjects, which indicates the potential of MPO as a biomarker for IBD.

6. Matrix metalloproteinases (MMPs). MMPs are a group of zinc-dependent endopeptidases with a conserved catalytic domain, and a Zn^{2+} present at the active site; collectively termed matrixins.[209, 210] MMP-9 along with MMP-1, 2, and 3, have been detected in significantly high levels in colonic biopsies from IBD patients.[211] MMP-9, also known as gelatinase B, has three repeat domains of type II fibronectin domain into the catalytic domain, which is used for binding to gelatin, collagens, or laminin (**Figure 3.12**). Baugh, M. D. et al. explored the expression of multiple MMP-1, MMP-2, MMP-3, and MMP-9 in patients with IBD.[212] A recent study evaluated the diagnostic value of fecal MMP-9 in different types of IBD using ELISA.[211] The results showed that the median concentration of fecal MMP-9 was 1.5 ng/ml in active CD patients, compared with 0.6 ng/ml in inactive CD patients; and 6.2 ng/ml in active UC patients, compared to 0.7 ng/ml in inactive UC patients. Fecal MMP-9 did not show a strong correlation with any of the disease activity indicative of CD. However, it did show a strong association with the clinical and endoscopic activities of UC. For UC patients with positive endoscopic activity, the sensitivity and specificity of fecal MMP-9 to diagnose UC were 96% and 75%, respectively.

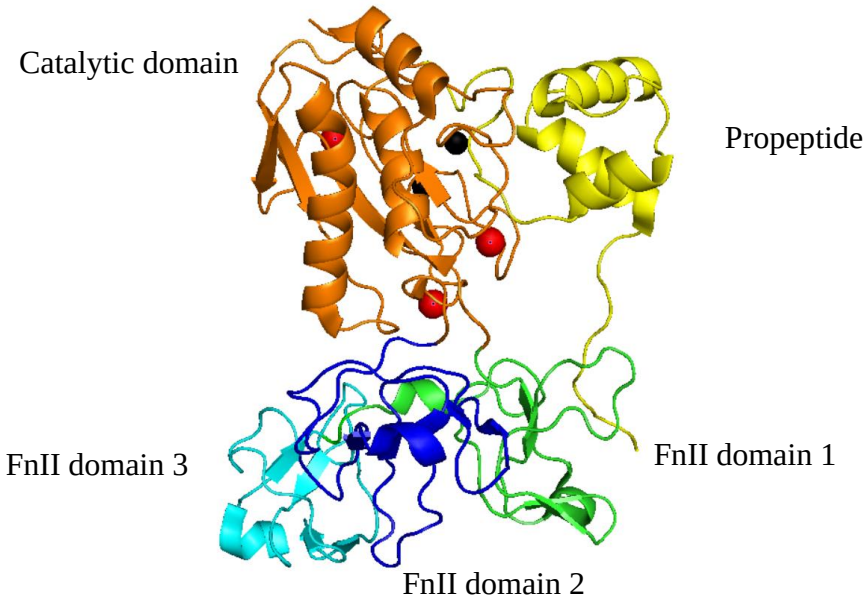

Figure 3.12 *Overall structure of proMMP-9. Structure downloaded from the NIH PDB database. ProMMP9 (PDB: 1L6J)*[213] *consists of 5 domains: propeptide (yellow color), catalytic domain (orange color) and 3 Fibronectin type II (FnII) domains (green, blue and cyan colors). Zn atoms were shown in black color and Ca atoms were shown in red color. ProMMP9 is enzymatic inactive and it can be activated by cleavage of propeptide. Zn is binding with catalytic domain, which is important for MMP9 enzymatic activity.*

7. Intestinal alkaline phosphatase (IAP). IAP belongs to a superfamily of metalloenzymes and is considered a crucial mucosal defense factor that works to maintain gut homeostasis.[214] While this enzyme is rarely found in the stomach of healthy subjects, it is present in the apical microvilli of the brush border of enterocytes found in the intestine. It is secreted apically and basolaterally by the enterocytes, and is expressed in the intestinal lumen, as well as the bloodstream, in response to inflammation.[214, 215] Another study performed by Park, Y. S. et al. evaluated the expression of IAP in the disease course of CD patients.[216] A total of 32 CD patients participated in the study and were monitored over the course of 14 months after biopsy sampling.

ELISA tests detected IAP concentrations in the intestinal mucosa; and samples were taken from inflamed and non-inflamed areas of the colon. Results showed that 31.3% of patients had lower IAP expression in inflamed mucosa compared to non-inflamed mucosa; the median value of IAP in inflamed mucosa was ~ 43 ng/ml, compared to 26 ng/ml in non-inflamed mucosa. Of the patients with this disparity in IAP levels, 90% experienced clinical recurrences of CD. This suggests that the concentration of IAP in the intestinal mucosa of CD patients may be associated with clinical recurrences of the disease, proving its usefulness as a potential biomarker for monitoring IBD.

Establishing the limit of detection and range of detection of the two biomarkers in IL10-/- mice, and development of assays to detect inflammatory biomarkers in our research group

We were interested in developing assays that could potentially be used in POCTs to monitor inflammation in IBD. Our long-term goal is to decrease the number of hospital visits and uncomfortable endoscopies for patients who have been diagnosed with IBD. If POCTs were available to monitor inflammation, IBD patients could use it in the privacy of their homes, test frequently and transmit the results to their physician. The physician could use the results to prescribe drugs or modify the drug dose, thereby reducing morbidity.

We first describe our efforts to establish the Limit of Detection (LOD) and range of detection of the two biomarkers (MMP-9 and TNF-α) in IL10-/- mice, followed by our efforts on assay development using mesoporous silica nanoparticles. MMP-9 level in mice fecal samples were detected by InnoZyme™ Gelatinase (MMP-2/MMP-9) Activity Assay kit (Catalog#: CBA003, Sigma). TNF-α level in mice serum samples were detected by TNF alpha Mouse ELISA Kit, High Sensitivity (Catalog#: BMS607HS, Thermo Fisher Scientific). Afterwards, we

developed assays to detect fecal MMP-9 and serum TNF-α using "cap and release" mesoporous silica nanoparticles (MSNs).

3.2 Mesoporous Silica Nanoparticles (MSNs) Introduction

3.2.1 A primer on MSN

MSNs have been drawn great attention as drug delivery system recent years. Due to its unique propensities, such as large loading capacity[217, 218], homogenous porosity[217], inertness and easy functionalization, it has been widely used in diagnostics[219, 220], drug delivery[221, 222], sensing[223, 224] and bioimaging[225]. There are two methods widely used to synthesize MSNs, one is solution-based synthesis, another is aerosol-based evaporation-induced self-assembly (EISA).[226]

Solution-based synthesis

Cetyltrimethylammonium bromide (CTAB) is most commonly used template molecule to synthesize MSNs. When it presents in concentrations greater than the critical micelle concentration in aqueous solution, it will form spherical micelles by self-assemble. After this, tetraethyl orthosilicate (TEOS) was added, it will form surface in hydrophilic interface of the micelles by electrostatic interaction. Followed by removing the template by calcination or acid extraction, MSNs will be produced (**Figure 3.13**). The dimensions of MSNs synthesized by this method range from 25 nm to 250 nm.[227]

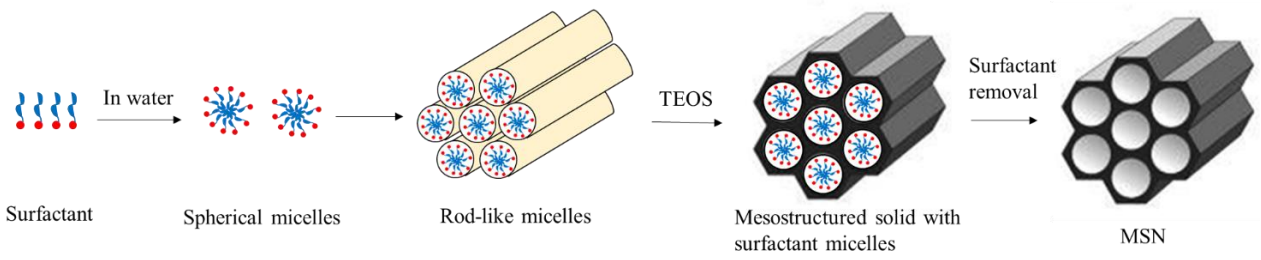

Figure 3.13 *Synthesis of MSN. Figure is taken from publisher with permission.*[228]

EISA

EISA begins with soluble silica and surfactant in ethanol/water solution with low concentration. As the solvent evaporate, the concentration of surfactant increases gradually, leading to self-assembly of silica/surfactant micelles and further form liquid-crystalline mesophases. The size of MSN synthesized by this method also has the particle size range from 25 nm to 250 nm.

3.2.2 Classification of MSN

Different types of MSN have been developed and used for drug delivery system, including Mobile Crystalline Material (MCM) system, Santa Barbara Amorphous (SBA) system, Korea Advanced Institute of Science and Technology (KIT) system and hollow MSNs.[229-231]

Table 3.4 *Different types of MSNs.*

MSN types	**Pore size (nm)**
MCM	1.5 – 8
SBA	2- 15
KIT	9
Hollow	100 - 150

MCM system including MCM-41, MCM-48, MCM-50, and MCM-41 is most commonly used for drug delivery. MCM-41 has a 2D hexagonal structure, characterized by a large surface area, a unidirectional pore system composed of a regular hexagonal array of tubes with high thermal stability.[232] Pore size of MCM-41 is around 1.5-8 nm.[232] MCM-48 has a 3D cubic structure, which has a larger surface area than MCM-41. The pore size of MCM-48 is around 2-5 nm. MCM-50 is characterized by 1D lamellar structure, which is formed by sheets or bilayers of surfactant molecules with hydrophilic head groups pointing towards silicate.[233]

SBA system, synthesized by polymer templates, mainly include SBA-1, SBA-2, SBA-3, SBA-11, SBA-12, SBA-15 and SBA-16. SBA-1, 2 and 3 were synthesized by cationic surfactants[234, 235], while SBA-11, 12, 15 and 16 were synthesized in acidic condition with non-ionic surfactants[236, 237]. The structure of SBA-15, similar to MCM-41, has a 2D hexagonal mesoporous structure, but with a thicker pore wall and larger pore size.[238]

KIT system including KIT-5 and KIT-6, KIT-5 has 1D cubic structure and KIT-6 has 3D network consisting of two interwoven nanochannels. TUD-1 is characterized by a foam-like mesoporous structure, which is disordered 3D network.[230]

Hollow MSNs have a larger pore size, around 100-150 nm, which has 3-15 times higher loading capacity than MCM.[239] As a result, lower amount of hollow MSNs are needed to achieve the desired cargos than MCM. Therefore, hollow MSNs have been widely used to deliver therapeutic drug recently.[240]

3.2.3 Application of MSN to detect IBD

Patients with IBD require long term management and frequent follow-up with their physician. The gold standard to detect and manage IBD is endoscopic evaluation to monitor inflammation and the procedure may be combined with biopsy to determine if there is cancerous growth.[241] However, this method is invasive and patients often experience pain and discomfort during these procedures, highlighting the need for a non-invasive and cost-effective technique to monitor inflammation. The concentration of fecal calprotectin is correlated with both endoscopic and histological inflammation scores in IBD.[241] Although a non-invasive procedure, the current assay for fecal calprotectin is not user-friendly and perceived as expensive for POC diagnosis. Here, we have explored the value of matrix metallopeptidase 9 (MMP-9) and tumor necrosis factor alpha (TNF-α) as alternative biomarkers. The level of MMP-9, a 92 kDa gelatinase, increases

during inflammation in IBD patients and is released into urine, stool and blood.[211, 212] TNF-α also increases during inflammation in serum.[242] The main goal of this study is to explore the correlation between concentrations of MMP-9, TNF-α and severity of colitis in IL10-/- mouse model, with a view to designing an effective tool for POC diagnostics for human IBD, since IL10-/- mouse model has similar condition with human IBD.

Here, we used MSNs to rapidly detect MMP-9 and TNF-α. First, we developed an assay using an MMP-9 substrate to cap MSNs; when MMP-9 in a sample is introduced, the enzyme opens the cap via cleavage of the substrate and the contents, i.e. the dye is released. A second assay was also developed, where TNF-α antibody is used to cap MSN; when samples containing TNF-α antigen is introduced, the antigen binds strongly to the antibody to open the cap and release the dyes.

3.3 Experiment Design

3.3.1 MMP-9 detection

We choose MCM-41 that is commercially available as the MSN because this MSN is well characterized and has been used in several studies[217, 218, 243]. For the cap, we chose an MMP-9 specific substrate, because MMP-9 specifically recognizes and cleaves the peptide sequence PLGMWSR[244]. Accordingly, to fully cap the pore of MSN, a peptide, PLGMWSRPLGMWSRPLGMWSR-pentynoic acid (peptide P), containing three repeats of the MMP-9 substrate, PLGMWSR, and pentynoic acid at the end for pore capping was designed[243]. This peptide P contains an alkyl group, which can be attached on the surface of MSN by click reaction with azide group on the MSN. We choose three repeating units of the peptide to ensure minimal leakage of the dyes from the pores of MSN. In this system, the alkyne group of pentynoic

acid reacts with the azide group modified on the surface of MSN and the cargo within the pore is released after peptide cleavage (**Figure 3.14**)

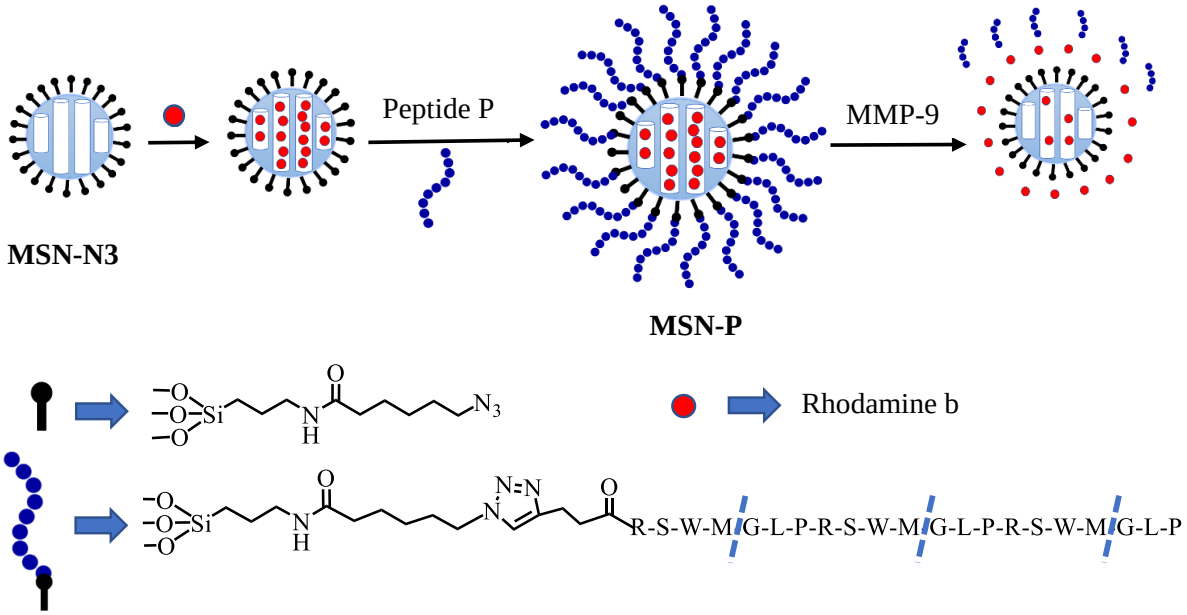

Figure 3.14 *Experimental design of MMP-9 substrate capped MSN. The external surface of MSN was modified by azide group, rhodamine b was loaded and capped using the peptide substrate. Introduction of MMP-9 releases the dye by cleaving the substrate.*

3.3.2 TNF-α detection

First, the MSN surface was modified with (3-Aminopropyl) triethoxysilane (APTES) to generate **MSN-NH2** that was positively charged in PBS buffer. **MSN-NH2** was subsequently suspended in fluorescein solution to load the dye via diffusion. Next, negatively charged TNF-α antibody was added for capping of **MSN-NH2** via electrostatic interactions. The presented TNF-α antigen could bind the antibody, open the gate and release the dye, which was detectable via fluorescence. (**Figure 3.15**)

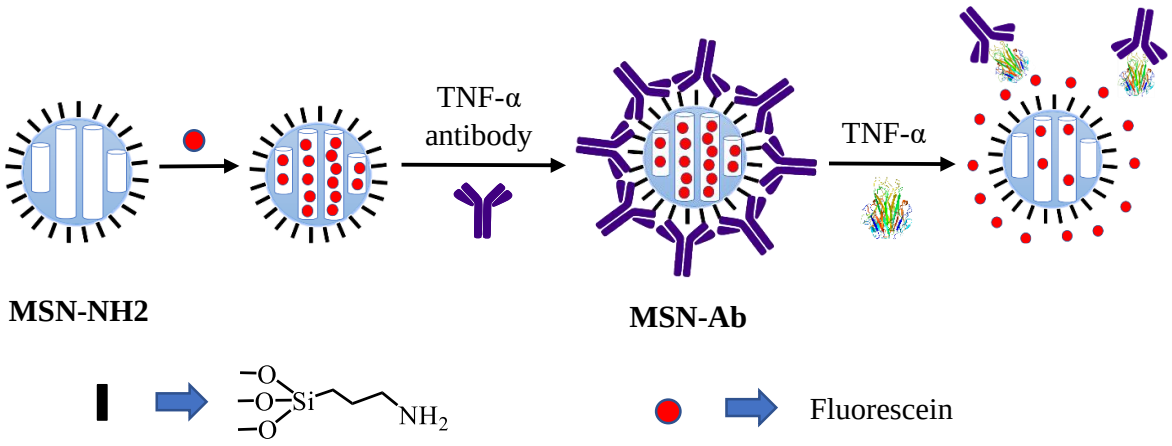

Figure 3.15 *Experimental design of TNF-α antibody capped MSN. MSN was modified by (3-aminopropyl) triethoxysilane (APTES) to afford MSN-NH2. After loading the dye, negatively charged TNF-α antibody was used to cap the nanoparticles. Introduction of TNF-α antigen results in tight binding of the antibody to the antigen and opens to cap to release the dye.*

3.4 Results and Discussions

3.4.1 Association between MMP-9 and TNF-α level with IBD severity.

MMP-9 detection with IL10-/- mouse model. First, we established the concentration of MMP-9 to monitor inflammation in wild-type and IL10-/- mice. IL10-/- mouse model is a genetic model that spontaneously develop colitis with age.[245] Mice fecal samples of wild-type (mice without colitis) and IL10-/- (with colitis) groups were detected with InnoZyme™ Gelatinase (MMP-2/MMP-9) Activity Assay kit. The results showed MMP-9 level in IL10-/- mice was significantly higher than that in the wild-type group (**Figure 3.16**). The mean MMP-9 levels were 18 ± 3 ng/ml (n = 3) in wild type mice and 31 ± 8 ng/ml (n = 3, $P < 0.05$) in IL10-/- mice. Next, we compared MMP-9 levels among IL10-/- mice of different ages, before (4 weeks-old) and after mice developed colitis (14 weeks-old) with the assay kit. The severity of colitis increased with ages of IL10-/- mice.[245] The mean MMP-9 levels were 12 ± 20 ng/ml (n = 8) and 28 ± 22 ng/ml

(n = 8, P < 0.005) in 4 week old mice and 14 week old mice, respectively, which shows that MMP-9 levels were higher with increasing severity of colitis (**Figure 3.17**). Fecal samples of IL10-/- mice treated with anti-TNF-α antibody, which is commonly used to treat IBD[246, 247], and non-treated IL10-/- mice that developed colitis were further compared (**Figure 3.18)**. Non-treated mice had higher levels (28 ± 22 ng/ml, n = 8) of MMP-9 than treated mice (7 ± 6 ng/ml, n = 8, P < 0.05), confirming that the MMP-9 concentration is correlated to severity of colitis. Taken together, these studies confirm that POC diagnostics that monitor MMP-9 levels could be used to monitor inflammation associated with IBD.

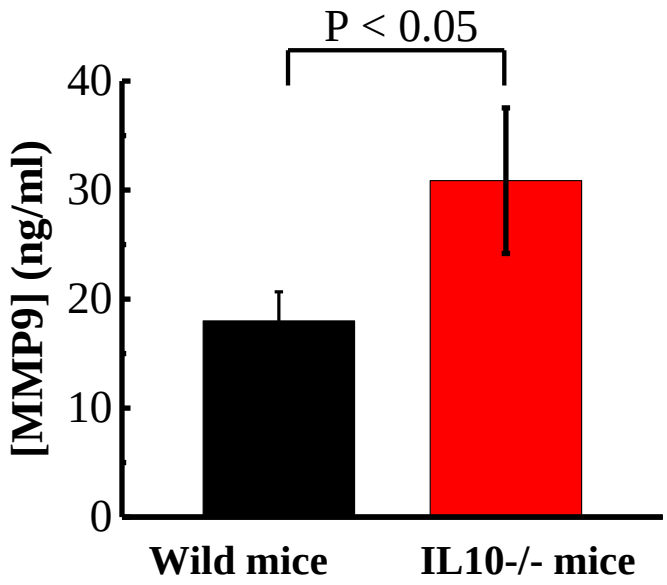

Figure 3.16 *The difference of fecal MMP-9 between wild mice (black column) and IL10-/- mice (red column) at 14 weeks-old, detected by fluorescence. The mean concentration of fecal MMP-9 in IL10-/- mice (31 ± 8 ng/ml, n = 3) is significantly higher than wild mice (18 ± 3 ng/ml, n = 3, P < 0.05). All experiments were performed in triplicate.*

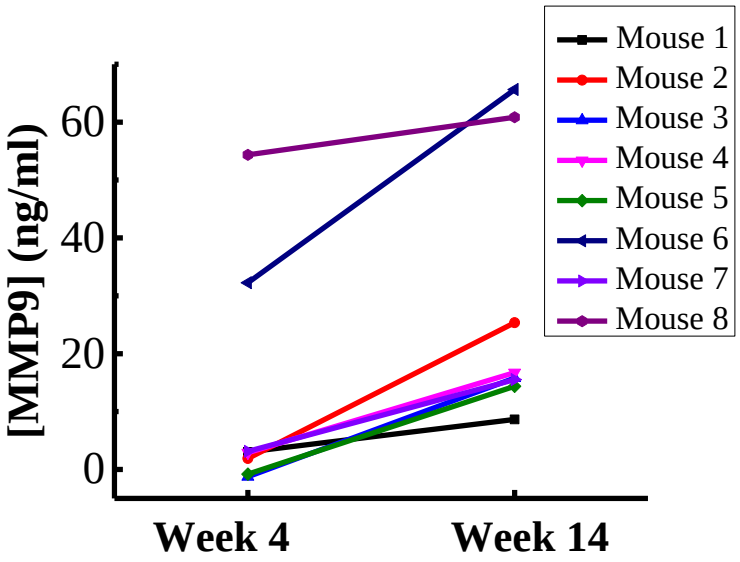

Figure 3.17 *The difference of fecal MMP-9 in different ages of IL10-/- mice. The mean concentration of fecal MMP-9 was detected by fluorescence at week 4 (12 ± 20 ng/ml, n = 8) and week 14 (28 ± 22 ng/ml, n = 8, P < 0.005). As age progresses, the concentration of fecal MMP-9 is higher. All experiments were performed in triplicate.*

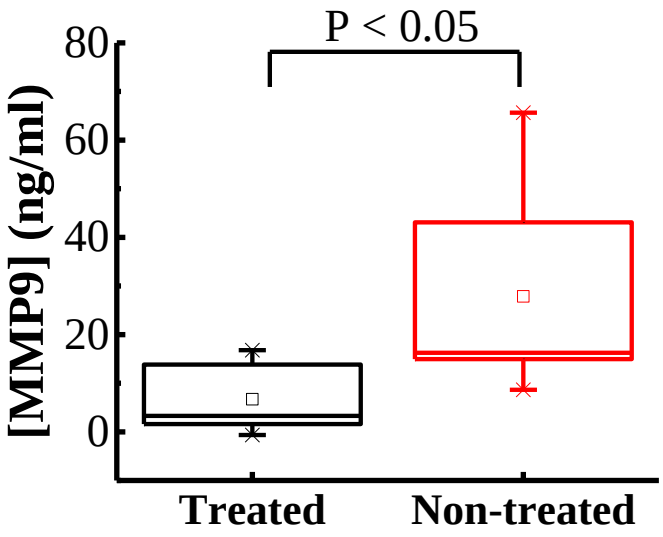

Figure 3.18 *The difference of fecal MMP-9 in anti-TNF-α treated and non-treated IL10-/- mice. The mean concentration of fecal MMP-9 in non-treated mice (red box, 28 ± 22 ng/ml, n =*

8) is higher than in anti-TNF-α-treated mice (black box, 7 ± 6 ng/ml, n = 8, P < 0.05). All experiments were performed in triplicate.

TNF-α detection with IL10-/- mouse model. We also established the serum TNF-α content increases with severity of IBD by comparing groups of mice of different ages, along with groups of anti-TNF-α-treated and non-treated IL10-/- mice. The differences in TNF-α levels in mice serum from different age groups (week 4 and week 14) are presented in **Figure 3.19** (Mean TNF-α concentration in week 4 vs week 14 = 1.0 ± 0.9 vs 4.7 ± 2.6 pg/ml, n = 7 vs 7, P < 0.01). Our data clearly revealed increasing TNF-α concentration in serum with severity of colitis. Differences in TNF-α levels in serum between anti-TNF-α treated and non-treated mice are presented in **Figure 3.20** (Mean TNF-α concentration in non-treated vs treated = 4.7 ± 2.6 vs 1.3 ± 1.5 pg/ml, n = 7 vs 7, P < 0.05). The mean serum TNF-α content was significantly higher in non-treated than treated mice in our experiments. Based on these findings, we propose that colitis conditions may be effectively evaluated by monitoring the serum TNF-α concentration.

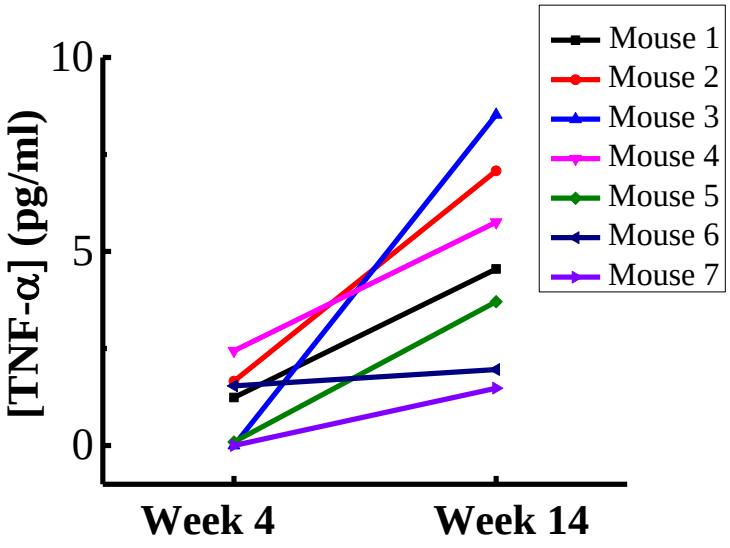

Figure 3.19 *The serum TNF-α concentration in different age of IL10-/- mice. The mean concentration of serum TNF-α was detected by purchased ELISA assay kit at week 4 (1.0 ± 0.9 pg/ml, n = 7) and week 14 (4.7 ± 2.6 pg/ml, n = 7, P < 0.01). As age progresses, the concentration of serum TNF-α is higher. All experiments were performed in triplicate.*

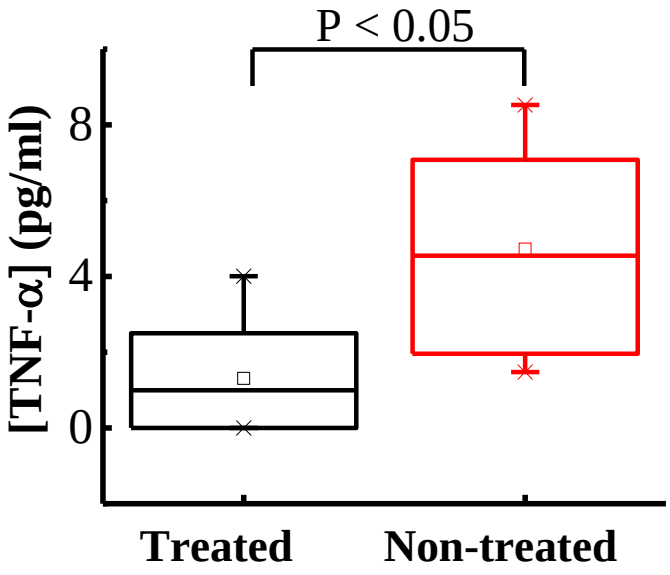

Figure 3.20 *TNF-α levels between anti-TNF-α treated and non-treated mice. The result shows that the concentration of serum TNF-α in non-treated mice (red box, 4.7 ± 2.6 pg/ml, n = 7) is significantly higher than treated mice (black box, 1.3 ± 1.5 pg/ml, n = 7, P < 0.05). All experiments were performed in triplicate.*

3.4.2 "Cap and release" MSN to detect MMP-9 and TNF-α.

After establishing the limit and range of detection of the two biomarkers, MMP-9 and TNF-α in wild type healthy and IL10-/- mice, we attempted to develop POC diagnostics to monitor inflammation associated with IBD.

MMP-9 detection. We examined rhodamine b release for MMP-9 substrate capped **MSN-P**. Briefly, 1 mg **MSN-P** was suspended in 1 ml PBS buffer and divided into two fractions, each containing 500 µg **MSN-P**. One fraction was treated with 50 µl PBS buffer as control and another with 50 µl (0.1 mg/ml) MMP-9. Both suspensions were incubated at 37°C and release of dye were detected at different time-points. The results are shown in **Figure 3.21**. Remarkable release of rhodamine b was observed in the presence of MMP-9 within minutes, while release was minimal in its absence. This demonstrates that the substrate cap was cleaved by MMP-9 to release the dye trapped in the pores of MSNs. To determine the limit of detection for MMP-9, we employed different concentrations for the release study (**Figure 3.22**). The limit of detection was measured as ~0.625 µg (1.1 µg/ml).

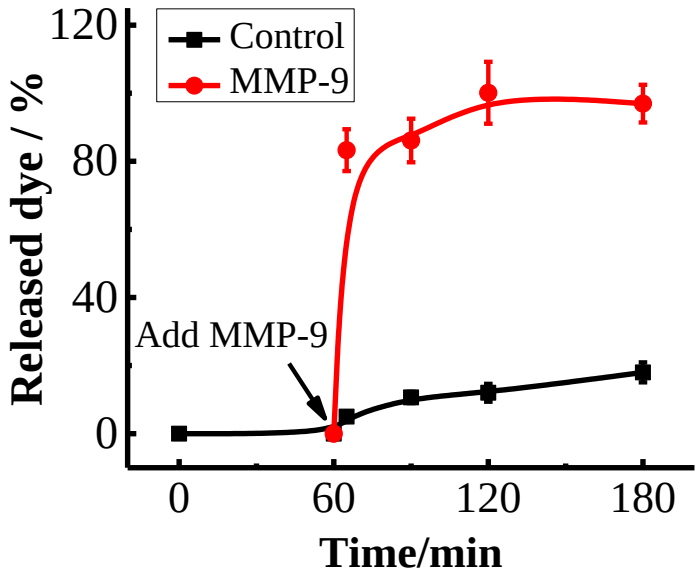

Figure 3.21 *Detection of MMP-9 using dye loaded MSNs. In the presence (red line, filled circles) of fecal MMP-9, dye release was significantly increased compared to the absence (black line, filled squares) of MMP-9. All experiments were performed in triplicate.*

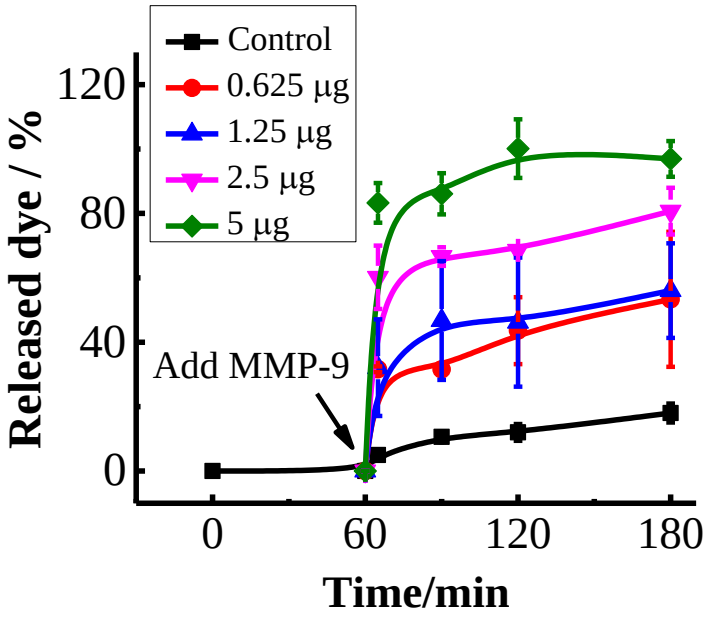

Figure 3.22 *The limit of detection for MMP-9. Different concentration of MMP-9 were used to detect the release in different time points (Control was shown in black line, filled squares; 0.625 µg MMP-9 was shown in red line, filled circles; 1.25 µg MMP-9 was shown in blue line, filled up triangles; 2.5 µg MMP-9 was shown in purple line, filled down triangles; 5 µg MMP-9 was shown in green line, filled diamonds). As the concentration of MMP-9 increases, the released dye will increase. The limit of detection was measured as ~0.625 µg (1.1 µg/ml). All experiments were performed in triplicate.*

TNF-α detection. We also examined the fluorescein release for TNF-α antibody capped MSNs, **MSN-Ab**. 1 ml suspended **MSN-Ab** in PBS was divided into two fractions, each containing 500 µl **MSN-Ab**. One fraction was treated with 12 µl PBS buffer as the control group and the other with 12 µl of 3 µg TNF-α antigen as the experimental group. Fluorescein release from both groups was detected at different time-points. Significant release was observed in the presence of TNF-α, while release was relatively small in its absence (**Figure 3.23**). Different

concentrations of TNF-α were used for the release study to measure the limit of detection (**Figure 3.24**). The data showed that the limit of detection was around ~0.5 µg (1 µg/ml).

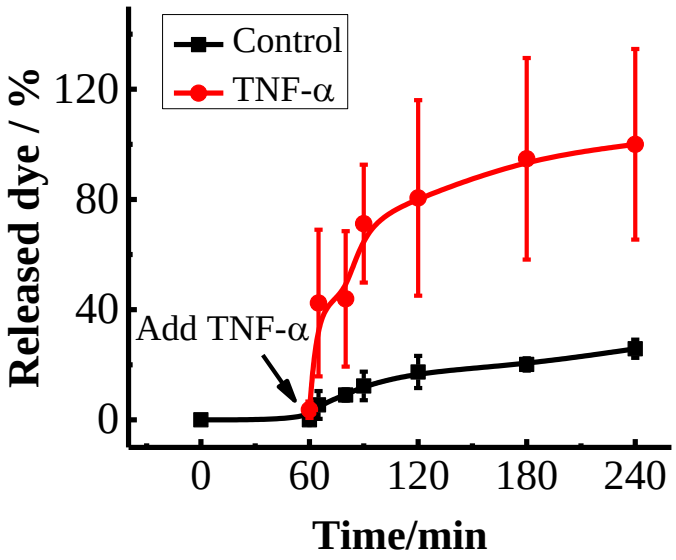

Figure 3.23 *Detection of TNF-α using dye loaded MSNs. The release study in the absence and presence of TNF-α. The released dye was significant in the presence (red line, filled circles) of TNF-α, while negligible release was found in the absence (black line, filled squares) of TNF-α. All experiments were performed in triplicate.*

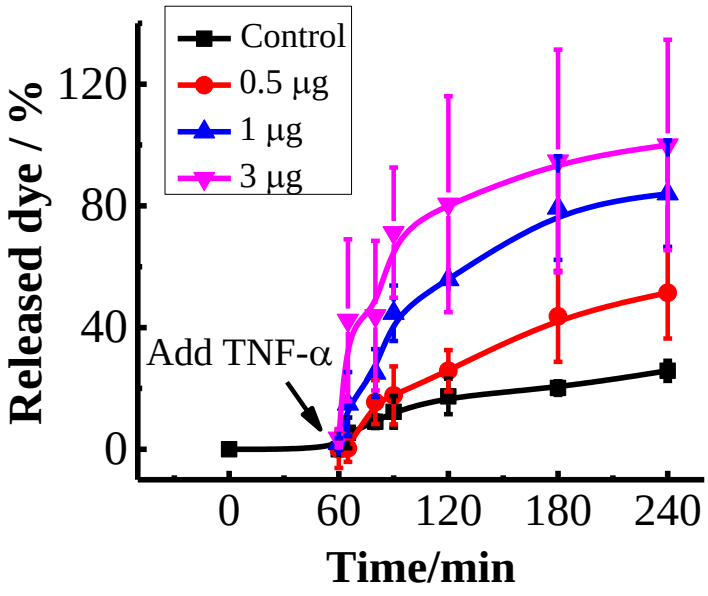

Figure 3.24 *The limit of detection for TNF-α. Different concentration of TNF-α were used to detect the release in different time points (Control was shown in black color, filled squares; 0.5 μg TNF-α was shown in red line, filled circles; 1 μg TNF-α was show in blue line, filled up triangles; 3 μg TNF-α was shown in purple line, filled down triangles). As the concentration of TNF-α increases, the released dye will increase. The limit of detection was ~0.5 μg (1 μg/ml). All experiments were performed in triplicate.*

3.5 Conclusion

IBD is an inflammatory disease of the gastrointestinal tract. IBD patients have to visit their physicians regularly to monitor inflammation and the typical procedure is endoscopy, which causes significant distress and discomfort to the patient. Additionally, inflammatory flareups have been determined to a variety of reasons, that includes stress, environmental factors, etc. which makes dosing of medication difficult for personalized medicine. If suitable biomarkers were identified in ex-vivo body fluids, it would lead to an increase in research efforts to develop POC diagnostics. Here, we investigated the association between fecal MMP-9 and serum TNF-α level

due to inflammation using an established IL10-/- mouse model that has been used to determine IBD severity.[245, 248] We found that these two biomolecules could be potentially used to monitor inflammation in IBD. We also developed assays to detect fecal MMP-9 and serum TNF-α. While the assays establish proof of concept that dye loaded MSNs can be used to monitor biomarker concentration and could be readily developed to POC diagnostics that requires minimal sample pretreatment, the limit of detection is higher. Efforts to improve sensitivity is currently underway and these studies will be reported soon.

In the future, we will work on the amplification of this system. We are going to load cysteine instead of dye into MSN, the released cysteine can activate caged papain and produce a series of enzymatic reaction to amplify the signal. Papain is a proteolytic enzyme that has a thiol group at its active site, which can be modified conveniently by mixing with methyl methanethiosulfonate to generate caged papain (papain-S-S-CH_3).[249] The thiol group from cysteine can react with caged papain result in the formation of active papain (papain-SH).[250] The active form of papain can catalyze chromogenic substrate and release fluorophore (**Figure 3.5**). According to this method, the signal can be amplified.

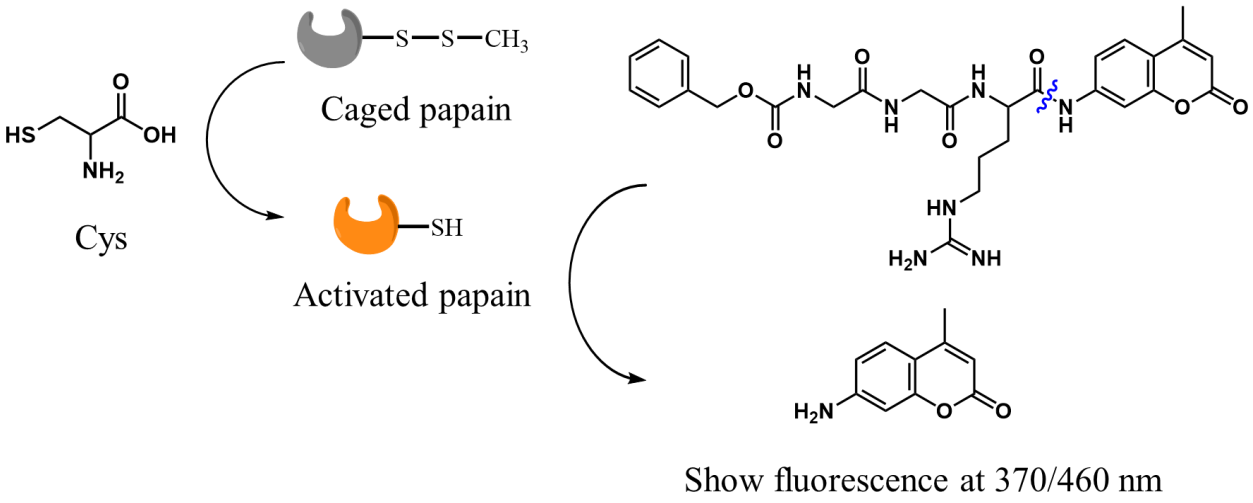

Figure 3.25 *Amplification of MSN signal.*

3.6 Experimental

3.6.1 MMP-9 and TNF-α concentration detection.

Materials: InnoZyme™ Gelatinase (MMP-2/MMP-9) Activity Assay kit (CBA003), Recombinant, active human MMP-9 (PF140), MCM-41 type mesostructured silica (CAS#: 7631-86-9), (3-Aminopropyl) triethoxysilane (APTES, CAS#: 919-30-2) were purchased from Sigma. TNF alpha Mouse ELISA Kit, High Sensitivity (Catalog#: BMS607HS) was purchase from Thermo Fisher Scientific. Wild mice and IL10-/- mice serum, fecal samples were obtained from Didier Merlin (Georgia State University)'s lab.

MMP-9 and TNF-α activity detection: 1000 ng/ml, 50 µl of MMP-9 enzyme was prepared, then 2-fold serial dilute 6 times with PBS buffer in 96 well plate. Followed by adding 30 µM, 50 µl MMP-9 substrate. The mixture was incubated in 37 ℃ for 3 h, then was detected fluorescence at 320/405 nm for 3 times. The standard curve for MMP-9 activity was shown in **Figure 3.26A**. TNF alpha Mouse ELISA Kit, High Sensitivity was used for TNF-α activity detection and the manufacturer's instructions was followed for the experiment. The standard curve for TNF-α activity was shown in **Figure 3.26B**.

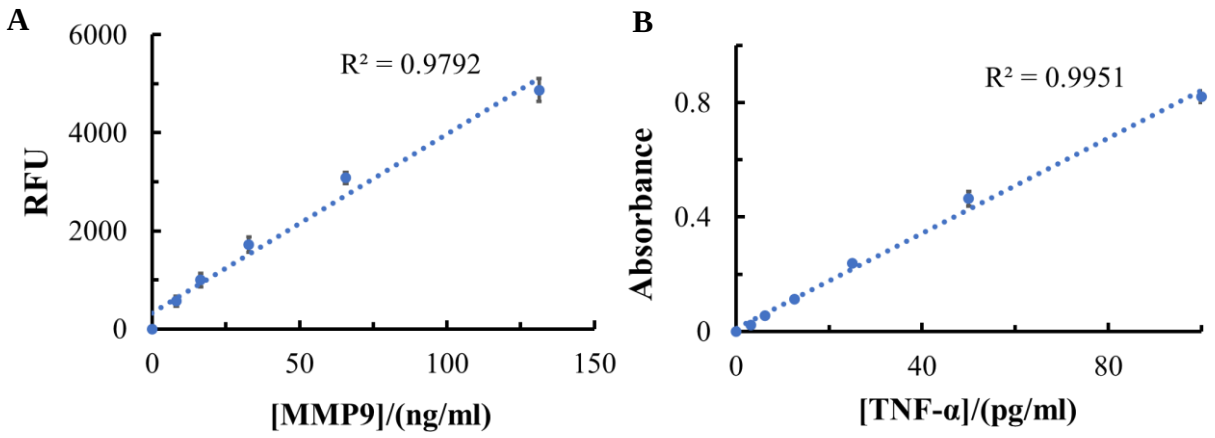

Figure 3.26 *Standard curve. A. Standard curve for MMP-9 activity; B. Standard curve for TNF-α activity. All experiments were performed in triplicate.*

Assays with mice fecal and serum samples: The mice feces were prepared as 100 mg/ml solution in PBS buffer, vortexed for 15 min, centrifugated in 14,000 g for 10 min and the supernatant was collected for experiment. Next, 20 µl of fecal sample was mixed with MMP-9 substrate to a total volume of 100 µl, MMP-9 substrate final concentration was 15 µM. The mixture was incubated in 37℃ for 3 hours and fluorescence was detected at 320/405 nm.

Mice serum samples 50 µl were used for TNF alpha Mouse ELISA Kit, High Sensitivity, Thermo Scientific, to detect TNF-α concentration in accordance with the manufacturer's instructions.

3.6.2 Fabrication and characterization of MSNs.

I. Chemical synthesis

General: Chemical reagents were of analytical grade, used as supplied, without further purification unless indicated. Analytical thin layer chromatography (TLC) was performed on silica gel 230-400 mesh (Silicycle, Quebec City, Canada). Plates were visualized under UV light, and/or by staining with acidic $CeH_8Mo_3N_2O_{12}$, followed by heating. 1H and 13C NMR spectra were recorded on Bruker 400 MHz spectrometer. Chemical shifts are reported in δ (ppm) units using 13C and residual 1H signals from deuterated solvents as references. Spectra were analyzed with MNova® (Mestrelab Research, Escondido, CA, USA).

Abbreviations: Sodium azide, NaN_3; Dimethylformamide, DMF; (3-Aminopropyl) triethoxysilane, APTES; MCM-41 type mesostructured silica, MCM-41; 2-(1H-benzotriazol-1-yl)-1,1,3,3-tetramethyluronium hexafluorophosphate, HBTU; N, N-Diisopropylethylamine,

DIPEA; Dichloromethane, DCM; Methanol, MeOH; Sodium sulfate, Na_2SO_4; Sodium metabisulfite, $Na_2S_2O_5$.

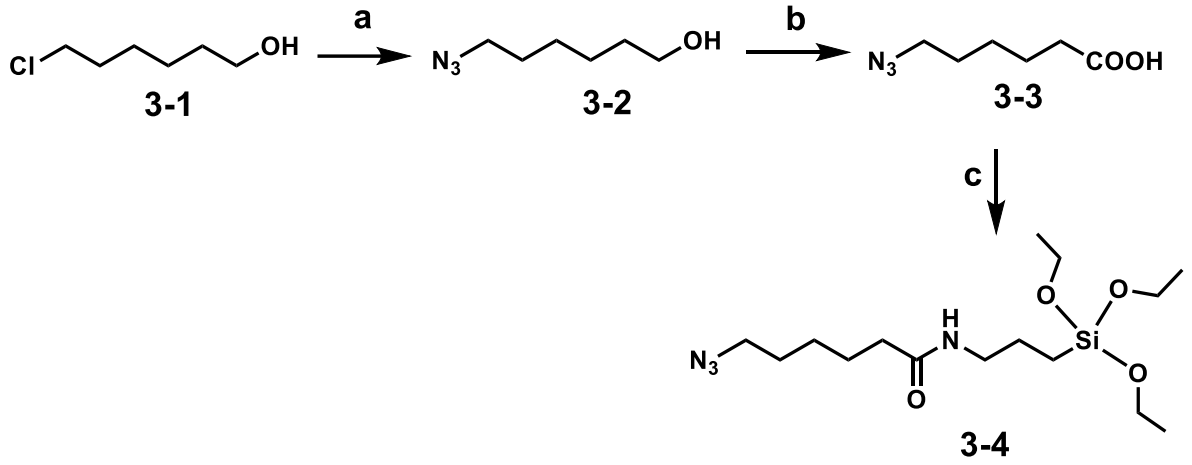

Scheme 3.1 *Reagents and Conditions:* (a) NaN_3, DMF, 80 °C, 12 h, 98%;[251] (b) 1M Jones' Reagent, acetone, 0°C-RT, 3 h, 99%;[251] (c) APTES, HBTU, DIPEA, DCM, RT, 16 h, 50%.[252]

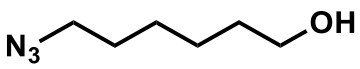

6-azidohexan-1-ol. To the solution of **3-1** (2.00 g, 11.86 mmol) in anhydrous DMF (10 mL) was added NaN_3 (1.08 g, 16.60 mmol), the reaction was stirred at 80 °C for 12 h. After completion of the reaction (TLC), the mixture was washed with deionized water, and the aqueous layer was extracted with ethyl acetate. The organic layers were collected, dried over Na_2SO_4, and concentrate under reduced pressure to afford **3-2** as a colorless oily material (1.96 g, 11.62 mmol, yield=98%).

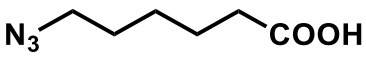

6-azidohexanoic acid. To the solution of chromium (VI) oxide (0.99 g, 9.92 mmol) in deionized water (7.72 mL), concentrated sulfuric acid (2.20 mL) was added dropwise at 0°C to form 1M Jones' Reagent. The Jones' Reagent was added to the solution of **3-2** (0.35 g, 2.48 mmol) in anhydrous acetone (7.72 mL) at 0 °C. The reaction was stirred at RT for 3 h. After completion

of the reaction (TLC), the mixture was washed with saturated $Na_2S_2O_5$ solution and 2M HCl at 0 °C, and the aqueous layer was extracted with ethyl acetate. The organic layers were collected, dried over Na_2SO_4, and concentrated to afford **3-3** (0.39 g, 2.46 mmol, yield=99%).

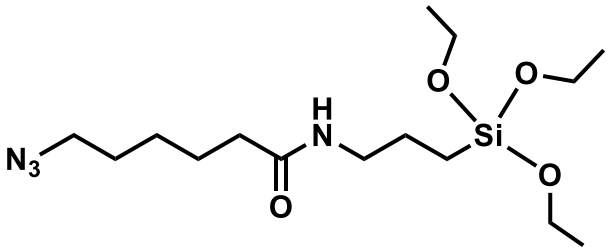

6-azido-N-(3-(triethoxysilyl)propyl)hexanamide. 3-3 (0.39 g, 2.46 mmol), HBTU (1.13 g, 2.98 mmol) and DIPEA (1.30 mL, 7.44 mmol) were successively dissolved in anhydrous CH_2Cl_2, and stirred under N_2 at RT for 30 min. Then APTES (0.70 mL, 2.98 mmol) was added, the mixture was stirred at RT for 16 h. After completion of the reaction (TLC), the crude product was purified by column (EtOAc:Hexane=1:1) to afford **3-4** as a colorless oily material (0.45 g, 1.25 mmol, yield=50%). 1H NMR (600 MHz, $CDCl_3$) δ 5.82 (s, 1H), 3.82 (q, J = 7.0 Hz, 6H), 3.37 – 3.17 (m, 4H), 2.17 (t, J = 7.5 Hz, 2H), 1.96 (s, 1H), 1.78 – 1.55 (m, 6H), 1.41 (ddd, J = 18.6, 8.9, 6.1 Hz, 2H), 1.23 (t, J = 7.0 Hz, 9H), 0.73 – 0.58 (m, 2H).

II. Fabrication and characterization of MSNs.

Synthesis of the MMP-9 substrate gated material. 6-Azido-N-(3-(triethoxysilyl) propyl) hexanamide was synthesized according to **Scheme 3.1**. The compound was characterized completely by ^{1}H-NMR and ^{13}C-NMR. Next, we modified MSN with 6-azido-N-(3-(triethoxysilyl) propyl) hexanamide. To this end, MCM-41 (0.1 g) was suspended in dry toluene (80 ml), following which 6-azido-N-(3-(triethoxysilyl)propyl)hexanamide (0.75 ml) was added and refluxed for 24 hours under nitrogen atmosphere[253]. The mixture was centrifuged at 10,000 rpm for 10 min, washed with toluene and methanol, and dried under vacuum to obtain **MSN-N3**.

To load the dye, a large excess of dye was used. 15 mg of **MSN-N3** was suspended in 2.5 ml of 2 mg/ml rhodamine b solution in DMF and stirred for 24 h. Next, 15 mg of peptide P, copper sulfate (11.24 mg) in 100 µL DI water, sodium ascorbate (17.83 mg) in 100 µL DI water and 500 µL t-butanol were added, and a microwave reaction was performed at 90℃ for 30 min.[254] The solution was centrifuged at 10,000 rpm for 5 min, washed with DI water and dried under vacuum to generate **MSN-P**. This material was washed extensively for twenty times was DI water followed by PBS buffer over ten days to remove dye that is adhered on the surface.

Synthesis of the TNF-α antibody gated material. First, to modify the surface of MSN with APTES, purchased MCM-41 (0.1 g) was suspended in dry toluene (80 ml) to which APTES (0.75 ml) was added, and refluxed for 24 hours under nitrogen atmosphere[253]. After the reaction, the mixture was centrifuged at 10,000 rpm for 10 min, washed with toluene and methanol, and dried under vacuum to generate **MSN-NH2**. The zeta potential of **MSN-NH2** was +14 mV while that of MSN was -28 mV (**Figure 3.27**), confirming that the surface was covered by the amino group. Next, 10 mg **MSN-NH2** was suspended in 2 ml of 200 µM fluorescein PBS solution and stirred for 24 hours, followed by the addition of 80 µl of 0.5 mg/ml TNF-α antibody and stirring for 6 hours. The mixture was centrifuged at 10,000 rpm for 5 min, washed with PBS buffer, and dried to generate **MSN-Ab**. As described previously, this material was washed extensively to remove excess dye.

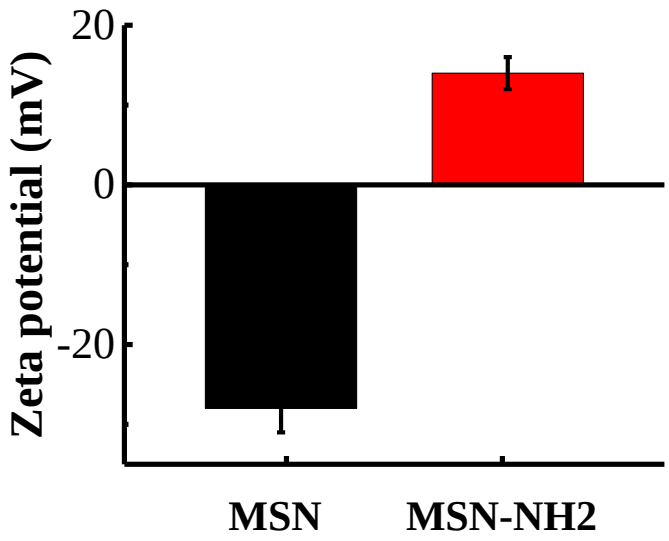

Figure 3.27 *Zeta potential of MSN and MSN-NH2. The black column represents the zeta potential of MSN is -28 mV, while red column represents the zeta potential of MSN-NH2 is +14 mV. It confirms that the surface of MSN-NH2 was cover by amino group. All experiments were performed in triplicate.*

4 CHAPTER 4 PROTEIN-GLYCAN INTERACTIONS: BINDING OF DIFFERENT NOROVIRUS VLPS TO A PANEL OF HISTO-BLOOD GROUP ANTIGENS

* Most of the work described in this chapter has been submitted in two publications and one more publication is in preparation:

1. Abasaheb N. Dhawane, Marta Diez-Valcarce, Bharat P. Gurale, Hieu Dinh, Jan Vinjé*, and Suri S. Iyer*. Synthesis and Evaluation of Biotinylated Bivalent HistoBlood Group Antigens for Capturing Human Noroviruses. *Bioconjug Chem* **2016,** *27* (8), 1822-9.

2. Amy E. Kirbya*, Yvonne Kienast, Milagros Aldeco, Molly Steele, Abasaheb Dhawane, Dandan Liu, Xikai Cui, Amrita Das, Suri S. Iyer* and Christine L. Moe. Snow Mountain Virus Recovery by Synthetic Human Histo-Blood Group Antigens is Heavily Influenced by Matrix Effects. *Scientific Reports*, **2020**, 10 (1), 4661.

3. Dandan Liu, Abasaheb N. Dhawane, Xiaohu Zhang, Xikai Cui, Marta Diez-Valcarce, Jan Vinjé, Xinqiu Yao, Donald Hamelberg and Suri S. Iyer*. Protein-Glycan Interactions: Binding of Different Norovirus VLPs to a Panel of Histo-Blood Group Antigens. Manuscript in preparation.

4.1 Norovirus Introduction

4.1.1 Norovirus epidemiology

Human noroviruses are the major cause of most epidemic outbreaks of gastroenteritis, leading to 218,000 deaths in children younger than five and 1.1 million hospitalizations worldwide each year.[255] Norovirus outbreaks typically occur in the winter months. . People infected by norovirus have severe nausea, vomiting and watery diarrhea within 12–24 hours exposure of

norovirus, which may lead death to severely immunocompromised people.[256] The outbreak was first described by Zahorsky, J. as 'winter vomiting disease' in 1929 due to its seasonal incidence and vomiting symptom.[257] The main route transmission is fecal-oral transmission, other transmission routes including food, water and environment contamination.[255] Waterborne outbreaks was first reported by Kaplan, J. E. et al. in 1982.[258] Multiple water systems linked with norovirus outbreaks, including municipal water systems, commercial ice consumption and potable water at camps.[259-261] To rapidly identify norovirus break, a criteria has been developed by Kaplan, J. E. et al..[262] It includes vomiting in more than half of symptomatic cases; mean or median incubation period of 24 – 48 hours; mean or median duration of illness of 12 – 60 hours; no bacterial pathogen isolated in stool culture.

Table 4.1 *The criteria to identify norovirus outbreaks. The table is taken from publisher with permission.*[262]

	Criteria to identify norovirus outbreaks
1	vomiting in more than half of symptomatic cases
2	Mean or median incubation period of 24 – 48 hours
3	Mean or median duration of illness of 12 – 60 hours
4	No bacterial pathogen isolated in stool culture

4.1.2 Norovirus structural proteins

Norovirus belongs to *Caliciviridae* family, it has a positive single-stranded RNA, which encodes three open reading frames (ORFs).[263] ORF1 encodes the nonstructural proteins, ORF2 and ORF3 encodes structure proteins: major capsid protein VP1 and minor structural protein VP2 respectively.[264]

Major capsid protein VP1

There are 90 dimers of VP1 on the norovirus virion, which is composed of 530 – 555 amino acids.[265] It forms a T = 3 icosahedral symmetry virion with 180 molecules of VP1. VP1 contains two conserved domains, which defines strain specificity. And it consists two domains: shell (S) domain and protruding (P) domain, P domain can be further divided into P1 and P2 domain (**Figure 4.1**).[266] The S domain forms a scaffold centered the viral RNA, whereas P domain stabilize the capsid and interact with cells. It was found that P2 domain plays an important role in binding histo-blood group antigens in the process of infection.[267] It is difficult to proliferate norovirus in human cell culture[268], therefore, VP1 was used to assembles virus-like particles (VLPs) that mimic norovirus particles. To prepare VLP, a recombinant baculovirus containing VP1 coding genes was cultured in mammalian or insect cells.[269] The expressed recombinant protein self-assembles into VLP spontaneously, which preserve the structure and antigenicity of virions.

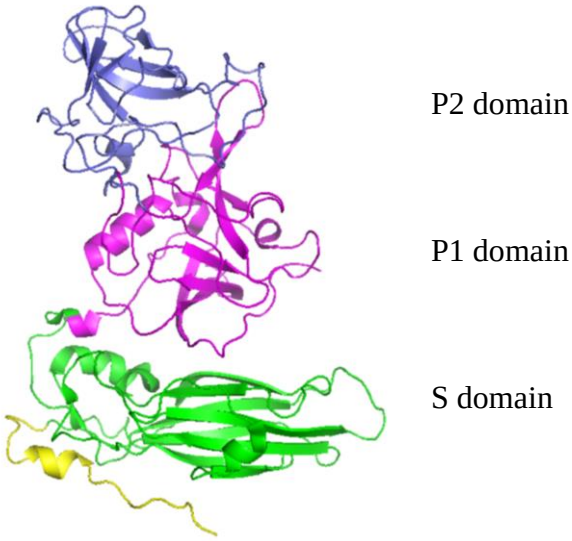

Figure 4.1 *Structure of VP1 monomer downloaded from NIH PDB database and PyMOL was used to show different domains (PDB: 6OUT).[270] P2 domain is shown in blue color, P1 domain*

is shown in purple color and S domain is shown in green color. There is a N-terminal arm shown in yellow color.

Minor capsid protein VP2

There are few copies of VP2 on the norovirus virion, which is consist of 208 – 268 amino acids. Although it is not necessary for recombinant VLP [271], it was found that absence of VP2 decreases the stability and size homogeneity of VLPs [272]. If both VP1 and VP2 coding genes were involved in the assembly of VLPs, the expression of VLPs increases.[273] VP2 is also essential for the production of infectious virions of feline calicivirus.[274] The lack of VP2 crystal structure makes it difficult to study more functions of it.

4.1.3 Histo-blood group antigens (HBGAs)

It was found that norovirus recognize human HBGAs as receptor when it infects humans.[275] Different types of norovirus bind to HBGAs with high diverse patterns. Studies on the binding patterns of norovirus with HBGAs are important for diagnostics and treatment of norovirus infection.

Studies on the interaction between norovirus and HBGAs have concentrated on the ABO, H, Lewis blood group antigens.[276] Different blood group systems were formed by adding specific carbohydrates to an oligosaccharide precursor that bind to lipids or proteins. Basically, there are four types of core structures carry ABH antigen activity[277] as shown in **Figure 4.2**. Type 1 and type 2 precursors are linked to proteins or lipid linked oligosaccharides, type 3 are linked to oligosaccharides, while type 4 are linked to lipids.[278] Glycosyltransferases are responsible for the synthesis of different types of antigens. Two different α(1,2) fucosyltransferases FUTI and FUTII add a fucose to the precursor by α1-2 linkage to form H type antigen.[279] FUTI comes from *H* gene in hematopoietic tissues, which has a high preference for type 2 and type 4 precursor chains; while

FUTII comes from *Se* gene in secretory tissues, which has a high preference for type 1 and type 3 precursor chain.[279] A type antigen was synthesized by adding galactosamine to the H type antigen by α(1,3) N-acetylglucosaminyltransferase. Whereas, B type antigen was synthesized by adding galactose to the H type antigen by α(1,3) galactosyltransferase.[280] Synthesis of Lewis (Le) antigen involves another type of fulcosyltransferase, for instance, Le a and x are synthesized by adding a fucose to N-acetylglucosamine with α1-4 or α1-3 linkage to the type 1 and type 2 precursor chains. Whereas, Le b and y are synthesized by adding a fucose to the same position to with α1-4 or α1-3 linkage to the type 1 and type 2 H type antigen.[281] The biosynthetic pathway was shown in **Figure 4.3.**

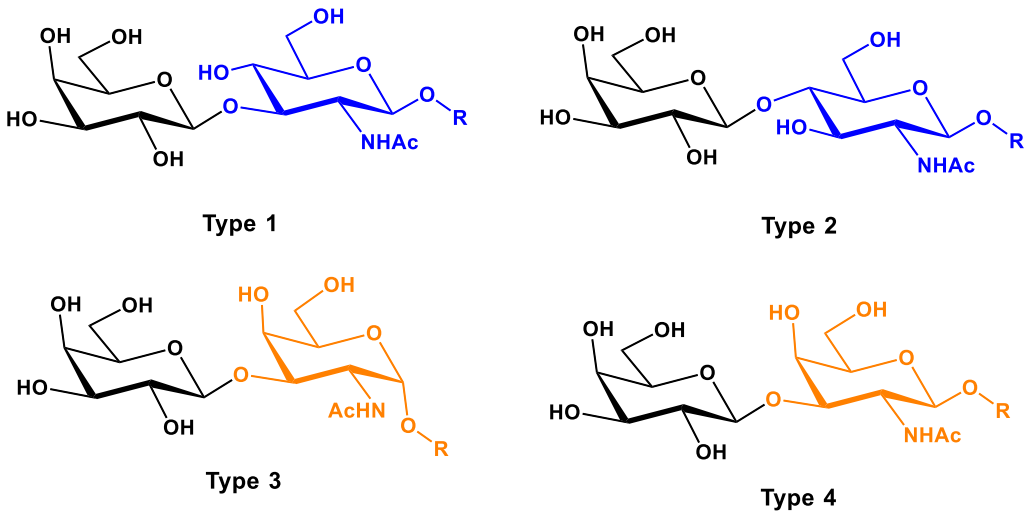

Figure 4.2 *Four types of precursor structures carrying ABH antigen. The differences between these structures were shown in different color, R represents lipid or protein. Type 1 shows a Gal β1-3 GlcNAc β1-R structure; type 2 shows a Gal β1-4 GlcNAc β1-R structure; type 3 shows a Gal β1-3 GalNAc α1-R structure; type 4 shows a Gal β1-3 GalNAc β1-R structure.*

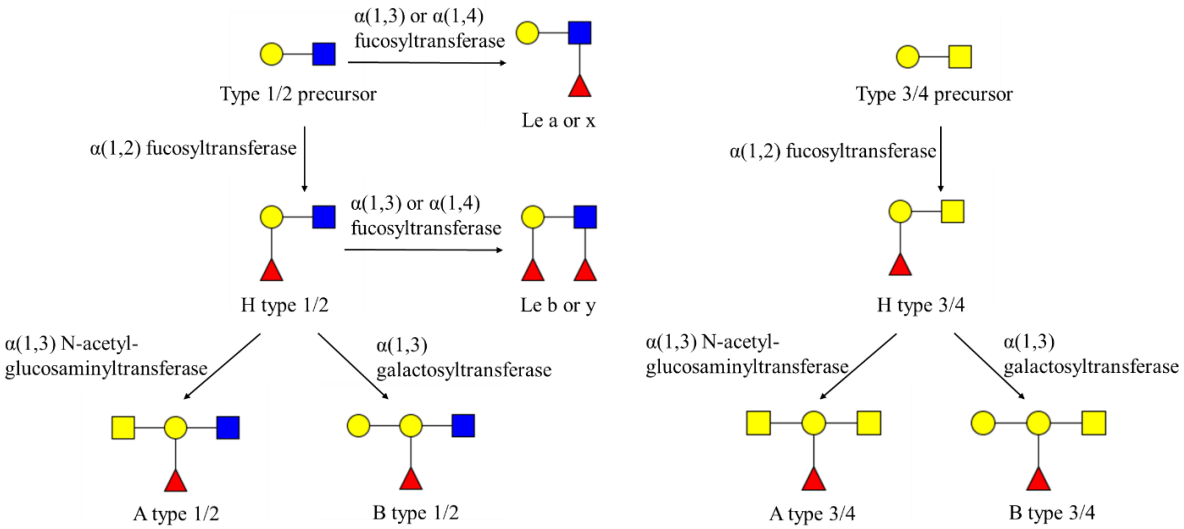

Figure 4.3 *Biosynthetic pathway for ABH and Lewis antigens. Yellow circle represents galactose; yellow square represents N-acetylglucosamine; blue square represents N-Acetylglucosamine; red triangle represents fucose. Figure is taken from publisher with permission.*[282]

4.1.4 Therapeutics of norovirus

There is no specific treatment for gastroenteritis caused by norovirus. Most people will recover in few days by preventing dehydration and controlling symptoms. One effective way to prevent norovirus outbreak is a vaccine. In recent years, several studies have been done to develop vaccine against norovirus by VLPs, however, a validated vaccine is still elusive.

4.1.5 Current diagnostics for norovirus

Norovirus antigen detection

Enzyme immunoassays. Several enzyme immunoassays (EIAs) have been developed commercially to detect norovirus in fecal samples, IDEIA Norovirus (Thermo Fisher Scientific, Basingstoke, UK) and Ridascreen Norovirus (R-Biopharm, Darmstadt, Germany) are most commonly used.[283, 284] Noroviruses are genogroup and genotype wildly diverse, the antibody

applied in the EIAs should be able to cross react with different genogroups and genotypes. Several studies have evaluated the value of commercial IDEIA Norovirus to detect norovirus in fecal samples.[285-287] The results showed that the sensitivity and specificity were ranged from 38.0% to 78.9% and 85.0% to 100.0% respectively. Similar as IDEIA Norovirus, the sensitivity and specificity of Ridascreen Norovirus were 32 – 92% and 65 – 100% respectively.[287-290] Multi samples test can increase the detection sensitivity of EIAs. Costantini, V. et al. have proved the sensitivity of IDEIA Norovirus increased from 44% by detecting 3 samples to 77% by detecting 5 samples per outbreak.[285] Therefore, a minimum of 6 outbreak samples is recommended for norovirus outbreak management.[291] The Ridascreen Norovirus third-generation test was approved by Food and Drug Administration (FDA) in 2011 to investigate norovirus outbreak. Compared to RT-PCR, enzyme immunoassay is more convenient and saving time.

Rapid immunochromatographic assays. A number of rapid immunoassays have been developed to detect norovirus antigen by lateral-flow immunochromatographic assays, which may provide as a POC tool. Ridaquick Norovirus (R-Biopharm, Darmstadt, Germany) and SD Bioline Norovirus (Standard Diagnostics, Inc., Kyonggi-do, South Korea) are most commonly used commercially available rapid tests.[292, 293] Studies have evaluated the sensitivity and specificity of Ridaquik Norovirus were 17 – 83% and 88 – 100% respectively.[292-294] For SD Bioline test, the sensitivity and specificity were 23 – 92% and 99 – 100% respectively.[295-297]

Molecular diagnostic tests

RT-PCR. RT-PCR is the golden standard for detection of different types norovirus. The first-generation RT-PCR assay used several primers based on only the first norovirus genome.[298, 299] It didn't perform well because the wild diversity of norovirus. The second-generation utilized sequences from different norovirus strains and the primers were designed by conserved regions of

the viral genome, which works well.[300, 301] other methods include, real time RT-PCR[286, 302], commercial RT-PCR[303, 304] and multiplex PCR/RT-PCR[305, 306]. Those methods improved the sensitivity and specificity of detection, and multiplex PCR/RT-PCR can detect hundreds of samples at one time. Overall, molecular test is more accurate than antigen test, however, the cost, need for trained personnel and equipment is prohibitive for low resource settings.

Summary

Taken together, there is a great need to develop alternate methods to accurately detect norovirus at POC. If POC were available, it would decrease morbidity and limit economic damage in an outbreak situation. Infected people could be isolated if identified early and economic activity could resume. As a first step towards the development of POC diagnostics, we studied the interactions between norovirus VLPs and its receptor, histo-blood group antigens. Our goal is to identify suitable glycoconjugates that could be used to capture norovirus in stool samples. Once identified, these glycoconjugates could be potentially be used in lateral flow assays similar to home pregnancy tests. A unique advantage of glycans is that these molecules can be produced in large quantities, are very stable in ambient conditions and can be characterized completely using NMR, mass spectroscopy and HPLC. Additionally, unlike antibodies, these small molecules can be easily and reproducibly conjugated to any diagnostic surface like nitrocellulose membranes or beads.

To identify suitable glycans that could bind to HBGAs, we choose SPR as the biophysical technique as this is a label free technique that is widely used to identify drugs, receptors and other small molecules. Described below is a primer on SPR, followed by a brief discussion on the synthesis of the glycans and the SPR studies. Also included computation studies that delineate some of the complex interactions between HBGAs and the synthetic glycoconjugates.

4.2 SPR Introduction

4.2.1 Principle of SPR

SPR is a label-free biosensing technique, and it can monitor the binding interaction in real time. All the interactions happen in the sensor chip, as shown in **Figure 4.4**. There's a prism in the bottom, a very thin gold was attached on the surface of the prism. The gold surface was coated with dextran or streptavidin, which can bind with ligand tightly. When the analyte flow through the ligand surface, it can catch analytes and give a signal. The principle of SPR involves total internal reflection and evanescent waves and surface plasmon.[307] When the light comes from higher refractive index medium to the lower refractive index, the total internal reflection can happen in the higher refractive index medium. This causes the formation of evanescent waves in the lower refractive index medium. The evanescent wave is enhanced when a gold film was put in the interface of two mediums and penetrate the gold film. The evanescent wave can excite the electron on the gold film, which makes the energy transfer from photon to metal electron. This phenomenon is called surface plasmon resonance. When it happens, the intensity of reflected light reduces, which can be captured by detector and express it as SPR response unit (RU) (**Figure 4.5**). When different analytes are injected to the solution, the refractive index of upper medium changes, the resonance angle θ will shift accordingly, which is detected as SPR signal (**Figure 4.6**).

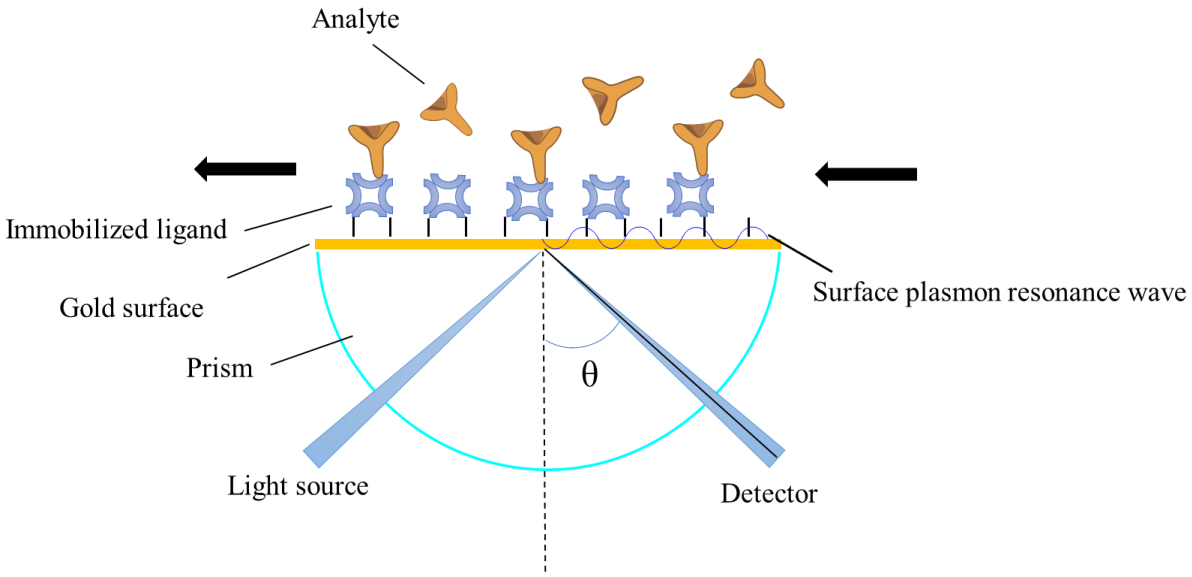

Figure 4.4 *Principle of SPR. The light source travels from prism to solution, the total internal reflection will happen in a certain angle. In this condition, the energy is transferred from photon to gold electron and results in the formation of surface plasmon resonance wave. Then a reduced reflection light beam can be detected by detector. When the analyte is injected in the solution and flow through the surface, the refractive index will change, which makes the change of refection angle. Figure is modified from publisher with permission.*[16]

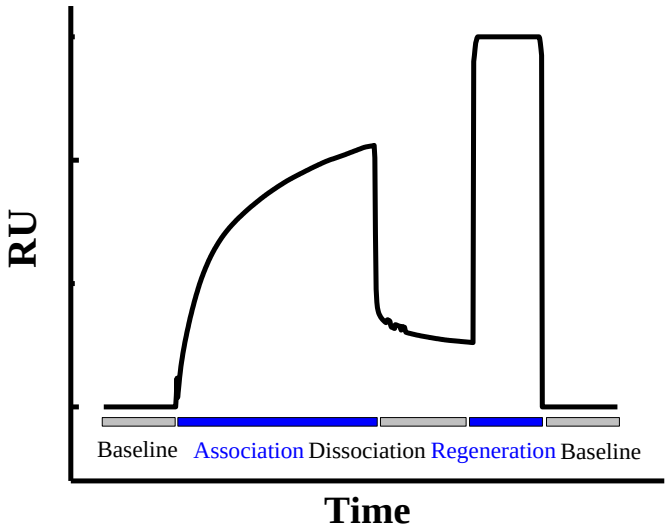

Figure 4.5 *SPR response unit changes as analytes binding and un-binding. When the buffer flow through the gold surface, it is shown as baseline in SPR. Continuous injection of analyte solution increase the RU, shown as association phase. After the injection stops, the RU decreases, which is shown as dissociation. Following, the regeneration solution is used to remove the bound analyte from the surface, the RU will go back to baseline and ready for next analyte to bind.*

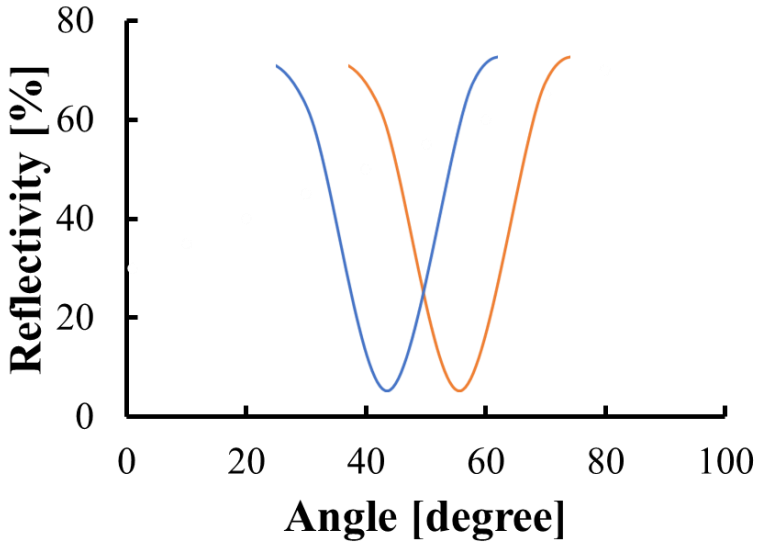

Figure 4.6 *SPR signal. The refractive index in the medium when analytes attached to the gold surface. The angle of reflection will change accordingly, which can be detected by detector and expressed as SPR signal response unit (RU). Figure is modified from publisher with permission.*[308]

4.2.2 Ligand immobilization

There are different types of chips coated with different materials on the surface available. Overall, they can be divided into two groups: covalent coupling sensor chips and capture coupling sensor chips. On the surface of covalent coupling sensor chips, they were coated with carboxymethylated dextran or no surface modification. Whereas, on the surface of capture

coupling sensor chips, they were coated with streptavidin, nitrilotriacetic acid (NTA), hydrophobic monolayer or lipophilic dextran. (**Table 4.2**)

Table 4.2 *Different type of sensor chips and their applications.*

Sensor types	**Sensor surface**	**Biocore chips**	**Applications**
Covalent coupling sensor chips	Gold	J1	Surface interaction and custom designs
	Carboxymethylated dextran	CM3, CM4, CM5, CM7	Protein-protein interaction and other molecules with amino groups
Capture coupling sensor chips	Streptavidin	SA	Capture biotinylated ligands
	NTA	NTA	Capture poly-histidine tagged ligands
	Hydrophobic monolayer	HPA	Capture lipid monolayers
	Lipophilic dextran	L1	Capture liposomes and lipid bilayers

For gold surface chips, sulfur and gold interaction is the most commonly used to immobilize ligand directly to gold surface. The thiol group will form strong bond with gold automatically, and the rest space of gold can be covered with thiolate PEG. Therefore, cysteine is widely used in the protein or peptide immobilization. By immobilizing protein, it can be used for protein-protein interaction.[309, 310] The surface of CM chips are coated with carboxymethylated dextran, which can interact with amino groups in protein or other molecules. Several intermediates are used to couple with exposed amino groups, such as aldehyde, epoxide and N-Hydroxy succinimide (NHS).[311] With covalent immobilization, the proteins immobilized are hardly inactivated by capture coupling, and the proteins are not necessary to be pure. Moreover, the covalent bond is strong, hard to dissociate in the process of regeneration.[312]

Capture coupling immobilization is based on the modification of the sensor chip to capture special tag modified proteins or molecules. Ligands are coated to the surface of gold and utilize the specific interactions between ligands and tags to immobilize target proteins or molecules. Streptavidin coated SA chips are widely used as non-covalent immobilization due to the high binding affinity between biotin and streptavidin (Kd ~10^{-14} M).[313] Some other affinity pairs have been used for the immobilization, such as chips coated with NTA is specific for histidine tag[314], coated glutathione is specific for S-transferase[315].

4.2.3 SPR applications

SPR has become a powerful technique in binding affinity detection. A lot of molecules can be involved in this detection, such as proteins, carbohydrates, lipids, nucleic acids, cells and small molecules. SPR is also used in other applications, including molecular interaction, conformational change analyses, mutation detection, drug and biomarker discovery.

SPR is widely used in the binding affinity analysis for different molecules, such as antibody-antigen[316], enzyme-substrate[317], ligand-receptor[318, 319], biomarker binding and drug discovery[320]. It also be used for determination of binding kinetics. The Langmuir model is widely used binding model to describe the interaction between ligand and analyte. Reaction rate (k_a and k_d) and equilibrium constant (K_D) are used to describe the interaction as shown in the following equation:

$$A + B \underset{k_d}{\overset{k_a}{\longleftrightarrow}} AB$$

The association constant k_a represents the formation rate of the complex AB, whereas the dissociation constant k_d represents the dissociation rate of AB. The detailed description of common constants is shown in **Table 4.3**.

Table 4.3 *Description of relevant kinetic parameters in SPR. The figure is taken from publisher with permission.*[321]

Constant	Definition	Description	Unit
Association rate constant, k_a	A + B ⟶ AB	Formation rate of the complex AB: number of AB formed per unit time at unit concentration of A and B	$M^{-1}s^{-1}$
Dissociation rate constant, k_d	AB ⟶ A + B	Dissociation rate of AB: number of AB dissociating per unit time	s^{-1}
Equilibrium association constant, K_A	$[AB]/[A][B] = k_a/k_d$	Association affinity	M^{-1}
Equilibrium dissociation constant, K_D	$[A][B]/[AB] = k_d/k_a$	Stability of AB	M

SPR can also be used verify conformational changes and mutation of proteins. SPR signal is strongly affected by optical thickness of metal film and the refractive index changes near the metal surface. When a protein goes through a conformational change, the optical indicators are also affected, which can be detected by SPR detector. Several studies have been used SPR to monitor structural transition in protein-small molecules interactions[322], proteins changes in different conditions[323, 324]. Han, S. H. et al. have detect mutation of protein p53 with SPR techinique.[325] It showed the RU of wild p53 was 4.7 higher than mutated protein each 100 nM.

4.3 Results and Discussions

4.3.1 Synthesis of the HBGA glycoconjugates: (Done by Dr. Abasaheb N. Dhawane, a former postdoctoral fellow in our group)

We developed biotinylated bivalent H, A and B-type glycoconjugates (**Figure 4.7**). The structure consists of two glycan headgroups, an aromatic scaffold that is relatively easy to

synthesize and a biotin, which allows conjugation to any streptavidin-coated surface. The spacers for these constructs were chosen to span the length of the binding sites in a P dimer, although we note that the glycan headgroups from a single glycoconjugate could bind to binding sites from two P subunits, which are not part of the P dimer.

The synthesis of the bivalent biotinylated H, A and B-type saccharides, and the scaffold is shown in schemes and the structures were confirmed by NMR. Our initial strategy was to synthesize the tri/tetrasaccharides bearing an azide group, followed by coupling with the alkyne bearing scaffold using Huisgen 1,3-dipolar cycloaddition conditions. The synthesis was completed after conjugation to an activated biotin, followed by deprotection of all protecting groups; however, this approach led to poor yields. We adopted an alternate strategy, where we coupled the biotin to the alkyne bearing scaffold before the cycloaddition reaction with tri/tetrasaccharides bearing an azide group followed by deprotection of protecting groups

Described in **Scheme 4.1** is an example of the complete synthesis of one of the target molecules. The details of the synthesis along with the complete characterization can be found in our publication (Dhawane, A. N. et al. *Bioconjugate Chemistry*).[326] Using this approach, a panel of chemically well-defined biotinylated glycoconjugates were synthesized and characterized. (**Figure 4.7**)

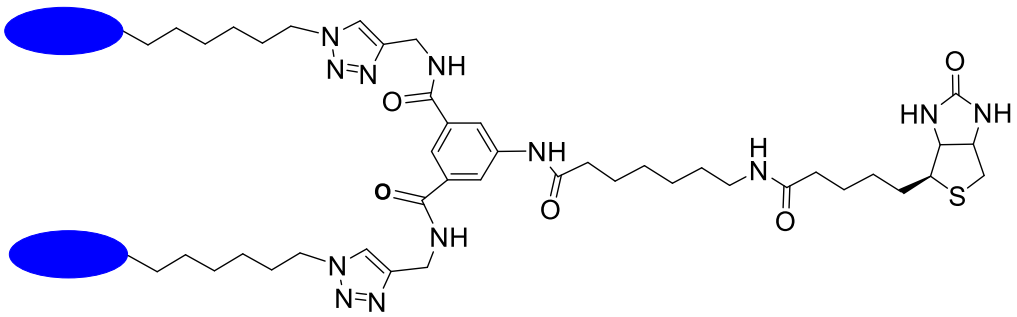

=

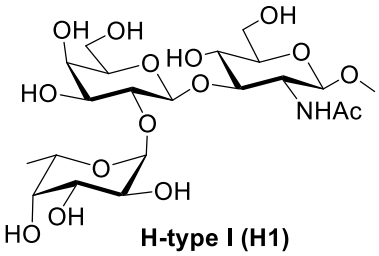

H-type I (H1)

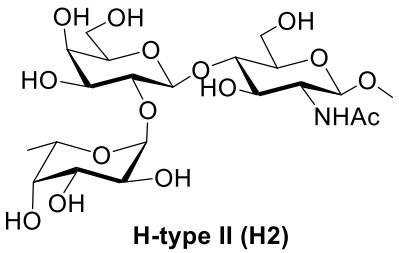

H-type II (H2)

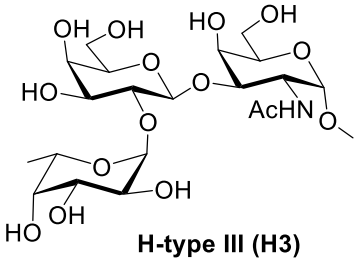

H-type III (H3)

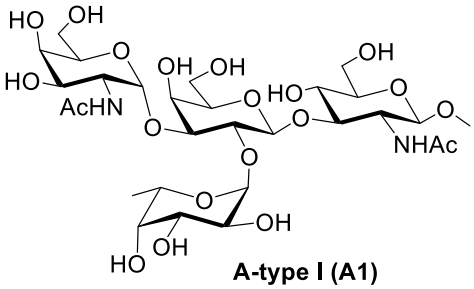

A-type I (A1)

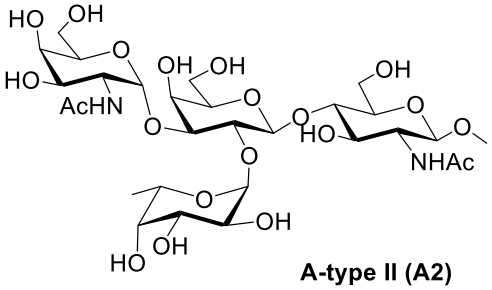

A-type II (A2)

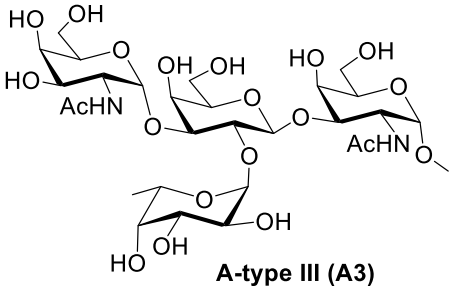

A-type III (A3)

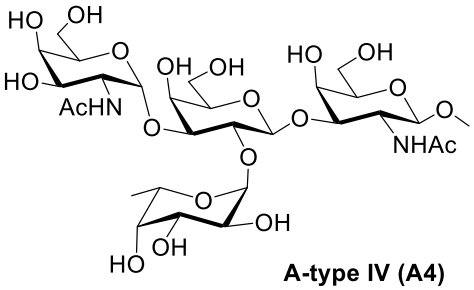

A-type IV (A4)

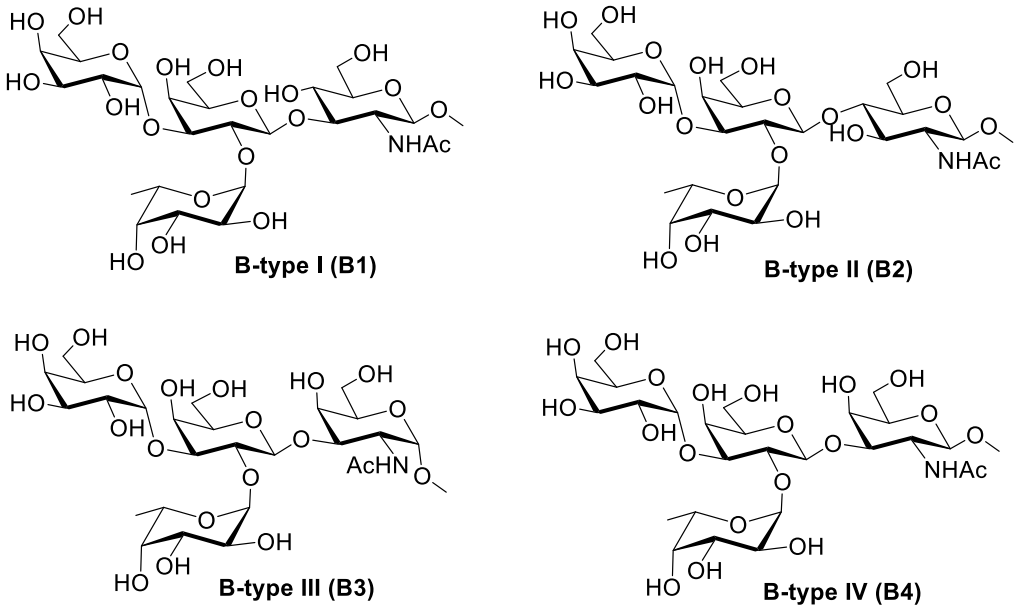

Figure 4.7 *Structures of the bivalent biotinylated H, A and B-type glycoconjugates. The blue ellipse represents the glycan headgroup and the spacer is a six-carbon spacer. The synthesis and characterization of most of the compounds has been reported in the Biconjugate Chemistry paper.*[326] *Figure is taken from publisher with permission.*[326]

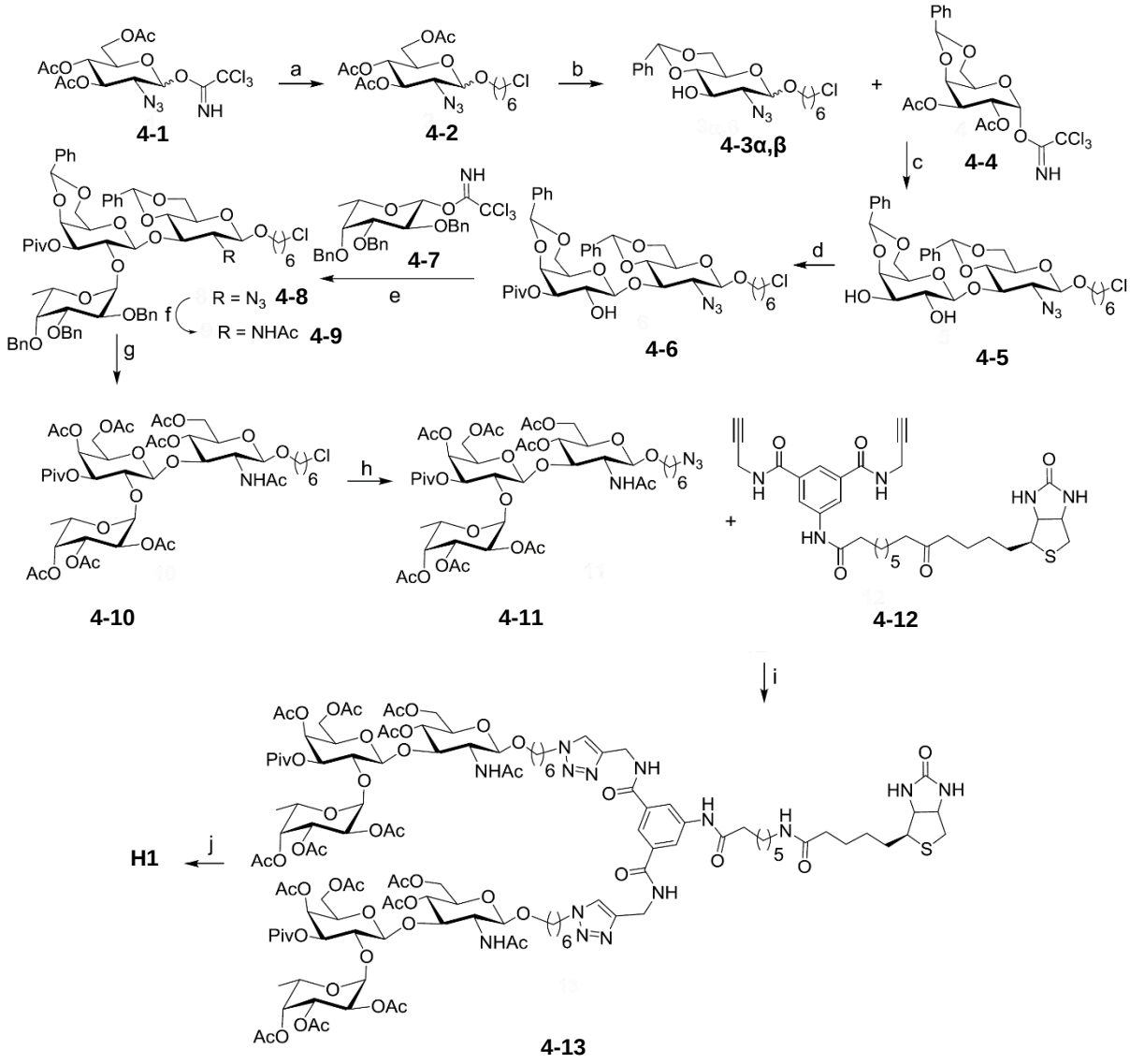

Scheme 4.1 *Reagents and Conditions*: a) 6-chloro hexanol, TMSOTf, DCM, 0°C-rt, 2h, 90%; b) i) $NaOCH_3$, MeOH, rt, 30 min, 85%; ii) $PhCH(OCH_3)_2$, CSA, ACN, rt, **3**α (28 %) and **3**β (41 %); c) i) TMSOTf, DCM, -40°C, 2h; ii) NaOMe, MeOH, rt, 1h; d) PivCl, pyridine, 45°C, 45 min., 75%; e) TMSOTf, Et_2O:DCM, -10°C, 60%; f) Zn dust, $CuSO_4$, Ac_2O, AcOH, rt, 3h, 75% g) i) $Pd(OH)_2/C$, H_2, ethyl acetate, rt, 4h; ii) Pyridine, Ac_2O, DMAP, 12h, 66% over two steps; h) NaN_3, DMF, 80°C, 90%; i) Cupric sulfate, Sodium ascorbate, *t*-BuOH:H_2O (7:3), rt, 24h, 80%; j) NaOMe, MeOH, rt, 12h, 75%.

4.3.2 SPR binding patterns for antigens

Next, we used SPR to detect the binding between glycoconjugates and VLPs. Biosensor sensor SA chip was used for the binding detection. The surface of SA chip was coated with streptavidin, which has very high binding affinity with biotin (Kd ~ 10^{-14} M).[313] The biotinylated antigens can be immobilized on the surface by binding with streptavidin. Afterwards, VLP can flow through the surface of the chip, if the VLP can bind with the antigens, the signal will increase, if the VLP does not bind with the antigens, the signal will not increase. After the binding experiment, the bound VLP can be removed by harsh condition, such as glycine solution with pH = 2.5. This step is called regeneration, which can move all the bound VLPs and bring the signal to the baseline. Hence, the chip can be reused to bind another VLP. The experiment design is shown in **Figure 4.8**.

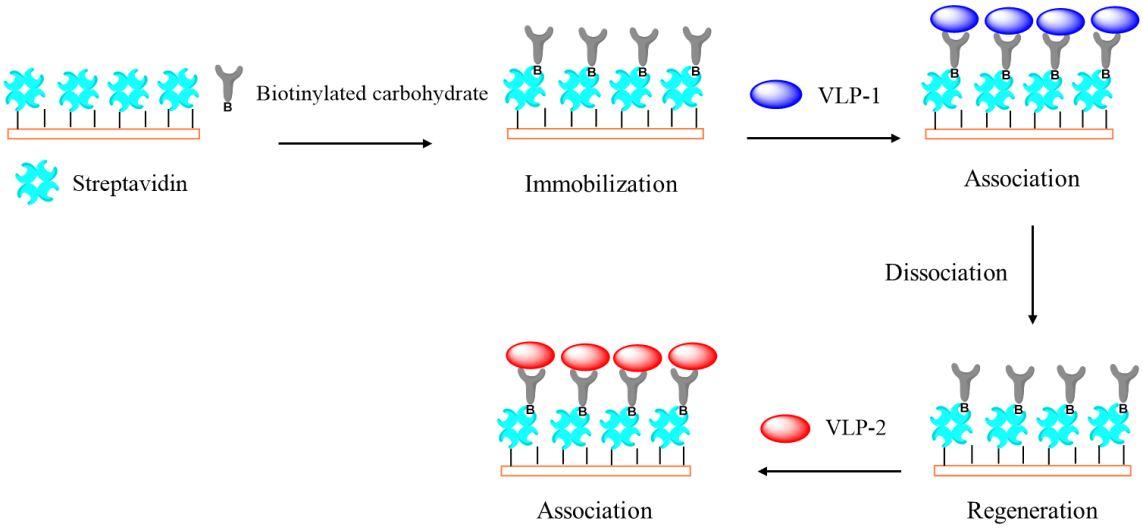

Figure 4.8 *Experimental design for detecting binding affinity of VLPs and biotinylated carbohydrate. The surface of SA chip was coated with streptavidin, biotinylated carbohydrate can bind with streptavidin with very high binding affinity. After immobilized with biotinylated*

carbohydrate, VLP-1 was flow through the surface to detect the binding affinity with the surface carbohydrate. Followed by regeneration to remove the bound VLP-1, the surface carbohydrate will be free to bind next VLP.

6 types of VLPs (GI.3, GII.2, GII.3, GII.4 New Orleans, GII.4 Sydney, GIV.1) were used to access the binding with the panel of glycans shown in **Figure 4.7**. The binding results for each VLP were shown in **Figure 4.9**. VLPs at 100 µg/ml concentration was injected for 300 seconds with flow rate of 5 µl/min. The increase in RU after 300 seconds is given in **Table 4.4**. The results showed that GI.3 VLP can bind with A4 with medium affinity (ΔRU = 689), while it binds with B2 (ΔRU = 1878) and B2 (ΔRU = 1958) with very high affinity and very weak affinity with B3 (ΔRU = 22) but it doesn't bind with H type antigens. The differences between A, B and H type antigens is that H type antigens are trisaccharide, while A type antigens have one more N-acetylgalactosamine attached in the end, B type antigens have one more galactose attached in the end. GII.2 VLP binds to A1 (ΔRU = 50) and A3 (ΔRU = 78) with weak affinity, no binding with B type and H type antigens. GII.3 VLP doesn't bind with any antigens. GII.4 New Orleans binds to A1 (ΔRU = 31), A3 (ΔRU = 42) and B1 (ΔRU = 148) with weak affinity, no binding with other antigens. GII.4 Sydney binds to A2 (ΔRU = 168), A3 (ΔRU = 133) and B2 (ΔRU = 98) with weak affinity, binds to A1 (ΔRU = 556) with medium affinity, binds to A4 (ΔRU = 2119) and B1 (ΔRU = 1022) with high affinity. GIV.1 VLP binds to A3 with medium affinity (ΔRU = 251), no binding with other antigens. Therefore, to further study the relations between binding sites and binding affinity of these two VLPs, we did computational calculation for Molecular dynamics (MD) simulations and binding free energy.

A. GI.3 VLP

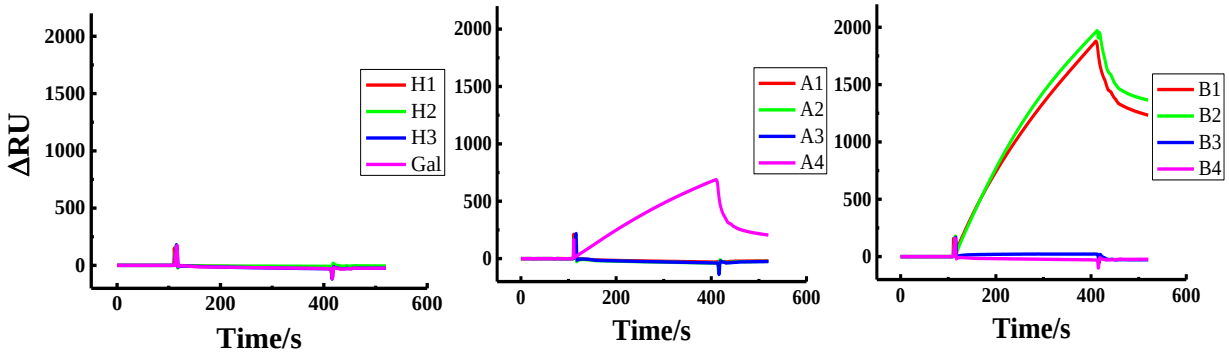

B. GII.2 VLP

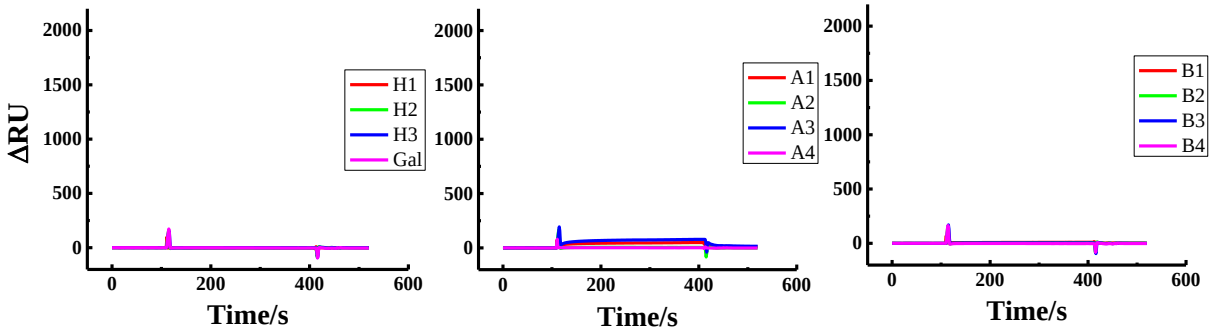

C. GII.3 VLP

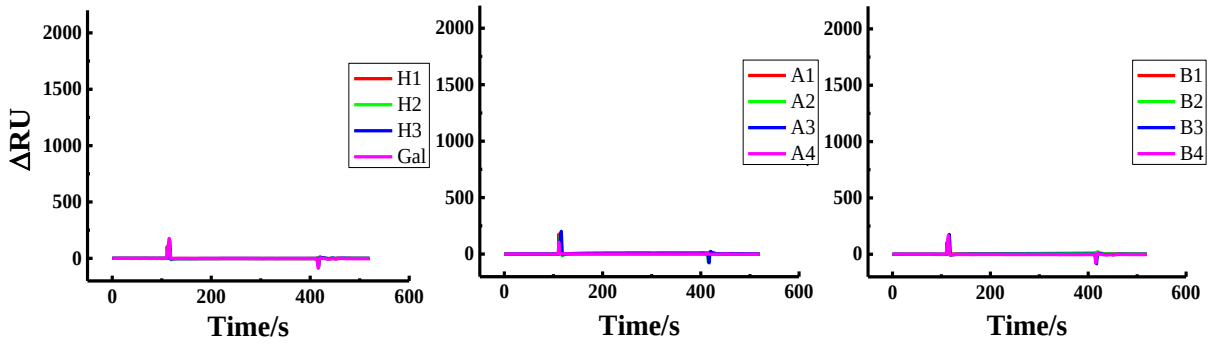

D. GII.4 New Orleans VLP

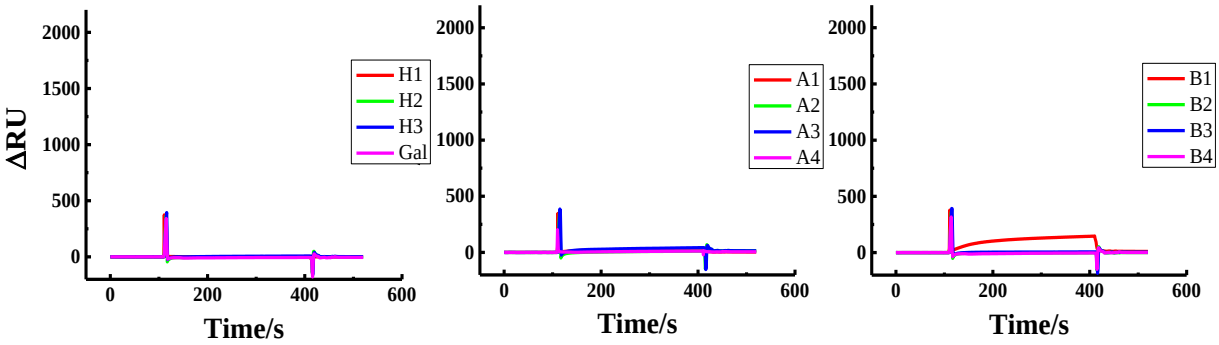

E. GII.4 Sydney VLP

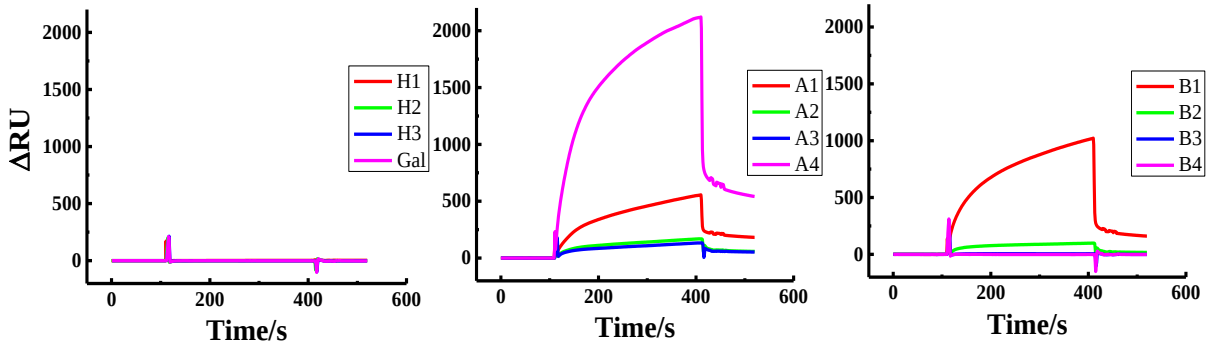

F. GIV.1 VLP

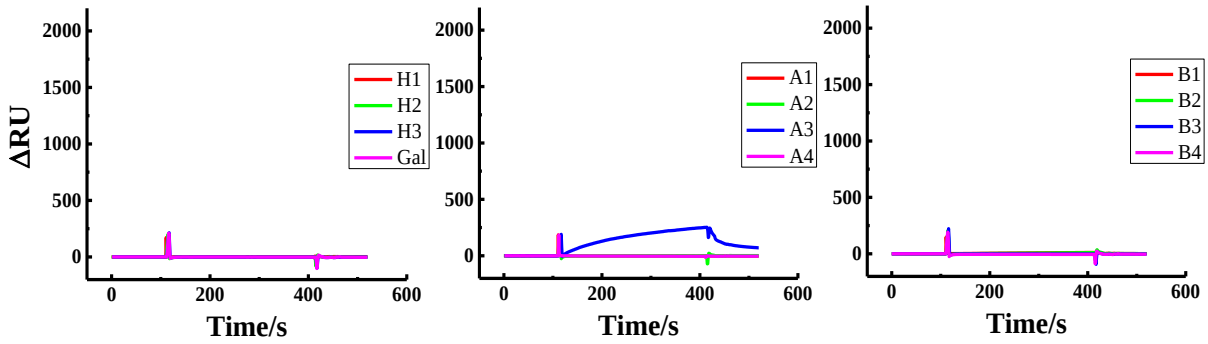

Figure 4.9 *Six types of norovirus VLPs binding with 11 types of HBGAs. A. GI.3 VLP binds to HBGAs. It shows GI.3 has low binding affinity with A4 type HBGA, very high binding affinity with B1 and B2 type HBGAs, very low binding affinity with B3 type HBGA and no binding with other HBGAs. B. GII.2 VLP binds to HBGAs. It shows GII.2 has very low binding affinity with A1*

and A3 type HBGAs, no binding with other HBGAs. C. GII.3 VLP binds to HBGAs. It shows GII.3 has no binding with any of the HBGAs. D. GII.4 New Orleans VLP binds to HBGAs. It shows GII.4 New Orleans has negligible binding with A1, A2 and A3, very low binding with B1, no binding with other HBGAs. E. GII.4 Sydney VLP binds to HBGAs. It shows GII.4 Sydney has very high binding with A4, mediate binding with B1, lower binding with A1, very low binding with A3, A4 and B2, no binding with other HBGAs. F. GIV.1 VLP binds to HBGAs. It shows GIV.1 has low binding with A3, no binding with other HBGAs. All experiments were performed twice.

Table 4.4 *The value of RU for VLPs and HBGAs binding.*

ΔRU Value												
HBGA / VLPs	Gal	H1	H2	H3	A1	A2	A3	A4	B1	B2	B3	B4
GI.3	NA[a]	NA	NA	NA	NA	NA	NA	689	1878	1958	22	NA
GII.2	NA	NA	NA	NA	50	NA	78	NA	NA	NA	NA	NA
GII.3	NA	NA	NA	NA	NA	NA	NA	NA	NA	NA	NA	NA
GII.4 New Orleans	NA	NA	NA	NA	31	NA	42	NA	148	NA	NA	NA
GII.4 Sydney	NA	NA	NA	NA	556	168	133	2119	1022	98	NA	NA
GIV.1	NA	NA	NA	NA	NA	NA	251	NA	NA	NA	NA	NA

[a]NA: ΔRU lower than 10.

4.3.3 Relative binding free energy for VLP and antigens (Done by Dr. Xinqiu Yao)

Molecular dynamics (MD) simulations and binding free energy calculations predict a rank of VP1-glycan associations consistent with experiments. Multiple hundred-nanosecond time scale simulations were performed, each for one of the VP1-glycan systems including Sydney-AIV, Sydney (R373N)-AIV, Sydney-AII, and New Orleans-AIV. Surface Plasmon Resonance (SPR) experiments show that the binding affinity between Sydney and AIV is strong while the affinity

of Sydney-AII or New Orleans-AIV is very weak. The Sydney (R373N) mutant was included to test whether the single point mutation of the binding site residue Arg373 underlies the distinct AIV binding affinities between Sydney and New Orleans. Principal Component Analysis (PCA) of the simulation trajectories reveals overall distinct global conformations among the systems, where major structural changes occur at both ligand binding and distal sites (**Figure 4.10**). Binding free energy was calculated for each conformational snapshot from the trajectory of a particular system. Statistics over all snapshots show that the binding affinity of Sydney-AIV is significantly higher than that of Sydney-AII or New Orleans-AIV, consistent with the SPR experiments (**Figure 4.11 A** and **Table 4.4**). Sydney (R373N) displays a medium binding affinity for AIV, weaker than wildtype Sydney but stronger than New Orleans. This suggests that the amino acid substitution at R373 contributes to the distinct AIV binding affinities between Sydney and New Orleans but does not fully account for the difference.

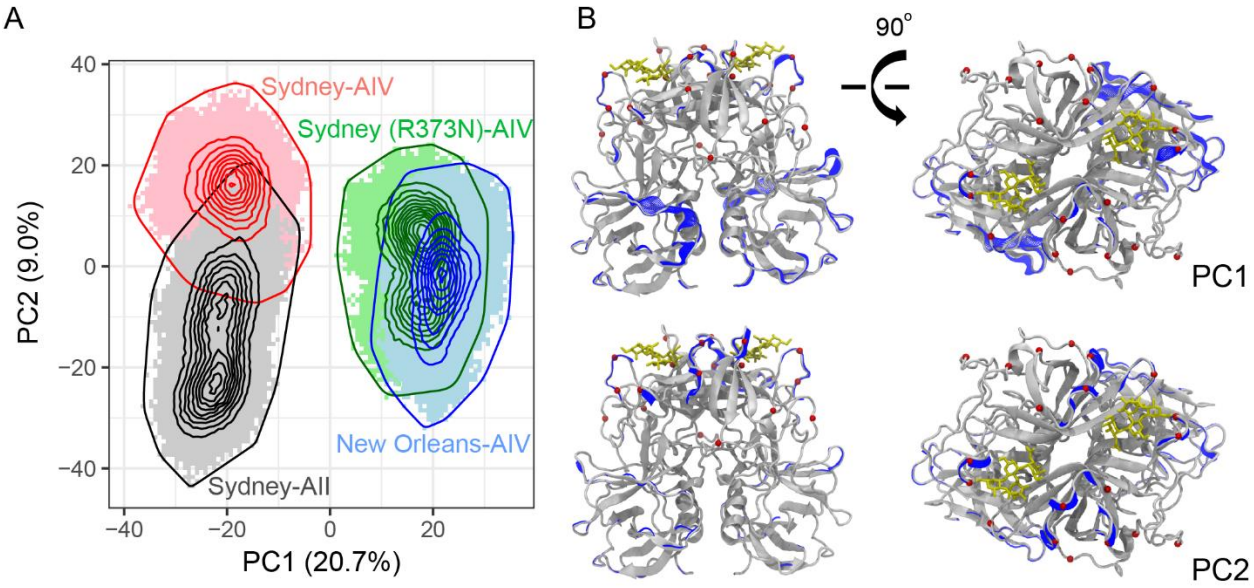

Figure 4.10 *Principal component analysis (PCA) reveals distinct global conformations. (A) Simulation-generated conformational snapshots (colored areas) are projected in the subspace*

spanned by the two principal components capturing the largest structural variance (PC1 and PC2; the number in the axis label indicates the percentage of variance captured by the corresponding PC). Probability density distributions of the conformational samples are represented as contour lines. The sampled space of each simulation is outlined. (B) Collective motions (blue shaded areas) represented by PC1 and PC2, respectively, mapped onto the VP1 homodimer (white cartoon) bound with ligands (yellow licorice). Red spheres, sites of amino acid substitutions between Sydney and New Orleans.

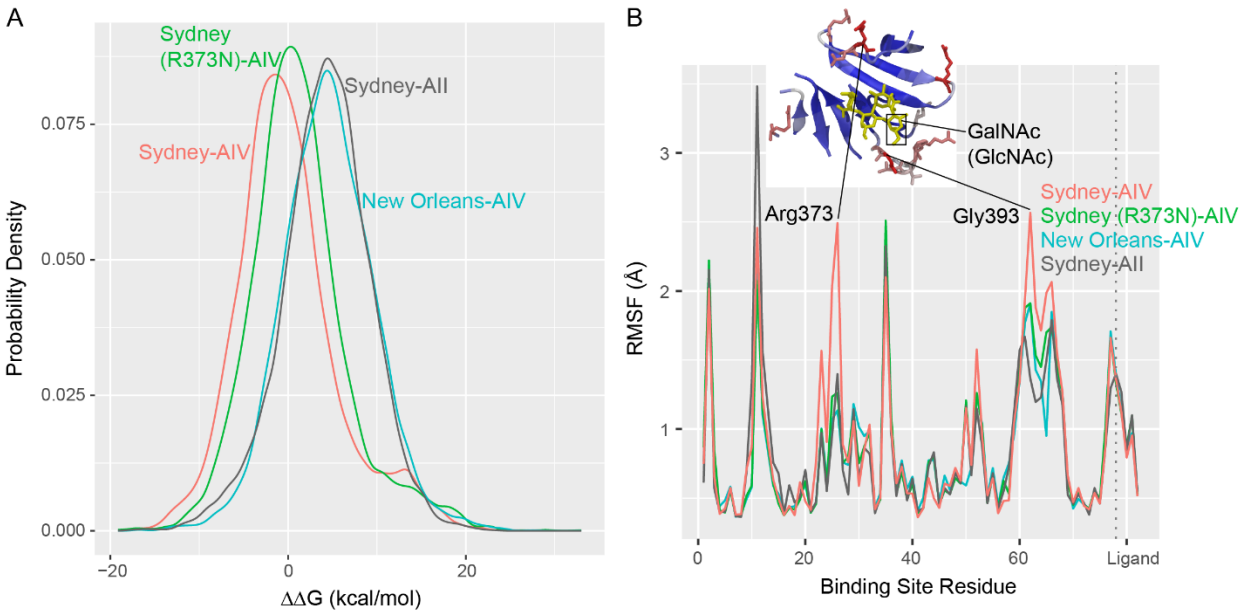

Figure 4.11 *Molecular dynamics and binding free energy calculations indicate that Sydney-AIV complex has the strongest ligand binding affinity and the most flexible binding site. (A) Probability density distributions of relative binding free energy with respect to the mean energy of Sydney-AIV under distinct VP1-glycan combinations. (B) Root mean square fluctuation (RMSF) for each binding site residue derived from MD simulations. The dotted line indicates the separation of protein and ligand residues. Two key residues showing the largest variation in RMSF across systems are labeled. Inset, molecular graphic of the binding site with protein colored by*

RMSF and ligand colored by yellow. The ligand and flexible binding site residues are represented as licorice. The sugar group distinguishing AIV and AII is highlighted with a black rectangle, where the name of the sugar for AIV (AII) is labeled.

***Table 4.5** Relative mean binding free energy with respect to Sydney-AIV (unit: kcal/mol; T=300 K).*

System	ΔΔH	-TΔΔS	ΔΔG
Sydney (R373N)-AIV	-0.140	1.403	1.263±0.072[a]
Sydney-AII	-3.180	7.436	4.256±0.064
New Orleans-AIV	-1.857	6.436	4.579±0.066

[a]mean±SEM.

Binding free energy analysis suggests that the specific Sydney-AIV binding is driven by entropic changes. The enthalpic and entropic part of the binding free energy display opposite directions of changes from Sydney-AIV to the other combinations – in terms of mean interaction energy (enthalpy) Sydney-AIV binding is the weakest; but the Sydney-AIV complex retains the largest portion of its flexibility upon ligand binding, leading to the overall strongest binding free energy due to a less loss in entropy of binding (**Table 4.5**). Energy decomposition on the basis of binding site residues indicates that in spite of the overall similar pattern of VP1-glycan interactions across systems, interactions around Arg373 and Gly393 are substantially altered upon either mutations at the binding site or the sugar substitution in the ligand (**Figure 4.12 & 4.13**). Intriguingly, Arg373 does not interact with the ligand directly (**Figure 4.12**) but the mutation at this site affects interactions between the neighboring Asp374 and the ligand (**Figure 4.13**). Consistent with the enthalpic analysis, the net interaction energy between the binding site of

Sydney and AIV is the weakest. However, the unique interaction pattern in Sydney-AIV may result in specific conformational dynamics that contribute to the enhanced entropy of the complex. To test this hypothesis, we performed residue wise root mean square fluctuation (RMSF) analysis. Results show that Sydney-AIV has the most flexible binding site, with largest difference of fluctuation occurring at residues Arg373 and Gly393 (**Figure 4.11B**). Residues Arg373 and Gly393 of Sydney are replaced with an asparagine and a serine, respectively, in New Orleans. In addition, the location of the sugar group distinguishing AIV (GalNAc) and AII (GlcNAc) is close to Gly393 (**Figure 4.11B**). These facts suggest that perturbation introduced by sequence variation or binding of distinct ligands considerably affects the flexibility of the protein, which in turn alters the overall entropy of the complex and ultimately the bind free energy. Intriguingly, although Sydney (R373N) is only different by one-amino acid from the wildtype, it has a substantially reduced flexibility at both Arg373 and Gly393, implying a dynamical coupling between the two residues.

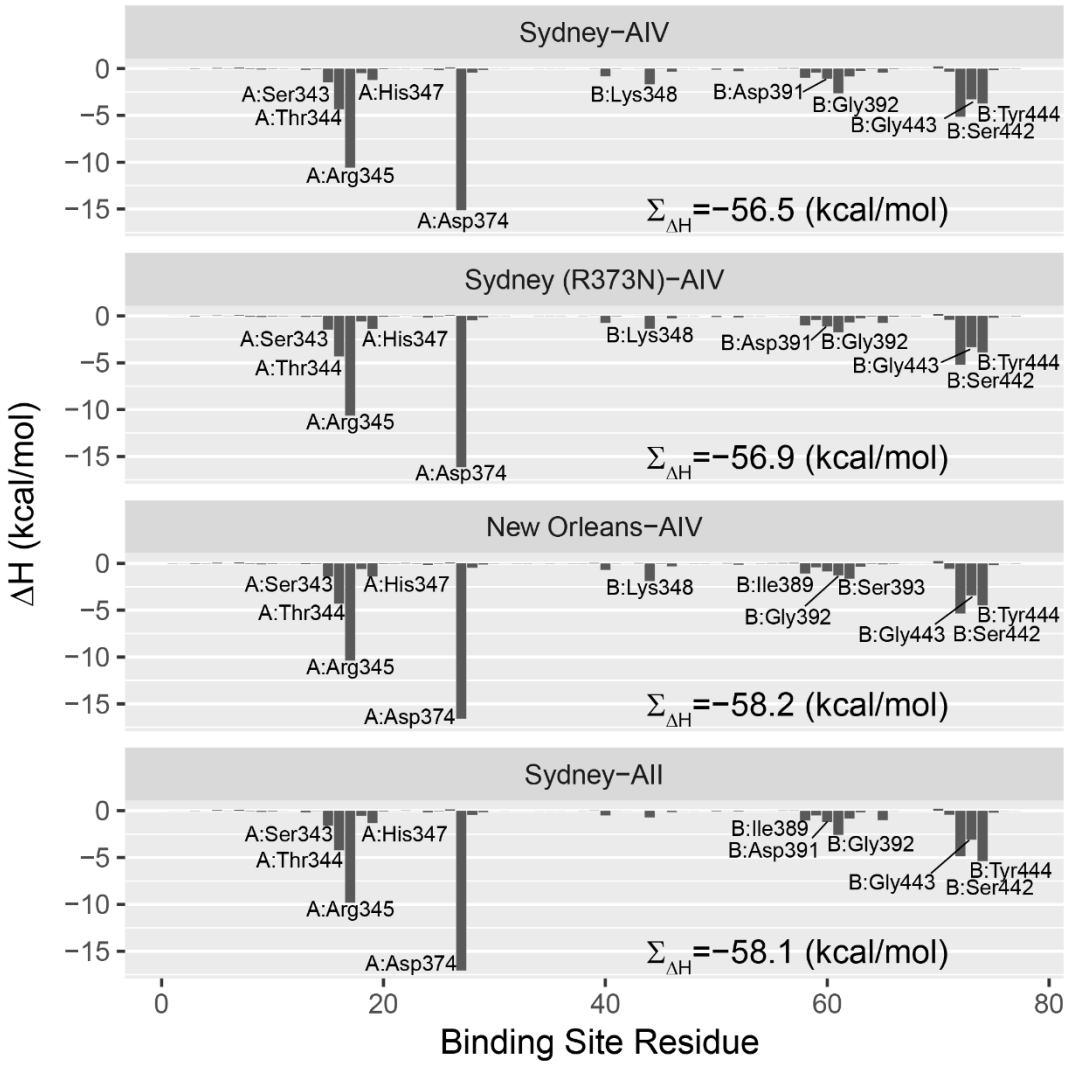

Figure 4.12 *The ligand interacts with binding site residues in an overall similar pattern across systems. Interaction energies are decomposed on the basis of residues and the energies belonging to binding site residues are shown.*

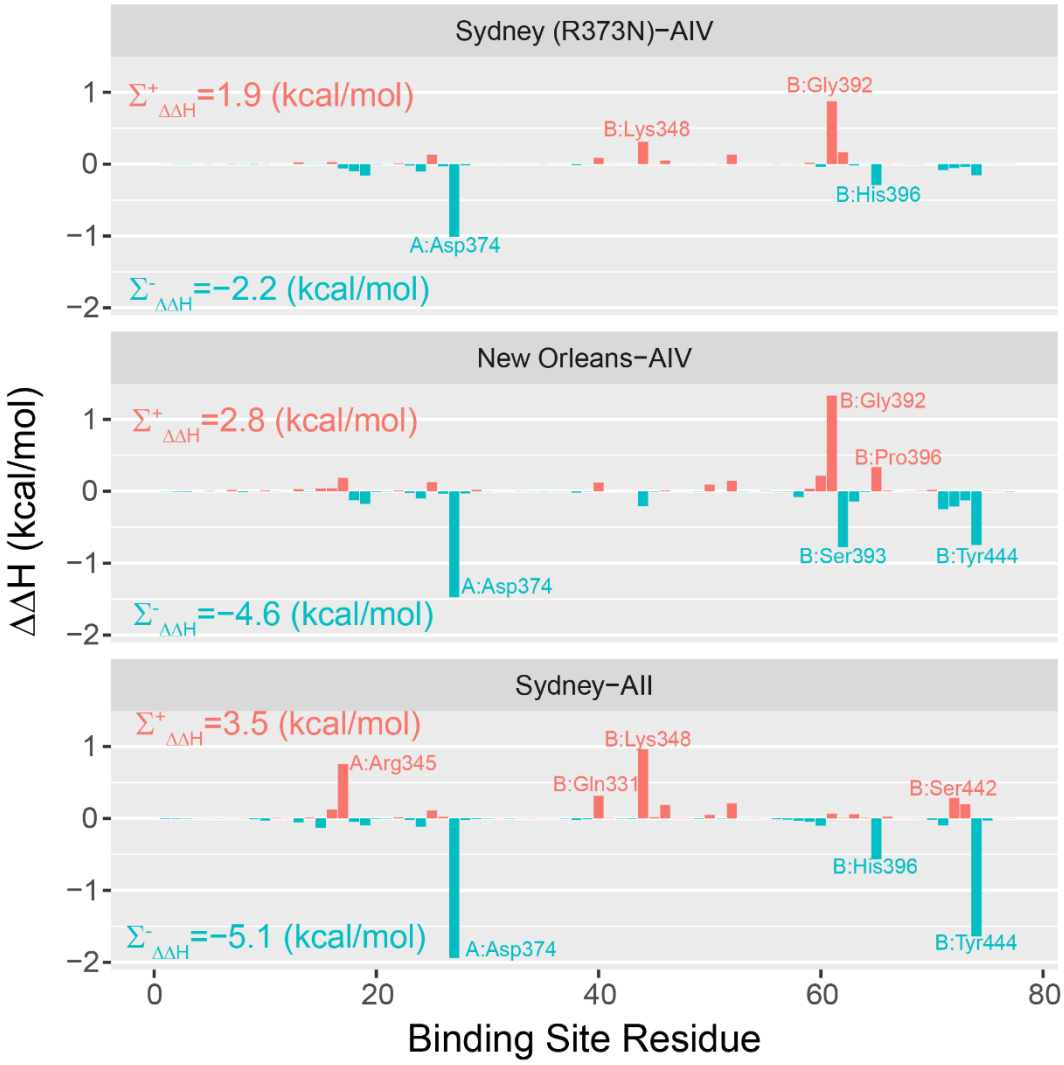

Figure 4.13 *Interaction energies at specific regions are perturbed upon mutations or binding distinct ligands. Interactions energies are decomposed on the basis of residues and the relative energies, with respect to Sydney-AIV, belonging to binding site residues are shown.*

4.4 Conclusion

The binding affinities between different norovirus VLPs and chemically synthesized HBGAs were studied. Different VLPs have different binding patterns with HBGAs. While we know that norovirus binds to HBGA glycans, the intricate details of binding is complicated because of the shallow binding pockets of the norovirus.[275] To further improve our understanding , we

performed molecular dynamic simulations, where we varied the amino acid sequence of one VLP and studied it's interaction with two sets of glycoconjugates. Molecular dynamics (MD) simulations and binding free energy calculations were used to predict the binding of GII.4 New Orleans and GII.4 Sydney and contributions of binding site residues. The computational prediction shows good correlations with SPR results. Single mutation was done for GII.4 Sydney, which implies the importance of binding site R373 for the binding affinity. These results further illustrate the reason for different binding affinities of VLPs. The differences in the binding affinities could potentially be used in POC diagnostics. We found that there are subtle differences in the binding affinities between a panel of HBGAs and different VLPs. We envision developing a microarray with a library of unique chemically defined glycans at specific locations. Exposure to a panel of norovirus genotypes would result in a fingerprint pattern of recognition, that could be used to accurately identify norovirus including genotypes.

4.5 Experimental

4.5.1 SPR binding assay

Materials: Biacore T200 machine, series S sensor chip SA (The surface was conjugated with streptavidin) and BIAdesorb solutions were from GE Healthcare Life Sciences company. Norovirus like particles (VLPs) were got from Centers for Disease Control and Prevention (CDC), biotinylated carbohydrates were synthesized in our laboratory. HBS-EP buffer was purchased from GE Healthcare Life Sciences, used for the immobilization step. Phosphate buffered saline (PBS, pH=7.4) was used for the VLPs and biotinylated carbohydrates binding step.

Immobilization: Immobilization was performed by streptavidin-biotin binding method in the Biacore T200 machine. The SA chip was used with temperature setting of 25℃ and HBS-EP running buffer. After cleaning the machine and inserting the chip, condition the sensor surface

with consecutive 1 min 1 M NaCl in 50 mM NaOH solution for 3 times to remove the streptavidin molecules that are not covalently attached to carboxymethyl dextran matrix. Followed by injection of HBS-EP running buffer until the baseline is stable. Then prepare 2 μg/ml of H1, H2, H3 compound and 10 μg/ml of biotinylated polyethylene glycol (PEG) with HBS-EP buffer. H1, H2, H3 compound were immobilized to channel 2, 3 and 4 separately until the resonance unit (RU) increase 380 (flow rate: 10 μl/min), then biotinylated PEG was flow through channel 1, 2, 3, 4 to block the remaining streptavidin sites. Channel 1 was covered with biotinylated PEG as control. HBS-EP buffer was used to wash biotinylated compounds not attached with streptavidin until the baseline is stable. A type and B type of HBGAs was immobilized in the same way. Biotinylated PEG, A1, A2, A3 were immobilized in chip-2; biotinylated PEG, B1, B2, B3 were immobilized in chip-3; biotinylated PEG, biotinylated galactose (Gal), A4, B4 were immobilized in chip-4.

SPR binding interaction: PBS running buffer was used for the binding process. Biotinylated HBGAs immobilized SA chip was inserted to the machine, PBS buffer was used to flow through the surface until the baseline is stable. Then GII.4-New Orleans VLP (100 μg/ml) was injected for 300 seconds with flow rate of 5 μl/min. After injection, PBS buffer was allowed to flow through for 10 min. Followed by regeneration with 10 mM glycine-HCl (pH=2.5) until it gets back to baseline. After regeneration, next VLP can be used to bind with the chip. The same procedure was used for the other VLPs and HBGAs binding.

4.5.2 Computational methods (Done by Dr. Xinqiu Yao)

Molecular dynamics simulations

MD simulations were performed using AMBER16[327] along with the AMBER ff14SB force field.[328, 329] Reoptimized parameters for backbone peptide-bond torsion angles were employed.[330] The GLYCAM06 force field[331] was used for glycan molecules. Four systems were considered:

Sydney-AIV, Sydney (R373N)-AIV, Sydney-AII, and New Orleans-AIV. The crystallographic structure of GII.4 human norovirus VP1 (Sydney) homodimer in complex with 2-fucosyllactose (PDB: 5J35)[332] was used as the starting conformation for the simulations containing wildtype Sydney VP1. The point mutation was introduced by simply replacing Arg373 with an asparagine using PyMOL 1.8 (Schrödinger, LLC) for the Sydney (R373N)-AIV simulation. The starting conformation of New Orleans was modeled using the SWISS-MODEL server with default parameters.[333] Arg and Lys were protonated, whereas Asp and Glu were deprotonated. The protonation states of His residues were determined based on their pKa values at pH 7.0 calculated using PROPKA 3.0[334] implemented in PDB2PQR 2.1.1.[335] The glycans AIV and AII were built with GLYCAM-Web (http://glycam.org) and were used to replace the ligand in the crystal structure by superimposing the common central galactose. Each system was solvated in an octahedron periodic box filled with pre-equilibrated TIP3P[336] water molecules, which extended at least 10 Å from any surface of the complex to each box face. Na^+ or Cl^- counter-ions were added to neutralize the systems. A series of energy minimization (EM) stages were performed, each having 2000 steps of steepest decent followed by 3000 steps of conjugate gradient. Position restraints were added for all atoms of the VP1-glycan complex with a force constant k=600 $kcal \cdot mol^{-1} \cdot Å^{-2}$ at the first stage of EM. Then, restraints were removed from the ligands but were retained for the protein atoms. Six additional EM stages followed, where restraints were imposed on the complex, but the force constant was gradually reduced from 600 to 0. The systems were heated up from 100K to 300K in five stages of 500-ps MD, each having a 1-fs time-step and position restraints for complex atoms (with k gradually reducing from 500 to 5). A further 1-ns equilibration MD was performed with a 2-fs time-step and no restraint. Subsequent 500-ns production MD was then performed under the same conditions as the equilibration, where the last

300-ns data were analyzed. Constant temperature (300K; Langevin thermostat with collision frequency γ=1.0 ps^{-1}) and constant pressure (1 bar; Monte Carlo barostat with coupling constant τ_p=1.0 ps) along with periodic boundary conditions were applied. The particle-mesh Ewald summation method[337] was employed to treat the long-range electrostatic interactions. For short-range non-bonded interactions, a 9-Å cutoff was used. All bonds involving hydrogen atoms were constrained with the SHAKE algorithm.[338] Each snapshot in the trajectories was saved every 1 ps.

Binding free energy calculations

The standard binding free energy was calculated similar to the work by Minh[339]

$$\Delta G^0 = -\beta^{-1} \ln\langle e^{-\beta B}\rangle + C$$
$$\approx \langle B\rangle - \frac{\beta}{2!}\langle (B - \langle B\rangle)^2\rangle + C$$

where <·> represents an ensemble average, B is the binding energy for a single conformational snapshot, β=(k_BT)$^{-1}$ is the inverse of Boltzmann's constant, k_B, times the temperature, T, and C is the free energy to confine the ligand to the binding site and is considered to be a constant across systems. The second line of the equation employs a cumulant expansion approximation up to the second order to simplify calculations of the exponential average. The first term, <B>, represents the enthalpic change, ΔH, upon ligand binding while the second term is related to the entropic change, $-T\Delta S$. In the statistical analysis (**Figure 4.10A**), the binding free energy for each simulation snapshot was computed by B plus the entropic term derived from the ensemble. The single-point binding energy B was estimated with the Molecular Mechanics/Generalized Born Surface Area (MM/GBSA) method implemented in AMBER16. Gas phase energies were computed with the ff14SB force field.[328, 329] The GB^{OBC} II model[340] and the LCPO method[341] were applied to calculate polar and nonpolar terms, respectively, of the solvation energy. The salt concentration was set to be 0.1 M. The MMPBSA.py script[342] of AMBER16 was

employed to run calculations over every 100 frames of a simulation. Calculations were performed for each binding site of the dimer separately and final results were derived from concatenated data of the two binding sites (cumulatively 600-ns data for each system).

RMSF and PCA

Residue wise root mean square fluctuation (RMSF) was calculated using the CPPTRAJ[343] command of AMBER16. Cartesian coordinates of equivalent binding site residues of the dimer derived from MD simulations were concatenated. Before calculations, all simulation snapshots were superimposed based on coordinates of main chain atoms (N, Cα, C, and O) of the binding site. Then, mass-weighted average of atomic fluctuations of each residue was computed by

$$\langle F \rangle = \frac{\sum_{i \in A} f_i \cdot M_i}{\sum_{i \in A} M_i}$$

where A contains all heavy atoms of the residue, M_i is the mass of atom i, and f_i is the fluctuation of atom i. The atomic fluctuation is defined by

$$f_i = \sqrt{\frac{1}{N-1} \sum_{j=1}^{N} \left\| r_i^j - \langle r_i \rangle \right\|^2}$$

where N is the total number of simulation frames, r_i^j is the position of atom i in frame j, and $<r_i>$ is the mean position of atom i.

Principal component analysis (PCA) was performed on the Cartesian coordinates of backbone atoms (N, Cα, and C) of VP1 dimer using CPPTRAJ. Prior to PCA, structures were superimposed based on backbone atoms. The variance-covariance matrix characterizing the correlated internal motions was then calculated and was diagonalized to obtain eigenvectors or principal components (PCs). The structural variance along each PC is given by the corresponding eigenvalue. The first two PCs capturing the largest structural variance were used to build the

subspace where simulation trajectories were projected for the subsequent inter-conformer relationship analysis. Molecular graphics were generated with VMD 1.9.3.[344] All other figures were made with Bio3D[345, 346] and ggplot2.[347]

REFERENCES

1. Price, C. P.; St John, A., Innovation in healthcare. The challenge for laboratory medicine. *Clin Chim Acta* **2014,** *427*, 71-8.

2. Vashist, S. K., Point-of-Care Diagnostics: Recent Advances and Trends. *Biosensors (Basel)* **2017,** *7* (4).

3. Segman, Y. J., Device and Method for Noninvasive Glucose Assessment. *J Diabetes Sci Technol* **2018,** *12* (6), 1159-1168.

4. Junker, R., Wahl, H.G. , POCT in the physician practice setting. In: Luppa P.B., Junker R. (eds) Point-of-Care Testing. Springer, Berlin, Heidelberg. https://doi.org/10.1007/978-3-662-54497-6_32. **2018**.

5. Grieshaber, D.; MacKenzie, R.; Voros, J.; Reimhult, E., Electrochemical Biosensors - Sensor Principles and Architectures. *Sensors (Basel)* **2008,** *8* (3), 1400-1458.

6. Damborsky, P.; Svitel, J.; Katrlik, J., Optical biosensors. *Essays Biochem* **2016,** *60* (1), 91-100.

7. Ganter, M. T.; Hofer, C. K., Coagulation monitoring: current techniques and clinical use of viscoelastic point-of-care coagulation devices. *Anesth Analg* **2008,** *106* (5), 1366-75.

8. Corstjens, A. M.; Ligtenberg, J. J.; van der Horst, I. C.; Spanjersberg, R.; Lind, J. S.; Tulleken, J. E.; Meertens, J. H.; Zijlstra, J. G., Accuracy and feasibility of point-of-care and continuous blood glucose analysis in critically ill ICU patients. *Crit Care* **2006,** *10* (5), R135.

9. Peeling, R. W.; Holmes, K. K.; Mabey, D.; Ronald, A., Rapid tests for sexually transmitted infections (STIs): the way forward. *Sex Transm Infect* **2006,** *82 Suppl 5*, v1-6.

10. Kosack, C. S.; Page, A. L.; Klatser, P. R., A guide to aid the selection of diagnostic tests. *Bull World Health Organ* **2017,** *95* (9), 639-645.

11. Cho, I. H.; Kim, D. H.; Park, S., Electrochemical biosensors: perspective on functional nanomaterials for on-site analysis. *Biomater Res* **2020,** *24*, 6.

12. Igor Cretescu, D. L., Liliana Rosemarie Manea Electrochemical Sensors for Monitoring of Indoor and Outdoor Air Pollution, Electrochemical Sensors Technology, Mohammed Muzibur Rahman and Abdullah Mohamed Asiri, IntechOpen, DOI: 10.5772/intechopen.68512. **2017**.

13. Heller, A., Amperometric biosensors. *Curr Opin Biotechnol* **1996,** *7* (1), 50-4.

14. Chaubey, A.; Malhotra, B. D., Mediated biosensors. *Biosens Bioelectron* **2002,** *17* (6-7), 441-56.

15. Berney, H. C.; Alderman, J.; Lane, W. A.; Collins, J. K., Development of a capacitive immunosensor: a comparison of monoclonal and polyclonal capture antibodies as the primary layer. *J Mol Recognit* **1998,** *11* (1-6), 175-7.

16. Nguyen, H. H.; Park, J.; Kang, S.; Kim, M., Surface plasmon resonance: a versatile technique for biosensor applications. *Sensors (Basel)* **2015,** *15* (5), 10481-510.

17. Bahadir, E. B.; Sezginturk, M. K., Lateral flow assays: Principles, designs and labels. *Trac-Trend Anal Chem* **2016,** *82*, 286-306.

18. Lucklum, R.; Hauptmann, P., Acoustic microsensors--the challenge behind microgravimetry. *Anal Bioanal Chem* **2006,** *384* (3), 667-82.

19. Hansen, K. M.; Thundat, T., Microcantilever biosensors. *Methods* **2005,** *37* (1), 57-64.

20. Maglio, O.; Costanzo, S.; Cercola, R.; Zambrano, G.; Mauro, M.; Battaglia, R.; Ferrini, G.; Nastri, F.; Pavone, V.; Lombardi, A., A Quartz Crystal Microbalance Immunosensor for Stem Cell Selection and Extraction. *Sensors (Basel)* **2017,** *17* (12).

21. Wang, H. C.; Lee, A. R., Recent developments in blood glucose sensors. *J Food Drug Anal* **2015,** *23* (2), 191-200.

22. Carraro, P., The point-of-care testing in the emergency department. *Emergency Care Journal* **2019,** *15* (2).

23. Kuszewski, K.; Brydak, L., The epidemiology and history of influenza. *Biomed Pharmacother* **2000,** *54* (4), 188-195.

24. Johnson, N. P. A. S.; Mueller, J., Updating the accounts: global mortality of the 1918-1920 "Spanish" influenza pandemic. *B Hist Med* **2002,** *76* (1), 105-115.

25. Brundage, J. F., Interactions between influenza and bacterial respiratory pathogens: implications for pandemic preparedness. *Lancet Infect Dis* **2006,** *6* (5), 303-312.

26. Viboud, C.; Simonsen, L.; Fuentes, R.; Flores, J.; Miller, M. A.; Chowell, G., Global Mortality Impact of the 1957-1959 Influenza Pandemic. *J Infect Dis* **2016,** *213* (5), 738-745.

27. Cockburn, W. C.; Delon, P. J.; Ferreira, W., Origin and progress of the 1968-69 Hong Kong influenza epidemic. *Bull World Health Organ* **1969,** *41* (3), 345-8.

28. Kilbourne, E. D., Influenza pandemics of the 20th century. *Emerging Infectious Diseases* **2006,** *12* (1), 9-14.

29. Lagace-Wiens, P. R. S.; Rubinstein, E.; Gumel, A., Influenza epidemiology-past, present, and future. *Crit Care Med* **2010,** *38*, E1-E9.

30. Shim, J. M.; Kim, J.; Tenson, T.; Min, J. Y.; Kainov, D. E., Influenza Virus Infection, Interferon Response, Viral Counter-Response, and Apoptosis. *Viruses* **2017,** *9* (8).

31. Russell, C. J.; Hu, M.; Okda, F. A., Influenza Hemagglutinin Protein Stability, Activation, and Pandemic Risk. *Trends Microbiol* **2018,** *26* (10), 841-853.

32. Te Velthuis, A. J.; Fodor, E., Influenza virus RNA polymerase: insights into the mechanisms of viral RNA synthesis. *Nat Rev Microbiol* **2016,** *14* (8), 479-93.

33. Samji, T., Influenza A: Understanding the Viral Life Cycle. *Yale Journal of Biology and Medicine* **2009,** *82* (4), 153-159.

34. von Itzstein, M., The war against influenza: discovery and development of sialidase inhibitors. *Nat Rev Drug Discov* **2007,** *6* (12), 967-74.

35. Shirvani, E.; Paldurai, A.; Varghese, B. P.; Samal, S. K., Contributions of HA1 and HA2 Subunits of Highly Pathogenic Avian Influenza Virus in Induction of Neutralizing Antibodies and Protection in Chickens. *Front Microbiol* **2020,** *11*, 1085.

36. Das, K.; Aramini, J. M.; Ma, L. C.; Krug, R. M.; Arnold, E., Structures of influenza A proteins and insights into antiviral drug targets. *Nat Struct Mol Biol* **2010,** *17* (5), 530-538.

37. Skehel, J. J.; Wiley, D. C., Receptor binding and membrane fusion in virus entry: The influenza hemagglutinin. *Annu Rev Biochem* **2000,** *69*, 531-569.

38. Samji, T., Influenza A: understanding the viral life cycle. *Yale J Biol Med* **2009,** *82* (4), 153-9.

39. Pinto, L. H.; Lamb, R. A., The M2 proton channels of influenza A and B viruses. *J Biol Chem* **2006,** *281* (14), 8997-9000.

40. Bossart-Whitaker, P.; Carson, M.; Babu, Y. S.; Smith, C. D.; Laver, W. G.; Air, G. M., Three-dimensional structure of influenza A N9 neuraminidase and its complex with the inhibitor 2-deoxy 2,3-dehydro-N-acetyl neuraminic acid. *J Mol Biol* **1993,** *232* (4), 1069-83.

41. Cohen, M.; Zhang, X. Q.; Senaati, H. P.; Chen, H. W.; Varki, N. M.; Schooley, R. T.; Gagneux, P., Influenza A penetrates host mucus by cleaving sialic acids with neuraminidase. *Virol J* **2013,** *10*, 321.

42. Behzadi, M. A.; Leyva-Grado, V. H., Overview of Current Therapeutics and Novel Candidates Against Influenza, Respiratory Syncytial Virus, and Middle East Respiratory Syndrome Coronavirus Infections. *Front Microbiol* **2019,** *10*.

43. Helenius, A., Unpacking the Incoming Influenza-Virus. *Cell* **1992,** *69* (4), 577-578.

44. Schnell, J. R.; Chou, J. J., Structure and mechanism of the M2 proton channel of influenza A virus. *Nature* **2008,** *451* (7178), 591-U12.

45. Hussain, M.; Galvin, H. D.; Haw, T. Y.; Nutsford, A. N.; Husain, M., Drug resistance in influenza A virus: the epidemiology and management. *Infect Drug Resist* **2017,** *10*, 121-134.

46. Ison, M. G., Antiviral Treatments. *Clin Chest Med* **2017,** *38* (1), 139-+.

47. Ikematsu, H.; Kawai, N., Laninamivir octanoate: a new long-acting neuraminidase inhibitor for the treatment of influenza. *Expert Rev Anti Infect Ther* **2011,** *9* (10), 851-7.

48. McClellan, K.; Perry, C. M., Oseltamivir: a review of its use in influenza (vol 61, pg 263, 2001). *Drugs* **2001,** *61* (6), 775-775.

49. Marty, F. M.; Vidal-Puigserver, J.; Clark, C.; Gupta, S. K.; Merino, E.; Garot, D.; Chapman, M. J.; Jacobs, F.; Rodriguez-Noriega, E.; Husa, P.; Shortino, D.; Watson, H. A.; Yates, P. J.; Peppercorn, A. F., Intravenous zanamivir or oral oseltamivir for hospitalised patients with influenza: an international, randomised, double-blind, double-dummy, phase 3 trial. *Lancet Respir Med* **2017,** *5* (2), 135-146.

50. Ison, M. G.; Fraiz, J.; Heller, B.; Jauregui, L.; Mills, G.; O'Riordan, W.; O'Neil, B.; Playford, E. G.; Rolf, J. D.; Sada-Diaz, E.; Elder, J.; Collis, P.; Hernandez, J. E.; Sheridan, W. P., Intravenous peramivir for treatment of influenza in hospitalized patients. *Antivir Ther* **2014,** *19* (4), 349-361.

51. Yildirim, D.; Ozdogru Sagdic, D.; Seflek, B.; Cimentepe, M.; Bayram, I.; Yarkin, F., Detection of influenza virus infections by molecular and immunofluorescence methods. *Mikrobiyol Bul* **2017,** *51* (4), 370-377.

52. Vasoo, S.; Stevens, J.; Singh, K., Rapid antigen tests for diagnosis of pandemic (Swine) influenza A/H1N1. *Clin Infect Dis* **2009,** *49* (7), 1090-3.

53. Leland, D. S.; Ginocchio, C. C., Role of cell culture for virus detection in the age of technology. *Clin Microbiol Rev* **2007,** *20* (1), 49-78.

54. Dziabowska, K.; Czaczyk, E.; Nidzworski, D., Detection Methods of Human and Animal Influenza Virus-Current Trends. *Biosensors-Basel* **2018,** *8* (4).

55. Vemula, S. V.; Zhao, J. Q.; Liu, J. K.; Wang, X.; Biswas, S.; Hewlett, I., Current Approaches for Diagnosis of Influenza Virus Infections in Humans. *Viruses-Basel* **2016,** *8* (4).

56. Mehlmann, M.; Bonner, A. B.; Williams, J. V.; Dankbar, D. M.; Moore, C. L.; Kuchta, R. D.; Podsiad, A. B.; Tamerius, J. D.; Dawson, E. D.; Rowlen, K. L., Comparison of the MChip to viral culture, reverse transcription-PCR, and the QuickVue influenza A+B test for rapid diagnosis of influenza. *J Clin Microbiol* **2007,** *45* (4), 1234-7.

57. Ahn, S. J.; Baek, Y. H.; Lloren, K. K. S.; Choi, W. S.; Jeong, J. H.; Antigua, K. J. C.; Kwon, H. I.; Park, S. J.; Kim, E. H.; Kim, Y. I.; Si, Y. J.; Hong, S. B.; Shin, K. S.; Chun, S.; Choi, Y. K.; Song, M. S., Rapid and simple colorimetric detection of multiple influenza viruses infecting humans using a reverse transcriptional loop-mediated isothermal amplification (RT-LAMP) diagnostic platform. *Bmc Infect Dis* **2019,** *19* (1), 676.

58. Zhao, J.; Liu, J.; Vemula, S. V.; Lin, C.; Tan, J.; Ragupathy, V.; Wang, X.; Mbondji-Wonje, C.; Ye, Z.; Landry, M. L.; Hewlett, I., Sensitive Detection and Simultaneous

Discrimination of Influenza A and B Viruses in Nasopharyngeal Swabs in a Single Assay Using Next-Generation Sequencing-Based Diagnostics. *Plos One* **2016,** *11* (9), e0163175.

59. Pingle, M. R.; Granger, K.; Feinberg, P.; Shatsky, R.; Sterling, B.; Rundell, M.; Spitzer, E.; Larone, D.; Golightly, L.; Barany, F., Multiplexed identification of blood-borne bacterial pathogens by use of a novel 16S rRNA gene PCR-ligase detection reaction-capillary electrophoresis assay. *J Clin Microbiol* **2007,** *45* (6), 1927-35.

60. Hoang Vu Mai, P.; Ung Thi Hong, T.; Nguyen Le Khanh, H.; Nguyen Thanh, T.; Le Thi, T.; Nguyen Vu, S.; Nguyen Phuong, A.; Tran Thi Thu, H.; Vuong Duc, C.; Le Quynh, M., Missed detections of influenza A(H1)pdm09 by real-time RT-PCR assay due to haemagglutinin sequence mutation, December 2017 to March 2018, northern Viet Nam. *Western Pac Surveill Response J* **2019,** *10* (1), 32-38.

61. Green, D. A.; StGeorge, K., Rapid Antigen Tests for Influenza: Rationale and Significance of the FDA Reclassification. *J Clin Microbiol* **2018,** *56* (10).

62. Allen, J. D.; Ross, T. M., H3N2 influenza viruses in humans: Viral mechanisms, evolution, and evaluation. *Hum Vaccin Immunother* **2018,** *14* (8), 1840-1847.

63. Hay, A. J.; Hayden, F. G., Oseltamivir resistance during treatment of H7N9 infection. *Lancet* **2013,** *381* (9885), 2230-2.

64. Morris, D. E.; Cleary, D. W.; Clarke, S. C., Secondary Bacterial Infections Associated with Influenza Pandemics. *Front Microbiol* **2017,** *8*.

65. Moscona, A., Drug therapy - Neuraminidase inhibitors for influenza. *New Engl J Med* **2005,** *353* (13), 1363-1373.

66. Leophonte, P., Azithromycin and Lower Respiratory-Tract Infections. *Pathol Biol* **1995,** *43* (6), 534-541.

67. Tan, T. Q.; Mason, E. O.; Wald, E. R.; Barson, E. J.; Schutze, G. E.; Bradley, J. S.; Givner, L. B.; Yogev, R.; Kim, K. S.; Kaplan, S. L., Clinical characteristics of children with complicated pneumonia caused by Streptococcus pneumoniae. *Pediatrics* **2002,** *110* (1).

68. Kash, J. C.; Walters, K. A.; Davis, A. S.; Sandouk, A.; Schwartzman, L. M.; Jagger, B. W.; Chertow, D. S.; Li, Q.; Kuestner, R. E.; Ozinsky, A.; Taubenberger, J. K., Lethal synergism of 2009 pandemic H1N1 influenza virus and Streptococcus pneumoniae coinfection is associated with loss of murine lung repair responses. *Mbio* **2011,** *2* (5).

69. Zhang, X. H.; Dhawane, A. N.; Sweeney, J.; He, Y.; Vasireddi, M.; Iyer, S. S., Electrochemical Assay to Detect Influenza Viruses and Measure Drug Susceptibility. *Angew Chem Int Edit* **2015,** *54* (20), 5929-5932.

70. Cui, X. K.; Das, A.; Dhawane, A. N.; Sweeney, J.; Zhang, X. H.; Chivukula, V.; Iyer, S. S., Highly specific and rapid glycan based amperometric detection of influenza viruses. *Chemical Science* **2017,** *8* (5), 3628-3634.

71. Das, A.; Cui, X. K.; Chivukula, V.; Iyer, S. S., Detection of Enzymes, Viruses, and Bacteria Using Glucose Meters. *Anal Chem* **2018,** *90* (19), 11589-11598.

72. Yang, W.; Liu, X. Y.; Peng, X. X.; Li, P.; Wang, T. X.; Tai, G. H.; Li, X. J.; Zhou, Y. F., Synthesis of novel N-acetylneuraminic acid derivatives as substrates for rapid detection of influenza virus neuraminidase. *Carbohyd Res* **2012,** *359*, 92-96.

73. Shrivastava, S.; Lee, W. I.; Lee, N. E., Culture-free, highly sensitive, quantitative detection of bacteria from minimally processed samples using fluorescence imaging by smartphone. *Biosens Bioelectron* **2018,** *109*, 90-97.

74. Liu, D. D.; Cui, X. K.; Dhawane, A. N.; Chivukula, V.; Iyer, S. S., Fluorescent sialic derivatives for the specific detection of influenza viruses. *Bioorg Med Chem Lett* **2019,** *29* (24).

75. Vavricka, C. J.; Li, Q.; Wu, Y.; Qi, J.; Wang, M.; Liu, Y.; Gao, F.; Liu, J.; Feng, E.; He, J.; Wang, J.; Liu, H.; Jiang, H.; Gao, G. F., Structural and functional analysis of laninamivir and its octanoate prodrug reveals group specific mechanisms for influenza NA inhibition. *PLoS Pathog* **2011,** *7* (10), e1002249.

76. Zhu, X. Y.; McBride, R.; Nycholat, C. M.; Yu, W. L.; Paulson, J. C.; Wilson, I. A., Influenza Virus Neuraminidases with Reduced Enzymatic Activity That Avidly Bind Sialic Acid Receptors. *Journal of Virology* **2012,** *86* (24), 13371-13383.

77. Gut, H.; Xu, G.; Taylor, G. L.; Walsh, M. A., Structural basis for Streptococcus pneumoniae NanA inhibition by influenza antivirals zanamivir and oseltamivir carboxylate. *J Mol Biol* **2011,** *409* (4), 496-503.

78. Carlescu, I.; Osborn, H. M. I.; Desbrieres, J.; Scutaru, D.; Popa, M., Synthesis of poly(aspartimide)-based bio-glycoconjugates. *Carbohyd Res* **2010,** *345* (1), 33-40.

79. Hodson, R., Inflammatory bowel disease. *Nature* **2016,** *540* (7634), S97.

80. Dahlhamer JM, Z. E., Ward BW, Wheaton AG, Croft JB., Prevalence of Inflammatory Bowel Disease Among Adults Aged ⩾18 Years — United States, . *MMWR Morb Mortal Wkly Rep 2016* **2015,** (65), 1166–1169.

81. Hoivik, M. L.; Moum, B.; Solberg, I. C.; Henriksen, M.; Cvancarova, M.; Bernklev, T.; Grp, I., Work disability in inflammatory bowel disease patients 10 years after disease onset: results from the IBSEN Study. *Gut* **2013,** *62* (3), 368-375.

82. Ungaro, R.; Mehandru, S.; Allen, P. B.; Peyrin-Biroulet, L.; Colombel, J. F., Ulcerative colitis. *Lancet* **2017,** *389* (10080), 1756-1770.

83. Kornbluth, A.; Sachar, D. B.; Gastroenterology, A. C., Ulcerative Colitis Practice Guidelines in Adults: American College of Gastroenterology, Practice Parameters Committee. *Am J Gastroenterol* **2010,** *105* (3), 501-523.

84. Jostins, L.; Ripke, S.; Weersma, R. K.; Duerr, R. H.; McGovern, D. P.; Hui, K. Y.; Lee, J. C.; Schumm, L. P.; Sharma, Y.; Anderson, C. A.; Essers, J.; Mitrovic, M.; Ning, K.; Cleynen, I.; Theatre, E.; Spain, S. L.; Raychaudhuri, S.; Goyette, P.; Wei, Z.; Abraham, C.; Achkar, J. P.; Ahmad, T.; Amininejad, L.; Ananthakrishnan, A. N.; Andersen, V.; Andrews, J. M.; Baidoo, L.; Balschun, T.; Bampton, P. A.; Bitton, A.; Boucher, G.; Brand, S.; Buning, C.; Cohain, A.; Cichon, S.; D'Amato, M.; De Jong, D.; Devaney, K. L.; Dubinsky, M.; Edwards, C.; Ellinghaus, D.; Ferguson, L. R.; Franchimont, D.; Fransen, K.; Gearry, R.; Georges, M.; Gieger, C.; Glas, J.; Haritunians, T.; Hart, A.; Hawkey, C.; Hedl, M.; Hu, X. L.; Karlsen, T. H.; Kupcinskas, L.; Kugathasan, S.; Latiano, A.; Laukens, D.; Lawrance, I. C.; Lees, C. W.; Louis, E.; Mahy, G.; Mansfield, J.; Morgan, A. R.; Mowat, C.; Newman, W.; Palmieri, O.; Ponsioen, C. Y.; Potocnik, U.; Prescott, N. J.; Regueiro, M.; Rotter, J. I.; Russell, R. K.; Sanderson, J. D.; Sans, M.; Satsangi, J.; Schreiber, S.; Simms, L. A.; Sventoraityte, J.; Targan, S. R.; Taylor, K. D.; Tremelling, M.; Verspaget, H. W.; De Vos, M.; Wijmenga, C.; Wilson, D. C.; Winkelmann, J.; Xavier, R. J.; Zeissig, S.; Zhang, B.; Zhang, C. K.; Zhao, H. Y.; Silverberg, M. S.; Annese, V.; Hakonarson, H.; Brant, S. R.; Radford-Smith, G.; Mathew, C. G.; Rioux, J. D.; Schadt, E. E.; Daly, M. J.; Franke, A.; Parkes, M.; Vermeire, S.; Barrett, J. C.; Cho, J. H.; IIBDGC, I. I. G. C., Host-microbe interactions have shaped the genetic architecture of inflammatory bowel disease. *Nature* **2012,** *491* (7422), 119-124.

85. Baumgart, D. C.; Sandborn, W. J., Crohn's disease. *Lancet* **2012,** *380* (9853), 1590-1605.

86. Kvasnovsky, C. L.; Aujla, U.; Bjarnason, I., Nonsteroidal anti-inflammatory drugs and exacerbations of inflammatory bowel disease. *Scand J Gastroenterol* **2015,** *50* (3), 255-63.

87. Williams, C.; Panaccione, R.; Ghosh, S.; Rioux, K., Optimizing clinical use of mesalazine (5-aminosalicylic acid) in inflammatory bowel disease. *Therap Adv Gastroenterol* **2011,** *4* (4), 237-48.

88. Selby, W. S.; Barr, G. D.; Ireland, A.; Mason, C. H.; Jewell, D. P., Olsalazine in active ulcerative colitis. *Br Med J (Clin Res Ed)* **1985,** *291* (6506), 1373-5.

89. Green, J. R.; Lobo, A. J.; Holdsworth, C. D.; Leicester, R. J.; Gibson, J. A.; Kerr, G. D.; Hodgson, H. J.; Parkins, K. J.; Taylor, M. D., Balsalazide is more effective and better tolerated than mesalamine in the treatment of acute ulcerative colitis. The Abacus Investigator Group. *Gastroenterology* **1998,** *114* (1), 15-22.

90. Sohrabpour, A. A.; Malekzadeh, R.; Keshavarzian, A., Current Therapeutic Approaches in Inflammatory Bowel Disease. *Curr Pharm Design* **2010,** *16* (33), 3668-3683.

91. Piper, J. M.; Ray, W. A.; Daugherty, J. R.; Griffin, M. R., Corticosteroid use and peptic ulcer disease: role of nonsteroidal anti-inflammatory drugs. *Ann Intern Med* **1991,** *114* (9), 735-40.

92. Dubois-Camacho, K.; Ottum, P. A.; Franco-Munoz, D.; De la Fuente, M.; Torres-Riquelme, A.; Diaz-Jimenez, D.; Olivares-Morales, M.; Astudillo, G.; Quera, R.; Hermoso, M. A., Glucocorticosteroid therapy in inflammatory bowel diseases: From clinical practice to molecular biology. *World J Gastroentero* **2017,** *23* (36), 6628-6638.

93. De Cassan, C.; Fiorino, G.; Danese, S., Second-Generation Corticosteroids for the Treatment of Crohn's Disease and Ulcerative Colitis: More Effective and Less Side Effects? *Digest Dis* **2012,** *30* (4), 368-375.

94. Lennard-Jones, J. E. L., A. J.; Newell, A. C.; Wilson, C. W. E.; Avery Jones, F.;, An assessment of prednisone, salazopyrin, and topical hydrocortisone hemisuccinate used as out-patient treatment for ulcerative colitis. *Gut* **1960,** *1* (3), 217-222.

95. Tremaine, W. J.; Hanauer, S. B.; Katz, S.; Winston, B. D.; Levine, J. G.; Persson, T.; Persson, A.; Grp, B. C. U. S., Budesonide CIR capsules (once or twice daily divided-dose) in active Crohn's disease: A randomized placebo-controlled study in the United States. *Am J Gastroenterol* **2002,** *97* (7), 1748-1754.

96. Present, D. H., 6-Mercaptopurine and other immunosuppressive agents in the treatment of Crohn's disease and ulcerative colitis. *Gastroenterol Clin North Am* **1989,** *18* (1), 57-71.

97. Zenlea, T.; Peppercorn, M. A., Immunosuppressive therapies for inflammatory bowel disease. *World J Gastroentero* **2014,** *20* (12), 3146-3152.

98. Feagan, B. G.; Alfadhli, A., Methotrexate in inflammatory bowel disease. *Gastroenterol Clin N* **2004,** *33* (2), 407-+.

99. Matsuda, S.; Koyasu, S., Mechanisms of action of cyclosporine. *Immunopharmacology* **2000,** *47* (2-3), 119-125.

100. Vermeire, S.; Noman, M.; Van Assche, G.; Baert, F.; D'Haens, G.; Rutgeerts, P., Effectiveness of concomitant immunosuppressive therapy in suppressing the formation of antibodies to infliximab in Crohn's disease. *Gut* **2007,** *56* (9), 1226-31.

101. Tracey, D.; Klareskog, L.; Sasso, E. H.; Salfeld, J. G.; Tak, P. P., Tumor necrosis factor antagonist mechanisms of action: A comprehensive review. *Pharmacol Therapeut* **2008,** *117* (2), 244-279.

102. Guo, Y.; Lu, N.; Bai, A., Clinical use and mechanisms of infliximab treatment on inflammatory bowel disease: a recent update. *Biomed Res Int* **2013,** *2013*, 581631.

103. Papamichael, K.; Lin, S.; Moore, M.; Papaioannou, G.; Sattler, L.; Cheifetz, A. S., Infliximab in inflammatory bowel disease. *Ther Adv Chronic Dis* **2019,** *10*, 2040622319838443.

104. Rawla, P.; Sunkara, T.; Raj, J. P., Role of biologics and biosimilars in inflammatory bowel disease: current trends and future perspectives. *J Inflamm Res* **2018,** *11*, 215-226.

105. Hanauer, S. B.; Feagan, B. G.; Lichtenstein, G. R.; Mayer, L. F.; Schreiber, S.; Colombel, J. F.; Rachmilewitz, D.; Wolf, D. C.; Olson, A.; Bao, W. H.; Rutgeerts, P.; Grp, A. I. S., Maintenance infliximab for Crohn's disease: the ACCENT I randomised trial. *Lancet* **2002,** *359* (9317), 1541-1549.

106. Rutgeerts, P.; Sandborn, W. J.; Feagan, B. G.; Reinisch, W.; Olson, A.; Johanns, J.; Travers, S.; Rachmilewitz, D.; Hanauer, S. B.; Lichtenstein, G. R.; de Villiers, W. J. S.; Present, D.; Sands, B. E.; Colombel, J. F., Infliximab for induction and maintenance therapy for ulcerative colitis. *New Engl J Med* **2005,** *353* (23), 2462-2476.

107. Schnitzler, F.; Fidder, H.; Ferrante, M.; Noman, M.; Arijs, I.; Van Assche, G.; Hoffman, I.; Van Steen, K.; Vermeire, S.; Rutgeerts, P., Long-term outcome of treatment with infliximab in 614 patients with Crohn's disease: results from a single-centre cohort. *Gut* **2009,** *58* (4), 492-500.

108. den Broeder, A.; van de Putte, L.; Rau, R.; Schattenkirchner, M.; Van Riel, P.; Sander, O.; Binder, C.; Fenner, H.; Bankmann, Y.; Velagapudi, R.; Kempeni, J.; Kupper, H., A single dose, placebo controlled study of the fully human anti-tumor necrosis factor-alpha antibody adalimumab (D2E7) in patients with rheumatoid arthritis. *J Rheumatol* **2002,** *29* (11), 2288-98.

109. Lapadula, G.; Marchesoni, A.; Armuzzi, A.; Blandizzi, C.; Caporali, R.; Chimenti, S.; Cimaz, R.; Cimino, L.; Gionchetti, P.; Girolomoni, G.; Lionetti, P.; Marcellusi, A.; Mennini,

F. S.; Salvarani, C., Adalimumab in the Treatment of Immune-Mediated Diseases. *Int J Immunopath Ph* **2014,** *27*, 33-48.

110. Sandborn, W. J.; Feagan, B. G.; Stoinov, S.; Honiball, P. J.; Rutgeerts, P.; Mason, D.; Bloomfield, R.; Schreiber, S., Certolizumab pegol for the treatment of Crohn's disease. *New Engl J Med* **2007,** *357* (3), 228-238.

111. Cunningham, G.; Samaan, M. A.; Irving, P. M., Golimumab in the treatment of ulcerative colitis. *Ther Adv Gastroenter* **2019,** *12*.

112. Spiceland, C. M.; Lodhia, N., Endoscopy in inflammatory bowel disease: Role in diagnosis, management, and treatment. *World J Gastroentero* **2018,** *24* (35), 4014-4020.

113. Annese, V.; Daperno, M.; Rutter, M. D.; Amiot, A.; Bossuyt, P.; East, J.; Ferrante, M.; Gotz, M.; Katsanos, K. H.; Kiesslich, R.; Ordas, I.; Repici, A.; Rosa, B.; Sebastian, S.; Kucharzik, T.; Eliakim, R.; Ecco, European evidence based consensus for endoscopy in inflammatory bowel disease. *Journal of Crohns & Colitis* **2013,** *7* (12), 982-1018.

114. Gomollon, F.; Dignass, A.; Annese, V.; Tilg, H.; Van Assche, G.; Lindsay, J. O.; Peyrin-Biroulet, L.; Cullen, G. J.; Daperno, M.; Kucharzik, T.; Rieder, F.; Almer, S.; Armuzzi, A.; Harbord, M.; Langhorst, J.; Sans, M.; Chowers, Y.; Fiorino, G.; Juillerat, P.; Mantzaris, G. J.; Rizzello, F.; Vavricka, S.; Gionchetti, P., 3rd European Evidence-based Consensus on the Diagnosis and Management of Crohn's Disease 2016: Part 1: Diagnosis and Medical Management. *Journal of Crohns & Colitis* **2017,** *11* (1), 3-25.

115. Jacobs, D. J.; Lee, S., Endoscopy for the Diagnosis of Inflammatory Bowel Disease. *Endoscopy* **2018**, 71-88.

116. Nahon, S.; Bouhnik, Y.; Lavergne-Slove, A.; Bitoun, A.; Panis, Y.; Valleur, P.; Vahedi, K.; Messing, B.; Matuchansky, C.; Rambaud, J. C., Colonoscopy accurately predicts the

anatomical severity of colonic Crohn's disease attacks: Correlation with findings from colectomy specimens. *Am J Gastroenterol* **2002,** *97* (12), 3102-3107.

117. Shergill, A. K.; Lightdale, J. R.; Bruining, D. H.; Acosta, R. D.; Chandrasekhara, V.; Chathadi, K. V.; Decker, G. A.; Early, D. S.; Evans, J. A.; Fanelli, R. D.; Fisher, D. A.; Fonkalsrud, L.; Foley, K.; Hwang, J. H.; Jue, T. L.; Khashab, M. A.; Muthusamy, V. R.; Pasha, S. F.; Saltzman, J. R.; Sharaf, R.; Cash, B. D.; DeWitt, J. M.; Comm, A. S. P., The role of endoscopy in inflammatory bowel disease. *Gastrointest Endosc* **2015,** *81* (5), 1101-U389.

118. Dajcman, D., The Role of a Colonoscopy in Inflammatory Bowel Disease (Ibd). *Zdr Vestn* **2008,** *77* (9), 623-627.

119. Feakins, R. M.; British Society of, G., Inflammatory bowel disease biopsies: updated British Society of Gastroenterology reporting guidelines. *J Clin Pathol* **2013,** *66* (12), 1005-26.

120. Theodossi, A.; Spiegelhalter, D. J.; Jass, J.; Firth, J.; Dixon, M.; Leader, M.; Levison, D. A.; Lindley, R.; Filipe, I.; Price, A.; et al., Observer variation and discriminatory value of biopsy features in inflammatory bowel disease. *Gut* **1994,** *35* (7), 961-8.

121. Kondrashina, E.; Schukina, O.; Kharitidis, A.; Botina, A.; Markova, E., Evaluation of histological parameters in patients with clinical remission of ulcerative colitis. *Journal of Crohns & Colitis* **2015,** *9*, S214-S214.

122. Lee, J. M.; Lee, K. M., Endoscopic Diagnosis and Differentiation of Inflammatory Bowel Disease. *Clin Endosc* **2016,** *49* (4), 370-5.

123. Panes, J.; Bouhnik, Y.; Reinisch, W.; Stoker, J.; Taylor, S. A.; Baumgart, D. C.; Danese, S.; Halligan, S.; Marincek, B.; Matos, C.; Peyrin-Biroulet, L.; Rimola, J.; Rogler, G.; van Assche, G.; Ardizzone, S.; Ba-Ssalamah, A.; Bali, M. A.; Bellini, D.; Biancone, L.; Castiglione, F.; Ehehalt, R.; Grassi, R.; Kucharzik, T.; Maccioni, F.; Maconi, G.; Magro, F.; Martin-Comin,

J.; Morana, G.; Pendse, D.; Sebastian, S.; Signore, A.; Tolan, D.; Tielbeek, J. A.; Weishaupt, D.; Wiarda, B.; Laghi, A., Imaging techniques for assessment of inflammatory bowel disease: joint ECCO and ESGAR evidence-based consensus guidelines. *J Crohns Colitis* **2013,** *7* (7), 556-85.

124. Lapp, R. T.; Spier, B. J.; Perlman, S. B.; Jaskowiak, C. J.; Reichelderfer, M., Clinical utility of positron emission tomography/computed tomography in inflammatory bowel disease. *Mol Imaging Biol* **2011,** *13* (3), 573-576.

125. Malham, M.; Hess, S.; Nielsen, R. G.; Husby, S.; Hoilund-Carlsen, P. F., PET/CT in the diagnosis of inflammatory bowel disease in pediatric patients: a review. *Am J Nucl Med Mol Imaging* **2014,** *4* (3), 225-30.

126. Mackalski, B. A.; Bernstein, C. N., New diagnostic imaging tools for inflammatory bowel disease. *Gut* **2006,** *55* (5), 733-41.

127. Horsthuis, K.; Bipat, S.; Bennink, R. J.; Stoker, J., Inflammatory bowel disease diagnosed with US, MR, scintigraphy, and CT: Meta-analysis of prospective studies. *Radiology* **2008,** *247* (1), 64-79.

128. Negaard, A.; Paulsen, V.; Sandvik, L.; Berstad, A. E.; Borthne, A.; Try, K.; Lygren, I.; Storaas, T.; Klow, N. E., A prospective randomized comparison between two MRI studies of the small bowel in Crohn's disease, the oral contrast method and MR enteroclysis. *Eur Radiol* **2007,** *17* (9), 2294-2301.

129. Nikolaus, S.; Schreiber, S., Diagnostics of inflammatory bowel disease. *Gastroenterology* **2007,** *133* (5), 1670-1689.

130. Biomarkers Definitions Working, G., Biomarkers and surrogate endpoints: preferred definitions and conceptual framework. *Clin Pharmacol Ther* **2001,** *69* (3), 89-95.

131. Tillett, S. W.; Francis, T., Serological reactions in pneumonia with a nonprotein somatic fraction of the Pneumococcus. *J Exp Med* **1930,** *52* (4), 561-571.

132. Pepys, M. B.; Hirschfield, G. M., C-reactive protein: a critical update. *J Clin Invest* **2003,** *111* (12), 1805-12.

133. Shine, B.; de Beer, F. C.; Pepys, M. B., Solid phase radioimmunoassays for human C-reactive protein. *Clin Chim Acta* **1981,** *117* (1), 13-23.

134. Bray, C.; Bell, L. N.; Liang, H.; Haykal, R.; Kaiksow, F.; Mazza, J. J.; Yale, S. H., Erythrocyte Sedimentation Rate and C-reactive Protein Measurements and Their Relevance in Clinical Medicine. *WMJ* **2016,** *115* (6), 317-21.

135. Fagan, E. A.; Dyck, R. F.; Maton, P. N.; Hodgson, H. J.; Chadwick, V. S.; Petrie, A.; Pepys, M. B., Serum levels of C-reactive protein in Crohn's disease and ulcerative colitis. *Eur J Clin Invest* **1982,** *12* (4), 351-9.

136. Solem, C. A.; Loftus, E. V., Jr.; Tremaine, W. J.; Harmsen, W. S.; Zinsmeister, A. R.; Sandborn, W. J., Correlation of C-reactive protein with clinical, endoscopic, histologic, and radiographic activity in inflammatory bowel disease. *Inflamm Bowel Dis* **2005,** *11* (8), 707-12.

137. Louis, E.; Vermeire, S.; Rutgeerts, M.; De Vos, M.; Van Gossum, A.; Pescatore, P.; Pelckmans, P.; Reynaert, H.; D'Haens, G.; Malaise, M.; Belaiche, J., A positive response to infliximab in Crohn disease: association with a higher systemic inflammation before treatment but not with -308 TNF gene polymorphism. *Scand J Gastroenterol* **2002,** *37* (7), 818–824.

138. Iwasa, R.; Yamada, A.; Sono, K.; Furukawa, R.; Takeuchi, K.; Suzuki, Y., C-reactive protein level at 2 weeks following initiation of infliximab induction therapy predicts outcomes in patients with ulcerative colitis: a 3 year follow-up study. *Bmc Gastroenterol* **2015,** *15*, 103.

139. Saadeh, C., The erythrocyte sedimentation rate: Old and new clinical applications. *Southern Med J* **1998,** *91* (3), 220-225.

140. Bridgen, M., The erythrocyte sedimentation rate - Still a helpful test when used judiciously. *Postgrad Med* **1998,** *103* (5), 253-+.

141. Dai, C.; Jiang, M.; Sun, M. J.; Cao, Q., Fecal Lactoferrin for Assessment of Inflammatory Bowel Disease Activity: A Systematic Review and Meta-Analysis. *J Clin Gastroenterol* **2019**.

142. Turner, D.; Mack, D. R.; Hyams, J.; LeLeiko, N.; Otley, A.; Markowitz, J.; Kasirer, Y.; Muise, A.; Seow, C. H.; Silverberg, M. S.; Crandall, W.; Griffiths, A. M., C-reactive protein (CRP), erythrocyte sedimentation rate (ESR) or both? A systematic evaluation in pediatric ulcerative colitis. *J Crohns Colitis* **2011,** *5* (5), 423-9.

143. Holtman, G. A.; Lisman-van Leeuwen, Y.; Reitsma, J. B.; Berger, M. Y., Noninvasive Tests for Inflammatory Bowel Disease: A Meta-analysis. *Pediatrics* **2016,** *137* (1).

144. Rump, J. A.; Scholmerich, J.; Gross, V.; Roth, M.; Helfesrieder, R.; Rautmann, A.; Ludemann, J.; Gross, W. L.; Peter, H. H., A new type of perinuclear anti-neutrophil cytoplasmic antibody (p-ANCA) in active ulcerative colitis but not in Crohn's disease. *Immunobiology* **1990,** *181* (4-5), 406-13.

145. Ruemmele, F. M.; Targan, S. R.; Levy, G.; Dubinsky, M.; Braun, J.; Seidman, E. G., Diagnostic accuracy of serological assays in pediatric inflammatory bowel disease. *Gastroenterology* **1998,** *115* (4), 822-9.

146. Vasiliauskas, E. A.; Plevy, S. E.; Landers, C. J.; Binder, S. W.; Ferguson, D. M.; Yang, H.; Rotter, J. I.; Vidrich, A.; Targan, S. R., Perinuclear antineutrophil cytoplasmic antibodies in patients with Crohn's disease define a clinical subgroup. *Gastroenterology* **1996,** *110* (6), 1810-9.

147. Mokhtarifar, A.; Ganji, A.; Sadrneshin, M.; Bahari, A.; Esmaeilzadeh, A.; Ghafarzadegan, K.; Nikpour, S., Diagnostic Value of ASCA and Atypical p-ANCA in Differential Diagnosis of Inflammatory Bowel Disease. *Middle East J Dig Dis* **2013,** *5* (2), 93-7.

148. Zholudev, A.; Zurakowski, D.; Young, W.; Leichtner, A.; Bousvaros, A., Serologic testing with ANCA, ASCA, and anti-OmpC in children and young adults with Crohn's disease and ulcerative colitis: diagnostic value and correlation with disease phenotype. *Am J Gastroenterol* **2004,** *99* (11), 2235-41.

149. Joossens, S.; Colombel, J. F.; Landers, C.; Poulain, D.; Geboes, K.; Bossuyt, X.; Targan, S.; Rutgeerts, P.; Reinisch, W., Anti-outer membrane of porin C and anti-I2 antibodies in indeterminate colitis. *Gut* **2006,** *55* (11), 1667-9.

150. Targan, S. R.; Landers, C. J.; Yang, H.; Lodes, M. J.; Cong, Y.; Papadakis, K. A.; Vasiliauskas, E.; Elson, C. O.; Hershberg, R. M., Antibodies to CBir1 flagellin define a unique response that is associated independently with complicated Crohn's disease. *Gastroenterology* **2005,** *128* (7), 2020-8.

151. Sitaraman, S. V.; Klapproth, J. M.; Moore, D. A., 3rd; Landers, C.; Targan, S.; Williams, I. R.; Gewirtz, A. T., Elevated flagellin-specific immunoglobulins in Crohn's disease. *Am J Physiol Gastrointest Liver Physiol* **2005,** *288* (2), G403-6.

152. Plevy, S.; Silverberg, M. S.; Lockton, S.; Stockfisch, T.; Croner, L.; Stachelski, J.; Brown, M.; Triggs, C.; Chuang, E.; Princen, F.; Singh, S., Combined serological, genetic, and inflammatory markers differentiate non-IBD, Crohn's disease, and ulcerative colitis patients. *Inflamm Bowel Dis* **2013,** *19* (6), 1139-48.

153. Korhonen, R.; Lahti, A.; Kankaanranta, H.; Moilanen, E., Nitric oxide production and signaling in inflammation. *Curr Drug Targets Inflamm Allergy* **2005,** *4* (4), 471-9.

154. Calcerrada, P.; Peluffo, G.; Radi, R., Nitric Oxide-Derived Oxidants with a Focus on Peroxynitrite: Molecular Targets, Cellular Responses and Therapeutic Implications. *Curr Pharm Design* **2011,** *17* (35), 3905-3932.

155. Kolios, G.; Valatas, V.; Ward, S. G., Nitric oxide in inflammatory bowel disease: a universal messenger in an unsolved puzzle. *Immunology* **2004,** *113* (4), 427-437.

156. Avdagic, N.; Zaciragic, A.; Babic, N.; Hukic, M.; Seremet, M.; Lepara, O.; Nakas-Icindic, E., Nitric oxide as a potential biomarker in inflammatory bowel disease. *Bosnian J Basic Med* **2013,** *13* (1), 5-9.

157. Wajant, H.; Pfizenmaier, K.; Scheurich, P., Tumor necrosis factor signaling. *Cell Death Differ* **2003,** *10* (1), 45-65.

158. Idriss, H. T.; Naismith, J. H., TNF alpha and the TNF receptor superfamily: structure-function relationship(s). *Microsc Res Tech* **2000,** *50* (3), 184-95.

159. Horiuchi, T.; Mitoma, H.; Harashima, S.; Tsukamoto, H.; Shimoda, T., Transmembrane TNF-alpha: structure, function and interaction with anti-TNF agents. *Rheumatology (Oxford)* **2010,** *49* (7), 1215-28.

160. Avdagic, N.; Babic, N.; Seremet, M.; Delic-Sarac, M.; Drace, Z.; Denjalic, A.; Nakas-Icindic, E., Tumor necrosis factor-alpha serum level in assessment of disease activity in inflammatory bowel diseases. *Med Glas (Zenica)* **2013,** *10* (2), 211-6.

161. Komatsu, M.; Kobayashi, D.; Saito, K.; Furuya, D.; Yagihashi, A.; Araake, H.; Tsuji, N.; Sakamaki, S.; Niitsu, Y.; Watanabe, N., Tumor necrosis factor-alpha in serum of patients with inflammatory bowel disease as measured by a highly sensitive immuno-PCR. *Clin Chem* **2001,** *47* (7), 1297-301.

162. Weichsel, A.; Maes, E. M.; Andersen, J. F.; Valenzuela, J. G.; Shokhireva, T.; Walker, F. A.; Montfort, W. R., Heme-assisted S-nitrosation of a proximal thiolate in a nitric oxide transport protein. *Proc Natl Acad Sci U S A* **2005,** *102* (3), 594-9.

163. Liang, S.; Dai, J.; Hou, S.; Su, L.; Zhang, D.; Guo, H.; Hu, S.; Wang, H.; Rao, Z.; Guo, Y.; Lou, Z., Structural basis for treating tumor necrosis factor alpha (TNFalpha)-associated diseases with the therapeutic antibody infliximab. *J Biol Chem* **2013,** *288* (19), 13799-807.

164. Mitsuyama, K.; Tomiyasu, N.; Takaki, K.; Masuda, J.; Yamasaki, H.; Kuwaki, K.; Takeda, T.; Kitazaki, S.; Tsuruta, O.; Sata, M., Interleukin-10 in the pathophysiology of inflammatory bowel disease: increased serum concentrations during the recovery phase. *Mediators Inflamm* **2006,** *2006* (6), 26875.

165. Fujino, S.; Andoh, A.; Bamba, S.; Ogawa, A.; Hata, K.; Araki, Y.; Bamba, T.; Fujiyama, Y., Increased expression of interleukin 17 in inflammatory bowel disease. *Gut* **2003,** *52* (1), 65-70.

166. Yamamoto-Furusho, J. K.; Miranda-Perez, E.; Fonseca-Camarillo, G.; Sanchez-Munoz, F.; Dominguez-Lopez, A.; Barreto-Zuniga, R., Colonic epithelial upregulation of interleukin 22 (IL-22) in patients with ulcerative colitis. *Inflamm Bowel Dis* **2010,** *16* (11), 1823.

167. Brocker, C.; Thompson, D.; Matsumoto, A.; Nebert, D. W.; Vasiliou, V., Evolutionary divergence and functions of the human interleukin (IL) gene family. *Hum Genomics* **2010,** *5* (1), 30-55.

168. Walter, M. R., The molecular basis of IL-10 function: from receptor structure to the onset of signaling. *Curr Top Microbiol Immunol* **2014,** *380,* 191-212.

169. Fiorentino, D. F.; Zlotnik, A.; Mosmann, T. R.; Howard, M.; O'Garra, A., IL-10 inhibits cytokine production by activated macrophages. *J Immunol* **1991,** *147* (11), 3815-22.

170. de Waal Malefyt, R.; Abrams, J.; Bennett, B.; Figdor, C. G.; de Vries, J. E., Interleukin 10(IL-10) inhibits cytokine synthesis by human monocytes: an autoregulatory role of IL-10 produced by monocytes. *J Exp Med* **1991,** *174* (5), 1209-20.

171. Howard, M.; O'Garra, A., Biological properties of interleukin 10. *Immunol Today* **1992,** *13* (6), 198-200.

172. Rousset, F.; Garcia, E.; Defrance, T.; Peronne, C.; Vezzio, N.; Hsu, D. H.; Kastelein, R.; Moore, K. W.; Banchereau, J., Interleukin 10 is a potent growth and differentiation factor for activated human B lymphocytes. *Proc Natl Acad Sci U S A* **1992,** *89* (5), 1890-3.

173. Levy, Y.; Brouet, J. C., Interleukin-10 prevents spontaneous death of germinal center B cells by induction of the bcl-2 protein. *J Clin Invest* **1994,** *93* (1), 424-8.

174. Iyer, S. S.; Cheng, G., Role of interleukin 10 transcriptional regulation in inflammation and autoimmune disease. *Crit Rev Immunol* **2012,** *32* (1), 23-63.

175. Kuhn, R.; Lohler, J.; Rennick, D.; Rajewsky, K.; Muller, W., Interleukin-10-deficient mice develop chronic enterocolitis. *Cell* **1993,** *75* (2), 263-74.

176. Pascual-Figal, D. A.; Januzzi, J. L., The biology of ST2: the International ST2 Consensus Panel. *Am J Cardiol* **2015,** *115* (7 Suppl), 3B-7B.

177. Villacorta, H.; Maisel, A. S., Soluble ST2 Testing: A Promising Biomarker in the Management of Heart Failure. *Arq Bras Cardiol* **2016,** *106* (2), 145-52.

178. Boga, S.; Alkim, H.; Koksal, A. R.; Ozagari, A. A.; Bayram, M.; Tekin Neijmann, S.; Sen, I.; Alkim, C., Serum ST2 in inflammatory bowel disease: a potential biomarker for disease activity. *J Investig Med* **2016,** *64* (5), 1016-24.

179. Milner, C. M.; Day, A. J., TSG-6: a multifunctional protein associated with inflammation. *J Cell Sci* **2003,** *116* (10), 1863-1873.

180. Bardos, T.; Kamath, R. V.; Mikecz, K.; Glant, T. T., Anti-inflammatory and chondroprotective effect of TSG-6 (tumor necrosis factor-alpha-stimulated gene-6) in murine models of experimental arthritis. *Am J Pathol* **2001,** *159* (5), 1711-21.

181. Yu, Q.; Zhang, S. H.; Wang, H. L.; Zhang, Y. F.; Feng, T.; Chen, B. L.; He, Y.; Zeng, Z. R.; Chen, M. H., TNFAIP6 is a potential biomarker of disease activity in inflammatory bowel disease. *Biomark Med* **2016,** *10* (5), 473-483.

182. Dabritz, J.; Musci, J.; Foell, D., Diagnostic utility of faecal biomarkers in patients with irritable bowel syndrome. *World J Gastroenterol* **2014,** *20* (2), 363-75.

183. Fagerhol, M. K.; Dale, I.; Andersson, T., A radioimmunoassay for a granulocyte protein as a marker in studies on the turnover of such cells. *Bull Eur Physiopathol Respir* **1980,** *16 Suppl*, 273-82.

184. von Roon, A. C.; Karamountzos, L.; Purkayastha, S.; Reese, G. E.; Darzi, A. W.; Teare, J. P.; Paraskeva, P.; Tekkis, P. P., Diagnostic precision of fecal calprotectin for inflammatory bowel disease and colorectal malignancy. *Am J Gastroenterol* **2007,** *102* (4), 803-13.

185. Shabani, F.; Farasat, A.; Mahdavi, M.; Gheibi, N., Calprotectin (S100A8/S100A9): a key protein between inflammation and cancer. *Inflamm Res* **2018,** *67* (10), 801-812.

186. Chatzikonstantinou, M.; Konstantopoulos, P.; Stergiopoulos, S.; Kontzoglou, K.; Verikokos, C.; Perrea, D.; Dimitroulis, D., Calprotectin as a diagnostic tool for inflammatory bowel diseases. *Biomed Rep* **2016,** *5* (4), 403-407.

187. Wang, S.; Wang, Z.; Shi, H.; Heng, L.; Juan, W.; Yuan, B.; Wu, X.; Wang, F., Faecal calprotectin concentrations in gastrointestinal diseases. *J Int Med Res* **2013,** *41* (4), 1357-61.

188. Michael R. Konikoff, M. L. A. D., MD, Role of Fecal Calprotectin as a Biomarker of Intestinal Inflammation in Inflammatory Bowel Disease. *Inflammatory Bowel Diseases* **2006,** *12* (6), 524-534.

189. Striz, I.; Trebichavsky, I., Calprotectin - a pleiotropic molecule in acute and chronic inflammation. *Physiol Res* **2004,** *53* (3), 245-53.

190. Freeman, K.; Willis, B. H.; Fraser, H.; Taylor-Phillips, S.; Clarke, A., Faecal calprotectin to detect inflammatory bowel disease: a systematic review and exploratory meta-analysis of test accuracy. *BMJ Open* **2019,** *9* (3), e027428.

191. Sipponen, T.; Savilahti, E.; Karkkainen, P.; Kolho, K. L.; Nuutinen, H.; Turunen, U.; Farkkila, M., Fecal calprotectin, lactoferrin, and endoscopic disease activity in monitoring anti-TNF-alpha therapy for Crohn's disease. *Inflamm Bowel Dis* **2008,** *14* (10), 1392-8.

192. Meijer, B.; Gearry, R. B.; Day, A. S., The role of S100A12 as a systemic marker of inflammation. *Int J Inflam* **2012,** *2012*, 907078.

193. Foell, D.; Kane, D.; Bresnihan, B.; Vogl, T.; Nacken, W.; Sorg, C.; Fitzgerald, O.; Roth, J., Expression of the pro-inflammatory protein S100A12 (EN-RAGE) in rheumatoid and psoriatic arthritis. *Rheumatology (Oxford)* **2003,** *42* (11), 1383-9.

194. Donato, R., Intracellular and extracellular roles of S100 proteins. *Microsc Res Tech* **2003,** *60* (6), 540-51.

195. Yang, Z.; Yan, W. X.; Cai, H.; Tedla, N.; Armishaw, C.; Di Girolamo, N.; Wang, H. W.; Hampartzoumian, T.; Simpson, J. L.; Gibson, P. G.; Hunt, J.; Hart, P.; Hughes, J. M.; Perry, M. A.; Alewood, P. F.; Geczy, C. L., S100A12 provokes mast cell activation: a potential amplification pathway in asthma and innate immunity. *J Allergy Clin Immunol* **2007,** *119* (1), 106-14.

196. Foell, D.; Seeliger, S.; Vogl, T.; Koch, H. G.; Maschek, H.; Harms, E.; Sorg, C.; Roth, J., Expression of S100A12 (EN-RAGE) in cystic fibrosis. *Thorax* **2003,** *58* (7), 613-7.

197. Camoretti-Mercado, B.; Karrar, E.; Nunez, L.; Bowman, M. A., S100A12 and the Airway Smooth Muscle: Beyond Inflammation and Constriction. *J Allergy Ther* **2012,** *3* (Suppl 1).

198. Foell, D.; Kucharzik, T.; Kraft, M.; Vogl, T.; Sorg, C.; Domschke, W.; Roth, J., Neutrophil derived human S100A12 (EN-RAGE) is strongly expressed during chronic active inflammatory bowel disease. *Gut* **2003,** *52* (6), 847-53.

199. Gonzalez-Chavez, S. A.; Arevalo-Gallegos, S.; Rascon-Cruz, Q., Lactoferrin: structure, function and applications. *Int J Antimicrob Agents* **2009,** *33* (4), 301 e1-8.

200. Legrand, D., Lactoferrin, a key molecule in immune and inflammatory processes. *Biochem Cell Biol* **2012,** *90* (3), 252-68.

201. Kane, S. V.; Sandborn, W. J.; Rufo, P. A.; Zholudev, A.; Boone, J.; Lyerly, D.; Camilleri, M.; Hanauer, S. B., Fecal lactoferrin is a sensitive and specific marker in identifying intestinal inflammation. *Am J Gastroenterol* **2003,** *98* (6), 1309-1314.

202. Kjeldsen, L.; Cowland, J. B.; Borregaard, N., Human neutrophil gelatinase-associated lipocalin and homologous proteins in rat and mouse. *Biochim Biophys Acta* **2000,** *1482* (1-2), 272-83.

203. Stallhofer, J.; Friedrich, M.; Konrad-Zerna, A.; Wetzke, M.; Lohse, P.; Glas, J.; Tillack-Schreiber, C.; Schnitzler, F.; Beigel, F.; Brand, S., Lipocalin-2 Is a Disease Activity Marker in Inflammatory Bowel Disease Regulated by IL-17A, IL-22, and TNF-alpha and Modulated by IL23R Genotype Status. *Inflamm Bowel Dis* **2015,** *21* (10), 2327-40.

204. Chakraborty, S.; Kaur, S.; Guha, S.; Batra, S. K., The multifaceted roles of neutrophil gelatinase associated lipocalin (NGAL) in inflammation and cancer. *Biochim Biophys Acta* **2012,** *1826* (1), 129-69.

205. Thorsvik, S.; Damas, J. K.; Granlund, A. V.; Flo, T. H.; Bergh, K.; Ostvik, A. E.; Sandvik, A. K., Fecal neutrophil gelatinase-associated lipocalin as a biomarker for inflammatory bowel disease. *J Gastroenterol Hepatol* **2017,** *32* (1), 128-135.

206. Weissmann, G.; Smolen, J. E.; Korchak, H. M., Release of inflammatory mediators from stimulated neutrophils. *N Engl J Med* **1980,** *303* (1), 27-34.

207. Krawisz, J. E.; Sharon, P.; Stenson, W. F., Quantitative assay for acute intestinal inflammation based on myeloperoxidase activity. Assessment of inflammation in rat and hamster models. *Gastroenterology* **1984,** *87* (6), 1344-50.

208. Saiki, T., Myeloperoxidase concentrations in the stool as a new parameter of inflammatory bowel disease. *Kurume Med J* **1998,** *45* (1), 69-73.

209. Egeblad, M.; Werb, Z., New functions for the matrix metalloproteinases in cancer progression. *Nat Rev Cancer* **2002,** *2* (3), 161-74.

210. Visse, R.; Nagase, H., Matrix metalloproteinases and tissue inhibitors of metalloproteinases: structure, function, and biochemistry. *Circ Res* **2003,** *92* (8), 827-39.

211. Farkas, K.; Sarodi, Z.; Balint, A.; Foldesi, I.; Tiszlavicz, L.; Szucs, M.; Nyari, T.; Tajti, J.; Nagy, F.; Szepes, Z.; Bor, R.; Annahazi, A.; Roka, R.; Molnar, T., The diagnostic value of a new fecal marker, matrix metalloprotease-9, in different types of inflammatory bowel diseases. *J Crohns Colitis* **2015,** *9* (3), 231-7.

212. Baugh, M. D.; Perry, M. J.; Hollander, A. P.; Davies, D. R.; Cross, S. S.; Lobo, A. J.; Taylor, C. J.; Evans, G. S., Matrix metalloproteinase levels are elevated in inflammatory bowel disease. *Gastroenterology* **1999,** *117* (4), 814-822.

213. Elkins, P. A.; Ho, Y. S.; Smith, W. W.; Janson, C. A.; D'Alessio, K. J.; McQueney, M. S.; Cummings, M. D.; Romanic, A. M., Structure of the C-terminally truncated human ProMMP9, a gelatin-binding matrix metalloproteinase. *Acta Crystallogr D Biol Crystallogr* **2002,** *58* (Pt 7), 1182-92.

214. Bilski, J.; Mazur-Bialy, A.; Wojcik, D.; Zahradnik-Bilska, J.; Brzozowski, B.; Magierowski, M.; Mach, T.; Magierowska, K.; Brzozowski, T., The Role of Intestinal Alkaline Phosphatase in Inflammatory Disorders of Gastrointestinal Tract. *Mediat Inflamm* **2017,** *2017*.

215. Lalles, J. P., Intestinal alkaline phosphatase: novel functions and protective effects. *Nutr Rev* **2014,** *72* (2), 82-94.

216. Park, S. Y.; Kim, J. Y.; Lee, S. M.; Chung, J. O.; Seo, J. H.; Kim, S.; Kim, D. H.; Park, C. H.; Ju, J. K.; Joo, Y. E.; Lee, J. H.; Kim, H. S.; Choi, S. K.; Rew, J. S., Lower expression of endogenous intestinal alkaline phosphatase may predict worse prognosis in patients with Crohn's disease. *Bmc Gastroenterol* **2018,** *18* (1), 188.

217. de la Torre, C.; Mondragon, L.; Coll, C.; Sancenon, F.; Marcos, M. D.; Martinez-Manez, R.; Amoros, P.; Perez-Paya, E.; Orzaez, M., Cathepsin-B Induced Controlled Release from Peptide-Capped Mesoporous Silica Nanoparticles. *Chem-Eur J* **2014,** *20* (47), 15309-15314.

218. Climent, E.; Bernardos, A.; Martinez-Manez, R.; Maquieira, A.; Marcos, M. D.; Pastor-Navarro, N.; Puchades, R.; Sancenon, F.; Soto, J.; Amoros, P., Controlled Delivery Systems Using Antibody-Capped Mesoporous Nanocontainers. *J Am Chem Soc* **2009,** *131* (39), 14075-14080.

219. Rosenholm, J. M.; Sahlgren, C.; Linden, M., Multifunctional Mesoporous Silica Nanoparticles for Combined Therapeutic, Diagnostic and Targeted Action in Cancer Treatment. *Curr Drug Targets* **2011,** *12* (8), 1166-1186.

220. Oroval, M.; Climent, E.; Coll, C.; Eritja, R.; Avino, A.; Marcos, M. D.; Sancenon, F.; Martinez-Manez, R.; Amoros, P., An aptamer-gated silica mesoporous material for thrombin detection. *Chem Commun* **2013,** *49* (48), 5480-5482.

221. Lu, C. H.; Willner, B.; Willner, I., DNA Nanotechnology: From Sensing and DNA Machines to Drug-Delivery Systems. *Acs Nano* **2013,** *7* (10), 8320-8332.

222. Bitar, A.; Ahmad, N. M.; Fessi, H.; Elaissari, A., Silica-based nanoparticles for biomedical applications. *Drug Discov Today* **2012,** *17* (19-20), 1147-1154.

223. Wan, X. J.; Wang, D.; Liu, S. Y., Fluorescent pH-Sensing Organic/Inorganic Hybrid Mesoporous Silica Nanoparticles with Tunable Redox-Responsive Release Capability. *Langmuir* **2010,** *26* (19), 15574-15579.

224. Tang, D.; Lin, Y.; Zhou, Q.; Lin, Y.; Li, P.; Niessner, R.; Knopp, D., Low-cost and highly sensitive immunosensing platform for aflatoxins using one-step competitive displacement reaction mode and portable glucometer-based detection. *Anal Chem* **2014,** *86* (22), 11451-8.

225. Zhang, X.; Yang, P. P.; Dai, Y. L.; Ma, P. A.; Li, X. J.; Cheng, Z. Y.; Hou, Z. Y.; Kang, X. J.; Li, C. X.; Lin, J., Multifunctional Up-Converting Nanocomposites with Smart Polymer Brushes Gated Mesopores for Cell Imaging and Thermo/pH Dual-Responsive Drug Controlled Release. *Adv Funct Mater* **2013,** *23* (33), 4067-4078.

226. Li, Z.; Zhang, Y.; Feng, N., Mesoporous silica nanoparticles: synthesis, classification, drug loading, pharmacokinetics, biocompatibility, and application in drug delivery. *Expert Opin Drug Deliv* **2019,** *16* (3), 219-237.

227. Butler, K. S.; Durfee, P. N.; Theron, C.; Ashley, C. E.; Carnes, E. C.; Brinker, C. J., Protocells: Modular Mesoporous Silica Nanoparticle-Supported Lipid Bilayers for Drug Delivery. *Small* **2016,** *12* (16), 2173-85.

228. Jadhav KS, D. P., Pande VV, Mesoporous Silica Nanoparticles (MSN): A Nanonetwork and Hierarchical Structure in Drug Delivery. *J Nanomed Res* **2015,** *2* (5), 00043.

229. Kresge, C. T.; Leonowicz, M. E.; Roth, W. J.; Vartuli, J. C.; Beck, J. S., Ordered Mesoporous Molecular-Sieves Synthesized by a Liquid-Crystal Template Mechanism. *Nature* **1992,** *359* (6397), 710-712.

230. Heikkila, T.; Salonen, J.; Tuura, J.; Hamdy, M. S.; Mul, G.; Kumar, N.; Salmi, T.; Murzin, D. Y.; Laitinen, L.; Kaukonen, A. M.; Hirvonen, J.; Lehto, V. P., Mesoporous silica material TUD-1 as a drug delivery system. *Int J Pharmaceut* **2007,** *331* (1), 133-138.

231. Kotcherlakota, R.; Barui, A. K.; Prashar, S.; Fajardo, M.; Briones, D.; Rodriguez-Dieguez, A.; Patra, C. R.; Gomez-Ruiz, S., Curcumin loaded mesoporous silica: an effective drug delivery system for cancer treatment. *Biomater Sci-Uk* **2016,** *4* (3), 448-459.

232. Kumar, D.; Schumacher, K.; von Hohenesche, C. D. F.; Grun, M.; Unger, K. K., MCM-41, MCM-48 and related mesoporous adsorbents: their synthesis and characterisation. *Colloid Surface A* **2001,** *187*, 109-116.

233. Feng, Y.; Panwar, N.; Tng, D. J. H.; Tjin, S. C.; Wang, K.; Yong, K. T., The application of mesoporous silica nanoparticle family in cancer theranostics. *Coordin Chem Rev* **2016,** *319*, 86-109.

234. Chen, F. X.; Xu, X. J.; Shen, S. C.; Kawi, S.; Hidajat, K., Microporosity of SBA-3 mesoporous molecular sieves. *Micropor Mesopor Mat* **2004,** *75* (3), 231-235.

235. Anunziata, O. A.; Beltramone, A. R.; Martinez, M. L.; Belon, L. L., Synthesis and characterization of SBA-3, SBA-15, and SBA-1 nanostructured catalytic materials. *J Colloid Interf Sci* **2007,** *315* (1), 184-190.

236. Zhao, D. Y.; Huo, Q. S.; Feng, J. L.; Chmelka, B. F.; Stucky, G. D., Nonionic triblock and star diblock copolymer and oligomeric surfactant syntheses of highly ordered, hydrothermally stable, mesoporous silica structures. *J Am Chem Soc* **1998,** *120* (24), 6024-6036.

237. Zhao, L.; Qin, H. Q.; Wu, R. A.; Zou, H. F., Recent advances of mesoporous materials in sample preparation. *J Chromatogr A* **2012,** *1228*, 193-204.

238. Hamdy, M. S.; Mul, G.; Jansen, J. C.; Ebaid, A.; Shan, Z.; Overweg, A. R.; Maschmeyer, T., Synthesis, characterization, and unique catalytic performance of the mesoporous material Fe-TUD-1 in Friedel-Crafts benzylation of benzene. *Catal Today* **2005,** *100* (3-4), 255-260.

239. Chen, F.; Hong, H.; Shi, S.; Valdovinos, H. F.; Barnhart, T. E.; Cai, W., Engineering of Hollow Mesoporous Silica Nanoparticles for Remarkably Enhanced Tumor Active Targeting Efficacy. *Eur J Nucl Med Mol I* **2014,** *41*, S322-S322.

240. Liu, J. J.; Luo, Z.; Zhang, J. X.; Luo, T. T.; Zhou, J.; Zhao, X. J.; Cai, K. Y., Hollow mesoporous silica nanoparticles facilitated drug delivery via cascade pH stimuli in tumor microenvironment for tumor therapy. *Biomaterials* **2016,** *83*, 51-65.

241. D'Haens, G.; Ferrante, M.; Vermeire, S.; Baert, F.; Noman, M.; Moortgat, L.; Geens, P.; Iwens, D.; Aerden, I.; Van Assche, G.; Van Olmen, G.; Rutgeerts, P., Fecal calprotectin is a surrogate marker for endoscopic lesions in inflammatory bowel disease. *Inflamm Bowel Dis* **2012,** *18* (12), 2218-24.

242. Komatsu, M.; Kobayashi, D.; Saito, K.; Furuya, D.; Yagihashi, A.; Araake, H.; Tsuji, N.; Sakamaki, S.; Niitsu, Y.; Watanabe, N., Tumor necrosis factor-alpha in serum of patients

with inflammatory bowel disease as measured by a highly sensitive immuno-PCR. *Clin Chem* **2001,** *47* (7), 1297-1301.

243. Coll, C.; Mondragon, L.; Martinez-Manez, R.; Sancenon, F.; Marcos, M. D.; Soto, J.; Amoros, P.; Perez-Paya, E., Enzyme-Mediated Controlled Release Systems by Anchoring Peptide Sequences on Mesoporous Silica Supports. *Angew Chem Int Edit* **2011,** *50* (9), 2138-2140.

244. Tranchant, I.; Vera, L.; Czarny, B.; Amoura, M.; Cassar, E.; Beau, F.; Stura, E. A.; Dive, V., Halogen Bonding Controls Selectivity of FRET Substrate Probes for MMP-9. *Chem Biol* **2014,** *21* (3), 408-413.

245. Keubler, L. M.; Buettner, M.; Hager, C.; Bleich, A., A Multihit Model: Colitis Lessons from the Interleukin-10-deficient Mouse. *Inflamm Bowel Dis* **2015,** *21* (8), 1967-75.

246. Adegbola, S. O.; Sahnan, K.; Warusavitarne, J.; Hart, A.; Tozer, P., Anti-TNF Therapy in Crohn's Disease. *Int J Mol Sci* **2018,** *19* (8).

247. Zhang, C.; Shu, W.; Zhou, G.; Lin, J.; Chu, F.; Wu, H.; Liu, Z., Anti-TNF-alpha Therapy Suppresses Proinflammatory Activities of Mucosal Neutrophils in Inflammatory Bowel Disease. *Mediators Inflamm* **2018,** *2018*, 3021863.

248. Wang, H.; Vilches-Moure, J. G.; Cherkaoui, S.; Tardy, I.; Alleaume, C.; Bettinger, T.; Lutz, A.; Paulmurugan, R., Chronic Model of Inflammatory Bowel Disease in IL-10(-/-) Transgenic Mice: Evaluation with Ultrasound Molecular Imaging. *Theranostics* **2019,** *9* (21), 6031-6046.

249. Rullmann, J. A.; Bellido, M. N.; van Duijnen, P. T., The active site of papain. All-atom study of interactions with protein matrix and solvent. *J Mol Biol* **1989,** *206* (1), 101-18.

250. deBoer, T. R.; Tarlton, N. J.; Yamaji, R.; Adams-Sapper, S.; Wu, T. Z.; Maity, S.; Vesgesna, G. K.; Sadlowski, C. M.; DePaola, P. t.; Riley, L. W.; Murthy, N., An Enzyme-

Mediated Amplification Strategy Enables Detection of beta-Lactamase Activity Directly in Unprocessed Clinical Samples for Phenotypic Detection of beta-Lactam Resistance. *Chembiochem* **2018,** *19* (20), 2173-2177.

251. Clave, G.; Boutal, H.; Hoang, A.; Perraut, F.; Volland, H.; Renard, P. Y.; Romieu, A., A novel heterotrifunctional peptide-based cross-linking reagent for facile access to bioconjugates. Applications to peptide fluorescent labelling and immobilisation. *Org Biomol Chem* **2008,** *6* (17), 3065-78.

252. Guo, C. H.; Hu, J. N.; Kao, L.; Pan, D. Y.; Luo, K.; Li, N.; Gu, Z. W., Pepetide Dendron-Functionalized Mesoporous Silica Nanoparticle-Based Nanohybrid: Biocompatibility and Its Potential as Imaging Probe. *Acs Biomater Sci Eng* **2016,** *2* (5), 860-870.

253. Tang, D. H.; Zhang, W. T.; Qiao, Z. N.; Liu, Y. L.; Huo, Q. S., Functionalized mesoporous silica nanoparticles as a catalyst to synthesize a luminescent polymer/silica nanocomposite. *Rsc Adv* **2016,** *6* (20), 16461-16466.

254. Lee, J.; Kim, H.; Han, S.; Hong, E.; Lee, K. H.; Kim, C., Stimuli-Responsive Conformational Conversion of Peptide Gatekeepers for Controlled Release of Guests from Mesoporous Silica Nanocontainers. *J Am Chem Soc* **2014,** *136* (37), 12880-12883.

255. Matthews, J. E.; Dickey, B. W.; Miller, R. D.; Felzer, J. R.; Dawson, B. P.; Lee, A. S.; Rocks, J. J.; Kiel, J.; Montes, J. S.; Moe, C. L.; Eisenberg, J. N.; Leon, J. S., The epidemiology of published norovirus outbreaks: a review of risk factors associated with attack rate and genogroup. *Epidemiol Infect* **2012,** *140* (7), 1161-72.

256. Rydell, G. E.; Kindberg, E.; Larson, G.; Svensson, L., Susceptibility to winter vomiting disease: a sweet matter. *Rev Med Virol* **2011,** *21* (6), 370-382.

257. Zahorsky, J., Hyperemesis Hiemis or the winter vomiting disease *Archives of Pediatrics & Adolescent Medicine* **1929,** *46*, 391-395

258. Kaplan, J. E.; Goodman, R. A.; Schonberger, L. B.; Lippy, E. C.; Gary, G. W., Gastroenteritis due to Norwalk virus: an outbreak associated with a municipal water system. *J Infect Dis* **1982,** *146* (2), 190-7.

259. Cannon, R. O.; Poliner, J. R.; Hirschhorn, R. B.; Rodeheaver, D. C.; Silverman, P. R.; Brown, E. A.; Talbot, G. H.; Stine, S. E.; Monroe, S. S.; Dennis, D. T.; et al., A multistate outbreak of Norwalk virus gastroenteritis associated with consumption of commercial ice. *J Infect Dis* **1991,** *164* (5), 860-3.

260. ter Waarbeek, H. L.; Dukers-Muijrers, N. H.; Vennema, H.; Hoebe, C. J., Waterborne gastroenteritis outbreak at a scouting camp caused by two norovirus genogroups: GI and GII. *J Clin Virol* **2010,** *47* (3), 268-72.

261. Koh, S. J.; Cho, H. G.; Kim, B. H.; Choi, B. Y., An outbreak of gastroenteritis caused by norovirus-contaminated groundwater at a waterpark in Korea. *J Korean Med Sci* **2011,** *26* (1), 28-32.

262. Kaplan, J. E.; Feldman, R.; Campbell, D. S.; Lookabaugh, C.; Gary, G. W., The frequency of a Norwalk-like pattern of illness in outbreaks of acute gastroenteritis. *Am J Public Health* **1982,** *72* (12), 1329-32.

263. Dan, W.; Jin, Y.; Tang, Z.; Li, Y.; Yao, H., Nucleotide composition and synonymous codon usage of open reading frames in Norovirus GII.4 variants. *J Biomol Struct Dyn* **2020,** *38* (16), 4764-4773.

264. Hardy, M. E., Norovirus protein structure and function. *FEMS Microbiol Lett* **2005,** *253* (1), 1-8.

265. Prasad, B. V.; Rothnagel, R.; Jiang, X.; Estes, M. K., Three-dimensional structure of baculovirus-expressed Norwalk virus capsids. *J Virol* **1994,** *68* (8), 5117-25.

266. Prasad, B. V.; Hardy, M. E.; Dokland, T.; Bella, J.; Rossmann, M. G.; Estes, M. K., X-ray crystallographic structure of the Norwalk virus capsid. *Science* **1999,** *286* (5438), 287-90.

267. Tan, M.; Huang, P.; Meller, J.; Zhong, W.; Farkas, T.; Jiang, X., Mutations within the P2 domain of norovirus capsid affect binding to human histo-blood group antigens: evidence for a binding pocket. *J Virol* **2003,** *77* (23), 12562-71.

268. Lay, M. K.; Atmar, R. L.; Guix, S.; Bharadwaj, U.; He, H.; Neill, F. H.; Sastry, K. J.; Yao, Q.; Estes, M. K., Norwalk virus does not replicate in human macrophages or dendritic cells derived from the peripheral blood of susceptible humans. *Virology* **2010,** *406* (1), 1-11.

269. Kamata, K.; Shinozaki, K.; Okada, M.; Seto, Y.; Kobayashi, S.; Sakae, K.; Oseto, M.; Natori, K.; Shirato-Horikoshi, H.; Katayama, K.; Tanaka, T.; Takeda, N.; Taniguchi, K., Expression and antigenicity of virus-like particles of norovirus and their application for detection of noroviruses in stool samples. *J Med Virol* **2005,** *76* (1), 129-36.

270. Jung, J.; Grant, T.; Thomas, D. R.; Diehnelt, C. W.; Grigorieff, N.; Joshua-Tor, L., High-resolution cryo-EM structures of outbreak strain human norovirus shells reveal size variations. *Proc Natl Acad Sci U S A* **2019,** *116* (26), 12828-12832.

271. Bertolotti-Ciarlet, A.; White, L. J.; Chen, R.; Prasad, B. V.; Estes, M. K., Structural requirements for the assembly of Norwalk virus-like particles. *J Virol* **2002,** *76* (8), 4044-55.

272. Bertolotti-Ciarlet, A.; Crawford, S. E.; Hutson, A. M.; Estes, M. K., The 3' end of Norwalk virus mRNA contains determinants that regulate the expression and stability of the viral capsid protein VP1: a novel function for the VP2 protein. *J Virol* **2003,** *77* (21), 11603-15.

273. Vongpunsawad, S.; Venkataram Prasad, B. V.; Estes, M. K., Norwalk Virus Minor Capsid Protein VP2 Associates within the VP1 Shell Domain. *J Virol* **2013,** *87* (9), 4818-25.

274. Sosnovtsev, S. V.; Belliot, G.; Chang, K. O.; Onwudiwe, O.; Green, K. Y., Feline calicivirus VP2 is essential for the production of infectious virions. *J Virol* **2005,** *79* (7), 4012-24.

275. Shirato, H., Norovirus and Histo-Blood Group Antigens. *Jpn J Infect Dis* **2011,** *64* (2), 95-103.

276. Huang, P.; Farkas, T.; Zhong, W.; Tan, M.; Thornton, S.; Morrow, A. L.; Jiang, X., Norovirus and histo-blood group antigens: demonstration of a wide spectrum of strain specificities and classification of two major binding groups among multiple binding patterns. *J Virol* **2005,** *79* (11), 6714-22.

277. Ravn, V.; Dabelsteen, E., Tissue distribution of histo-blood group antigens. *Apmis* **2000,** *108* (1), 1-28.

278. Clausen, H.; Hakomori, S., ABH and related histo-blood group antigens; immunochemical differences in carrier isotypes and their distribution. *Vox Sang* **1989,** *56* (1), 1-20.

279. Ewald, D. R.; Sumner, S. C. J., Blood type biochemistry and human disease. *Wires Syst Biol Med* **2016,** *8* (6), 517-535.

280. Itzkowitz, S. H.; Dahiya, R.; Byrd, J. C.; Kim, Y. S., Blood group antigen synthesis and degradation in normal and cancerous colonic tissues. *Gastroenterology* **1990,** *99* (2), 431-42.

281. Marionneau, S.; Cailleau-Thomas, A.; Rocher, J.; Le Moullac-Vaidye, B.; Ruvoen, N.; Clement, M.; Le Pendu, J., ABH and Lewis histo-blood group antigens, a model for the meaning of oligosaccharide diversity in the face of a changing world. *Biochimie* **2001,** *83* (7), 565-573.

282. Marionneau, S.; Cailleau-Thomas, A.; Rocher, J.; Le Moullac-Vaidye, B.; Ruvoen, N.; Clement, M.; Le Pendu, J., ABH and Lewis histo-blood group antigens, a model for the meaning of oligosaccharide diversity in the face of a changing world. *Biochimie* **2001,** *83* (7), 565-73.

283. Costantini, V.; Grenz, L.; Fritzinger, A.; Lewis, D.; Biggs, C.; Hale, A.; Vinje, J., Diagnostic accuracy and analytical sensitivity of IDEIA Norovirus assay for routine screening of human norovirus. *J Clin Microbiol* **2010,** *48* (8), 2770-8.

284. Kirby, A.; Gurgel, R. Q.; Dove, W.; Vieira, S. C.; Cunliffe, N. A.; Cuevas, L. E., An evaluation of the RIDASCREEN and IDEIA enzyme immunoassays and the RIDAQUICK immunochromatographic test for the detection of norovirus in faecal specimens. *J Clin Virol* **2010,** *49* (4), 254-7.

285. Costantini, V.; Grenz, L.; Fritzinger, A.; Lewis, D.; Biggs, C.; Hale, A.; Vinje, J., Diagnostic Accuracy and Analytical Sensitivity of IDEIA Norovirus Assay for Routine Screening of Human Norovirus. *J Clin Microbiol* **2010,** *48* (8), 2770-2778.

286. Burton-MacLeod, J. A.; Kane, E. M.; Beard, R. S.; Hadley, L. A.; Glass, R. I.; Ando, T., Evaluation and comparison of two commercial enzyme-linked immunosorbent assay kits for detection of antigenically diverse human noroviruses in stool samples. *J Clin Microbiol* **2004,** *42* (6), 2587-2595.

287. Castriciano, S.; Luinstra, K.; Petrich, A.; Smieja, M.; Lee, C.; Jang, D.; Portillo, E.; Chernesky, M., Comparison of the RIDASCREEN norovirus enzyme immunoassay to IDEIA NLV GI/GII by testing stools also assayed by RT-PCR and electron microscopy. *J Virol Methods* **2007,** *141* (2), 216-9.

288. Gray, J. J.; Kohli, E.; Ruggeri, F. M.; Vennema, H.; Sanchez-Fauquier, A.; Schreier, E.; Gallimore, C. I.; Iturriza-Gomara, M.; Giraudon, H.; Pothier, P.; Di Bartolo, I.; Inglese, N.; de

Bruin, E.; van der Veer, B.; Moreno, S.; Montero, V.; de Llano, M. C.; Hoehne, M.; Diedrich, S. M., European multicenter evaluation of commercial enzyme immunoassays for detecting norovirus antigen in fecal samples. *Clin Vaccine Immunol* **2007,** *14* (10), 1349-1355.

289. Geginat, G.; Kaiser, D.; Schrempf, S., Evaluation of third-generation ELISA and a rapid immunochromatographic assay for the detection of norovirus infection in fecal samples from inpatients of a German tertiary care hospital. *Eur J Clin Microbiol Infect Dis* **2012,** *31* (5), 733-7.

290. Rovida, F.; Campanini, G.; Sarasini, A.; Adzasehoun, K. M.; Piralla, A.; Baldanti, F., Comparison of immunologic and molecular assays for the diagnosis of gastrointestinal viral infections. *Diagn Microbiol Infect Dis* **2013,** *75* (1), 110-1.

291. Division of Viral Diseases, N. C. f. I.; Respiratory Diseases, C. f. D. C.; Prevention, Updated norovirus outbreak management and disease prevention guidelines. *MMWR Recomm Rep* **2011,** *60* (RR-3), 1-18.

292. Derrington, P.; Schreiber, F.; Day, S.; Curtis, C.; Lyon, M., Norovirus Ridaquick: a new test for rapid diagnosis of norovirus. *Pathology* **2009,** *41* (7), 687-688.

293. Battaglioli, G.; Nazarian, E. J.; Lamson, D.; Musser, K. A.; George, K. S., Evaluation of the RIDAQuick norovirus immunochromatographic test kit. *Journal of Clinical Virology* **2012,** *53* (3), 262-264.

294. Bruins, M. J.; Wolfhagen, M. J. H. M.; Schirm, J.; Ruijs, G. J. H. M., Evaluation of a rapid immunochromatographic test for the detection of norovirus in stool samples. *Eur J Clin Microbiol* **2010,** *29* (6), 741-743.

295. Kim, H. S.; Hyun, J.; Kim, J. S.; Song, W.; Kang, H. J.; Lee, K. M., Evaluation of the SD Bioline Norovirus rapid immunochromatography test using fecal specimens from Korean gastroenteritis patients. *J Virol Methods* **2012,** *186* (1-2), 94-8.

296. Park, K. S.; Baek, K. A.; Kim, D. U.; Kwon, K. S.; Bing, S. H.; Park, J. S.; Nam, H. S.; Lee, S. H.; Choi, Y. J., Evaluation of a new immunochromatographic assay kit for the rapid detection of norovirus in fecal specimens. *Ann Lab Med* **2012,** *32* (1), 79-81.

297. Ambert-Balay, K.; Pothier, P., Evaluation of 4 immunochromatographic tests for rapid detection of norovirus in faecal samples. *J Clin Virol* **2013,** *56* (3), 194-8.

298. Deleon, R.; Matsui, S. M.; Baric, R. S.; Herrmann, J. E.; Blacklow, N. R.; Greenberg, H. B.; Sobsey, M. D., Detection of Norwalk Virus in Stool Specimens by Reverse Transcriptase-Polymerase Chain-Reaction and Nonradioactive Oligoprobes. *J Clin Microbiol* **1992,** *30* (12), 3151-3157.

299. Xi, J.; Wang, J. X.; Graham, D. Y.; Estes, M. K., Detection of Norwalk Virus in Stool by Polymerase Chain-Reaction. *J Clin Microbiol* **1992,** *30* (10), 2529-2534.

300. LeGuyader, F.; Estes, M. K.; Hardy, M. E.; Neill, F. H.; Green, J.; Brown, D. W. G.; Atmar, R. L., Evaluation of a degenerate primer for the PCR detection of human caliciviruses - Brief report. *Arch Virol* **1996,** *141* (11), 2225-2235.

301. Vinje, J.; Vennema, H.; Maunula, L.; von Bonsdorff, C. H.; Hoehne, M.; Schreier, E.; Richards, A.; Green, J.; Brown, D.; Beard, S. S.; Monroe, S. S.; de Bruin, E.; Svensson, L.; Koopmans, M. P. G., International collaborative study to compare reverse transcriptase PCR assays for detection and genotyping of noroviruses. *J Clin Microbiol* **2003,** *41* (4), 1423-1433.

302. Ishida, S.; Yoshizumi, S.; Ikeda, T.; Miyoshi, M.; Okano, M.; Okui, T., Sensitive and rapid detection of norovirus using duplex TaqMan reverse transcription-polymerase chain reaction. *J Med Virol* **2008,** *80* (5), 913-20.

303. Bon, F.; Giraudon, H.; Sancey, C.; Barranger, C.; Joannes, M.; Pothier, P.; Kohli, E., Development and evaluation of a new commercial test allowing the simultaneous detection of

noroviruses and sapoviruses by reverse transcription-PCR and microplate hybridization. *J Clin Microbiol* **2004,** *42* (5), 2218-20.

304. Kele, B.; Lengyel, G.; Deak, J., Comparison of an ELISA and two reverse transcription polymerase chain reaction methods for norovirus detection. *Diagn Microbiol Infect Dis* **2011,** *70* (4), 475-8.

305. Liu, J.; Kibiki, G.; Maro, V.; Maro, A.; Kumburu, H.; Swai, N.; Taniuchi, M.; Gratz, J.; Toney, D.; Kang, G.; Houpt, E., Multiplex reverse transcription PCR Luminex assay for detection and quantitation of viral agents of gastroenteritis. *J Clin Virol* **2011,** *50* (4), 308-13.

306. Khare, R.; Espy, M. J.; Cebelinski, E.; Boxrud, D.; Sloan, L. M.; Cunningham, S. A.; Pritt, B. S.; Patel, R.; Binnicker, M. J., Comparative evaluation of two commercial multiplex panels for detection of gastrointestinal pathogens by use of clinical stool specimens. *J Clin Microbiol* **2014,** *52* (10), 3667-73.

307. Tang, Y. J.; Zeng, X. Q.; Liang, J., Surface Plasmon Resonance: An Introduction to a Surface Spectroscopy Technique. *J Chem Educ* **2010,** *87* (7), 742-746.

308. Prabowo, B. A.; Purwidyantri, A.; Liu, K. C., Surface Plasmon Resonance Optical Sensor: A Review on Light Source Technology. *Biosensors (Basel)* **2018,** *8* (3).

309. Park, K.; Lee, J. M.; Jung, Y.; Habtemariam, T.; Salah, A. W.; Fermin, C. D.; Kim, M., Combination of cysteine- and oligomerization domain-mediated protein immobilization on a surface plasmon resonance (SPR) gold chip surface. *Analyst* **2011,** *136* (12), 2506-11.

310. Lee, J. M.; Park, H. K.; Jung, Y.; Kim, J. K.; Jung, S. O.; Chung, B. H., Direct immobilization of protein g variants with various numbers of cysteine residues on a gold surface. *Anal Chem* **2007,** *79* (7), 2680-7.

311. Drescher, D. G.; Ramakrishnan, N. A.; Drescher, M. J., Surface plasmon resonance (SPR) analysis of binding interactions of proteins in inner-ear sensory epithelia. *Methods Mol Biol* **2009,** *493*, 323-43.

312. Douzi, B., Protein-Protein Interactions: Surface Plasmon Resonance. *Methods Mol Biol* **2017,** *1615*, 257-275.

313. Dundas, C. M.; Demonte, D.; Park, S., Streptavidin-biotin technology: improvements and innovations in chemical and biological applications. *Appl Microbiol Biotechnol* **2013,** *97* (21), 9343-53.

314. Patrie, S. M.; Mrksich, M., Self-assembled monolayers for MALDI-TOF mass spectrometry for immunoassays of human protein antigens. *Anal Chem* **2007,** *79* (15), 5878-87.

315. Ha, T. H.; Jung, S. O.; Lee, J. M.; Lee, K. Y.; Lee, Y.; Park, J. S.; Chung, B. H., Oriented immobilization of antibodies with GST-fused multiple Fc-specific B-domains on a gold surface. *Anal Chem* **2007,** *79* (2), 546-56.

316. Zeder-Lutz, G.; Zuber, E.; Witz, J.; Van Regenmortel, M. H., Thermodynamic analysis of antigen-antibody binding using biosensor measurements at different temperatures. *Anal Biochem* **1997,** *246* (1), 123-32.

317. Wegner, G. J.; Wark, A. W.; Lee, H. J.; Codner, E.; Saeki, T.; Fang, S.; Corn, R. M., Real-time surface plasmon resonance imaging measurements for the multiplexed determination of protein adsorption/desorption kinetics and surface enzymatic reactions on peptide microarrays. *Anal Chem* **2004,** *76* (19), 5677-84.

318. Cooper, M. A.; Hansson, A.; Lofas, S.; Williams, D. H., A vesicle capture sensor chip for kinetic analysis of interactions with membrane-bound receptors. *Anal Biochem* **2000,** *277* (2), 196-205.

319. Pattnaik, P., Surface plasmon resonance: applications in understanding receptor-ligand interaction. *Appl Biochem Biotechnol* **2005,** *126* (2), 79-92.

320. Huber, W.; Mueller, F., Biomolecular interaction analysis in drug discovery using surface plasmon resonance technology. *Curr Pharm Des* **2006,** *12* (31), 3999-4021.

321. Schasfoort, R. B. M., Chapter 1 Introduction to Surface Plasmon Resonance. In *Handbook of Surface Plasmon Resonance (2),* The Royal Society of Chemistry: 2017; pp 1-26.

322. Geitmann, M.; Danielson, U. H., Studies of substrate-induced conformational changes in human cytomegalovirus protease using optical biosensor technology. *Anal Biochem* **2004,** *332* (2), 203-14.

323. Sota, H.; Hasegawa, Y.; Iwakura, M., Detection of conformational changes in an immobilized protein using surface plasmon resonance. *Anal Chem* **1998,** *70* (10), 2019-24.

324. Mannen, T.; Yamaguchi, S.; Honda, J.; Sugimoto, S.; Kitayama, A.; Nagamune, T., Observation of charge state and conformational change in immobilized protein using surface plasmon resonance sensor. *Anal Biochem* **2001,** *293* (2), 185-93.

325. Han, S. H.; Kim, S. K.; Park, K.; Yi, S. Y.; Park, H. J.; Lyu, H. K.; Kim, M.; Chung, B. H., Detection of mutant p53 using field-effect transistor biosensor. *Anal Chim Acta* **2010,** *665* (1), 79-83.

326. Dhawane, A. N.; Diez-Valcarce, M.; Gurale, B. P.; Dinh, H.; Vinje, J.; Iyer, S. S., Synthesis and Evaluation of Biotinylated Bivalent HistoBlood Group Antigens for Capturing Human Noroviruses. *Bioconjug Chem* **2016,** *27* (8), 1822-9.

327. D.A. Case, R. M. B., D.S. Cerutti, T.E. Cheatham III, T.A. Darden, R.E. Duke, T.J. Giese, H. Gohlke, A.W. Goetz, N. Homeyer, S. Izadi, P. Janowski, J. Kaus, A. Kovalenko, T.S. Lee, S. LeGrand, P. Li, C. Lin, T. Luchko, R. Luo, B. Madej, D. Mermelstein, K.M. Merz, G. Monard, H.

Nguyen, H.T. Nguyen, I. Omelyan, A. Onufriev, D.R. Roe, A. Roitberg, C. Sagui, C.L. Simmerling, W.M. Botello-Smith, J. Swails, R.C. Walker, J. Wang, R.M. Wolf, X. Wu, L. Xiao, P.A. Kollman, *AMBER 16*. 1st ed.; University of California: San Francisco, 2016; p 923.

328. Hornak, V.; Abel, R.; Okur, A.; Strockbine, B.; Roitberg, A.; Simmerling, C., Comparison of multiple Amber force fields and development of improved protein backbone parameters. *Proteins* **2006,** *65*, 712-725.

329. Maier, J. A.; Martinez, C.; Kasavajhala, K.; Wickstrom, L.; Hauser, K. E.; Simmerling, C., ff14SB: Improving the Accuracy of Protein Side Chain and Backbone Parameters from ff99SB. *J Chem Theory Comput* **2015,** *11* (8), 3696-3713.

330. Doshi, U.; Hamelberg, D., Reoptimization of the AMBER force field parameters for peptide bond (Omega) torsions using accelerated molecular dynamics. *J Phys Chem B* **2009,** *113* (52), 16590-16595.

331. Kirschner, K. N.; Yongye, A. B.; Tschampel, S. M.; Gonzalez-Outeirino, J.; Daniels, C. R.; Foley, B. L.; Woods, R. J., GLYCAM06: a generalizable biomolecular force field. Carbohydrates. *J Comput Chem* **2008,** *29* (4), 622-55.

332. Berman, H. M.; Westbrook, J.; Feng, Z.; Gilliland, G.; Bhat, T. N.; Weissig, H.; Shindyalov, I. N.; Bourne, P. E., The Protein Data Bank. *Nucleic Acids Res* **2000,** *28* (1), 235-242.

333. Biasini, M.; Bienert, S.; Waterhouse, A.; Arnold, K.; Studer, G.; Schmidt, T.; Kiefer, F.; Gallo Cassarino, T.; Bertoni, M.; Bordoli, L.; Schwede, T., SWISS-MODEL: modelling protein tertiary and quaternary structure using evolutionary information. *Nucleic Acids Res* **2014,** *42* (Web Server issue), W252-8.

334. Olsson, M. H.; Sondergaard, C. R.; Rostkowski, M.; Jensen, J. H., PROPKA3: Consistent Treatment of Internal and Surface Residues in Empirical pKa Predictions. *J Chem Theory Comput* **2011,** *7* (2), 525-37.

335. Dolinsky, T. J.; Nielsen, J. E.; McCammon, J. A.; Baker, N. A., PDB2PQR: an automated pipeline for the setup of Poisson-Boltzmann electrostatics calculations. *Nucleic Acids Res* **2004,** *32* (Web Server issue), W665-7.

336. Jorgensen, W. L.; Chandrasekhar, J.; Madura, J. D.; Impey, R. W.; Klein, M. L., Comparison of simple potential functions for simulating liquid water. *J Chem Phys* **1983,** *79* (2), 926-935.

337. Darden, T.; York, D.; Pedersen, L., Particle mesh Ewald: An N·log(N) method for Ewald sums in large systems. *J Chem Phys* **1993,** *98* (12), 10089-10092.

338. Ryckaert, J.-P.; Ciccotti, G.; Berendsen, H. J. C., Numerical integration of the cartesian equations of motion of a system with constraints: molecular dynamics of n-alkanes. *J Comput Phys* **1977,** *23*, 327-341.

339. Minh, D. D., Implicit ligand theory: rigorous binding free energies and thermodynamic expectations from molecular docking. *J Chem Phys* **2012,** *137* (10), 104106.

340. Onufriev, A.; Bashford, D.; Case, D. A., Exploring protein native states and large-scale conformational changes with a modified generalized born model. *Proteins* **2004,** *55* (2), 383-94.

341. Weiser, J.; Shenkin, P. S.; Still, W. C., Approximate atomic surfaces from linear combinations of pairwise overlaps (LCPO). *J Comput Chem* **1999,** *20* (2), 217-230.

342. Miller, B. R., 3rd; McGee, T. D., Jr.; Swails, J. M.; Homeyer, N.; Gohlke, H.; Roitberg, A. E., MMPBSA.py: An Efficient Program for End-State Free Energy Calculations. *J Chem Theory Comput* **2012,** *8* (9), 3314-21.

343. Roe, D. R.; Cheatham, T. E., 3rd, PTRAJ and CPPTRAJ: software for processing and analysis of molecular dynamics trajectory Data. *J Chem Theory Comput* **2013,** *9* (7), 3084-3095.

344. Humphrey, W.; Dalke, A.; Schulten, K., VMD: visual molecular dynamics. *J Mol Graph* **1996,** *14*, 33-38.

345. Grant, B. J.; Rodrigues, A. P.; ElSawy, K. M.; McCammon, J. A.; Caves, L. S., Bio3d: an R package for the comparative analysis of protein structures. *Bioinformatics* **2006,** *22*, 2695-2696.

346. Skjærven, L.; Yao, X.-Q.; Scarabelli, G.; Grant, B. J., Integrating protein structural dynamics and evolutionary analysis with Bio3D. *BMC Bioinformatics* **2014,** *15*, 399.

347. Wickham, H., *ggplot2: Elegant graphics for data analysis*. 2nd ed.; Springer-Verlag New York: New York, 2016; p 260.